6 Off-lattice models

6.1 FLUIDS

6.1.1 *NVT* ensemble and the virial theorem

The examination of the equation of state of a two-dimensional model fluid (the hard disk system) was the very first application of the importance sampling Monte Carlo method in statistical mechanics (Metropolis *et al.*, 1953), and since then the study of both atomic and molecular fluids by Monte Carlo simulation has been a very active area of research. Remember that statistical mechanics can deal well analytically with very dilute fluids (ideal gases), and it can also deal well with crystalline solids (making use of the harmonic approximation and perfect crystal lattice periodicity and symmetry), but the treatment of strongly correlated dense fluids (and their solid counterparts, amorphous glasses) is much more difficult. Even the description of short range order in fluids in a thermodynamic state far away from any phase transition is a non-trivial matter (unlike the lattice models discussed in the last chapter, where far away from phase transitions the molecular field approximation, or a variant thereof, is usually both good enough and easily worked out, and the real interest is generally in phase transition problems).

The discussion in this chapter will consider only symmetric particles; for the consideration of hard rods, spherocylinders, etc., the reader is referred elsewhere (Frenkel and Smit, 1996).

We are concerned here with classical mechanics only (the extension to the quantum case will be treated in Chapter 8) and then momenta of the particles cancel out from the statistical averages of any observables A, which are given as

$$\langle A \rangle_{N,V,T} = \frac{1}{Z} \int d\mathbf{X} A(\mathbf{X}) e^{-U(\mathbf{X})/k_B T}. \tag{6.1}$$

Here we have specialized the treatment to a case where there are N point particles in a box of volume V in thermal equilibrium at a given temperature T. This situation is called the NVT-ensemble of statistical mechanics. The phase space $\{\mathbf{X}\}$ is spanned by all the coordinates $\mathbf{r}_i$ of the N point particles, i.e. $\{\mathbf{X}\} = \{\mathbf{r}_1, \mathbf{r}_2, \ldots, \mathbf{r}_N\}$ and is $3N$-dimensional. Each point in that space contributes

to the average Eqn. (6.1) with the Boltzmann weight,

$$P(\mathbf{X}) = e^{-U(\mathbf{X})/k_B T}/Z, \tag{6.2}$$

which is the continuum analog of the weight that we have encountered for the discrete lattice models (Eqn. (4.5)). Here $U(\mathbf{X})$ is not the total energy, of course, but only the total potential energy (the kinetic energy has cancelled out from the average). Often it is assumed that $U(\mathbf{X})$ is simply a sum of pair-wise interactions $u(\mathbf{r}_i - \mathbf{r}_j)$ between point particles at positions $\mathbf{r}_i$, $\mathbf{r}_j$,

$$U(\mathbf{X}) = \sum_{i<j} u(\mathbf{r}_i - \mathbf{r}_j), \tag{6.3}$$

but sometimes three-body and four-body interactions, etc., are also included. A standard choice for a pair-wise potential is the Lennard–Jones interaction

$$U_{LJ}(r) = 4\varepsilon[(\sigma/r)^{12} - (\sigma/r)^6], \tag{6.4}$$

ε being the strength and σ the range of this potential.

Problem 6.1 Determine the location and depth of the minimum of the Lennard–Jones potential. At which distance has this potential decayed to about 1/1000 of its depth in the minimum?

Many other potentials have also been used in the literature; examples include the use of hard-core interactions to represent the repulsion at short distances,

$$u(r) = \infty, \quad r < r_0, \quad u(r) = 0, \quad r > r_0, \tag{6.5}$$

additional soft-sphere attractions,

$$u(r) = \infty, \quad r < r_0, \quad u(r) = -\varepsilon, \quad r_0 \le r < r_1, \quad u(r) = 0, \quad r > r_1 \tag{6.6}$$

and inverse power law potentials,

$$u(r) = (\sigma/r)^n, \quad n = \text{integer}, \tag{6.7}$$

etc.

Just as in the Monte Carlo algorithm for a lattice classical spin model, where a spin ($\mathbf{S}_i$) was randomly selected and a new spin orientation was proposed as the basic Monte Carlo step, we now select a particle i at random and consider a random displacement $\boldsymbol{\delta}$ from its old position $\mathbf{r}_i' = \mathbf{r}_i + \boldsymbol{\delta}$ to a new position. This displacement vector $\boldsymbol{\delta}$ is chosen randomly and uniformly from some volume region, ΔV, whose size is fixed such that the acceptance probability for the proposed move is on average neither close to unity nor close to zero. As in the case of the lattice model, the acceptance probability for the move, $W(\mathbf{r}_i \to \mathbf{r}_i')$, depends on the energy change $\Delta U = U(\mathbf{r}_i') - U(\mathbf{r}_i)$, given by the Boltzmann factor

$$W(\mathbf{r}_i - \mathbf{r}_i') = \min\{1, \exp(-\Delta U/k_B T)\}. \tag{6.8}$$

The implementation of the algorithm is thus quite analogous to the lattice case and can be summarized by the following steps:

'Off-lattice' Metropolis Monte Carlo method

(1) Choose an initial state (to avoid difficulties when particles are very close to each other and U thus very large, one frequently distributes particles on the sites of a regular face-centered cubic lattice).
(2) Consider a particle with a randomly chosen label i and calculate a trial position $\mathbf{r}_i' = \mathbf{r}_i + \boldsymbol{\delta}$.
(3) Calculate the energy change ΔU which results from this displacement.
(4) If $\Delta U < 0$ the move is accepted; go to (2).
(5) If $\Delta U > 0$, a random number η is chosen such that $0 < \eta < 1$.
(6) If $\eta < \exp(-\Delta U / k_B T)$, accept the move and in any case go then to (2). Note that if such a trial move is rejected, the old configuration is again counted in the averaging.

From this algorithm it is straightforward to calculate quantities like the average potential energy $\langle U \rangle_{NVT}$, or structural information like the radial pair distribution function $g(r)$, but in order to obtain the equation of state, one would also like to know the pressure p. Since this is an intensive variable, it is not so straightforward to obtain it from Monte Carlo sampling as it would be for any density of extensive variable. Nevertheless there is again a recipe from statistical mechanics that helps us, namely the virial theorem

$$p = \rho k_B T + \frac{1}{dV} \left\langle \sum_{i<j} \mathbf{f}(\mathbf{r}_i - \mathbf{r}_j) \cdot (\mathbf{r}_i - \mathbf{r}_j) \right\rangle, \tag{6.9}$$

where $\rho \equiv N/V$ is the particle density, $\mathbf{f}(\mathbf{r}_i - \mathbf{r}_j)$ is the force between particles i and j, and d is the spatial dimension. Since for the continuous, pair-wise interactions considered above, such as those in Eqns. (6.4) and (6.7), the forces are easily related to derivatives du/dr of these potentials and one can re-express the virial theorem in terms of the pair distribution function. In $d = 3$ dimensions this yields

$$p = \rho k_B T - \frac{2}{3} \pi \rho^2 \int_0^\infty dr\, r^3 \frac{du(r)}{dr} g(r). \tag{6.10}$$

Of course, these expressions for the pressure do not work for potentials that are discontinuous, such as those in Eqns. (6.5) and (6.6), and other techniques then have to be used instead. Finally, we note that the internal energy and the compressibility can also be conveniently expressed in terms of the pair

distribution function which in $d = 3$ dimensions is

$$\langle U \rangle / N = 2\pi\rho \int_0^\infty dr\, r^2 u(r) g(r), \tag{6.11a}$$

$$\kappa/\kappa_{\mathrm{id}} = 1 + 4\pi\rho \int_0^\infty dr\, r^2 \left[g(r) - 1 \right], \tag{6.11b}$$

where κ_{id} is the ideal gas compressibility.

At this point, we return to the problem that was already briefly alluded to above, namely that Eqns. (6.9) and (6.10) cannot be applied for systems of hard particles and related problems, such as the Asakura–Oosawa potential describing the effective interaction between colloids in a colloid–polymer mixture – this potential contains a hard core repulsion plus a soft attraction of the form

$$u(r < r_{\mathrm{c}}) = -\mathrm{const} \left(1 - \frac{3r}{2r_{\mathrm{c}}} + \frac{1}{2} \left(\frac{r}{r_{\mathrm{c}}} \right)^3 \right), \tag{6.12}$$

r_{c} being the range of the attractive part. A simple solution to this problem was suggested by De Miguel and Jackson (2006): one considers virtual volume changes from V to $V' = V(1 - \zeta)$, where ζ is very small. While in the old configuration (with volume V) there cannot be any pair of particles whose hard core potentials overlap, overlaps are allowed in the state created by the volume change. The quantity that is sampled then is the probability $P_{\mathrm{nov}}(\zeta)$ that no overlap occurs. One can show that for sufficiently small ζ one has $P_{\mathrm{nov}}(\zeta) = \exp(-b\zeta)$, and the constant b is related to the pressure contribution due to the hard cores, namely

$$p_{\mathrm{hc}} / (\rho k_{\mathrm{B}} T) = 1 + b/N. \tag{6.13}$$

If a soft attraction also is present, the contribution p_{sa} due to the latter then is easily estimated from the virial formula, i.e. the second part on the right-hand side of Eqn. (6.10), as usual, and the total pressure is then $p = p_{\mathrm{hc}} + p_{\mathrm{sa}}$ (Deb *et al.*, 2012).

These techniques can also be generalized to the case of systems in a thin film geometry confined by two walls a distance D apart. In such a system, there is an essential anisotropy of the pressure tensor $p_{\alpha\beta}(z)$, z being the coordinate in the direction perpendicular to the planar walls. While the 'normal pressure' $p_{\mathrm{N}} = p_{zz}$ is homogeneous in the system, the components $p_{xx}(z)$, $p_{yy}(z)$ have a non-trivial z-dependence. The average tangential pressure p_{T}, defined as

$$p_{\mathrm{T}} = \frac{1}{2D} \int_0^D (p_{xx}(z) + p_{yy}(z)) dz, \tag{6.14}$$

is of particular interest, because it is related to the surface tension of the fluid γ_{wf} against the walls via

$$\gamma_{\mathrm{wf}} = D(p_{\mathrm{N}} - p_{\mathrm{T}}), \quad D \to \infty. \tag{6.15}$$

In this case the approach outlined above is slightly generalized by considering virtual volume changes (of the system of volume $V = L \times L \times D$, with periodic boundary conditions only in the x and y directions, but hard walls at $z = 0$ and $z = D$). D and L vary independently,

$$D \to D' = D(1 - \zeta), \quad L \to L'(1 - \eta), \tag{6.16}$$

and, in practice, ζ and η often need to be extremely small ($\sim 10^{-4}$). Computing again the non-overlap probabilities $P_{\text{nov}}(\zeta) \approx 1 - b_{\text{N}}\zeta$, $P_{\text{nov}}(\eta) \approx 1 - b_{\text{T}}\eta$, we find

$$p_{N,\text{hc}}/(\rho k_{\text{B}}T) = 1 + b_{\text{N}}/N, \quad p_{T,\text{hc}}/(\rho k_{\text{B}}T) = 1 + b_{\text{T}}/N. \tag{6.17}$$

While simulations of hard sphere fluids (Deb *et al.*, 2012) show that the method works in principle, high accuracy is difficult to reach: the limit $D \to \infty$ in Eqn. (6.15) means that D must be chosen large enough so that the two walls are basically non-interacting. In practice, that means that D should be of the order of 20 hard sphere diameters. Noting, then, that for hard spheres near the crystallization transition $p_{\text{hc}}/k_{\text{B}}T$ is of the order of 10 (where the hard sphere diameter is the unit of length), while $\gamma_{\text{wf}}/k_{\text{B}}T$ is of order 1, it is clear that an extremely good accuracy in the sampling of b_{N} and b_{T} is required, if γ_{wf} is computed using Eqns. (6.15) and 6.17), since p_{N} and p_{T} differ only by the order of 1%. So, in many cases alternative approaches, based on thermodynamic integration methods or generalized ensemble techniques, are more efficient (see Section 6.8 for a description of these techniques and application examples).

Problem 6.2 Write a program that approximates $g(r)$ via a histogram, binning together particles that fall within a distance interval $[r, r + \Delta r]$ from each other.

Problem 6.3 Generalize Eqns. (6.10)–(6.11) to dimensions $d = 2$ and $d = 4$.

6.1.2 *NpT* ensemble

The isobaric-isothermal ensemble is very often used in Monte Carlo simulations of fluids and solids, in particular when one wishes to address problems such as the fluid–solid transition or transitions among different solid phases. At such first order transitions, first derivatives (such as internal energy U, volume V) of the appropriate thermodynamic potential exhibit a jump (e.g. ΔU, ΔV). Using such an extensive variable (like the volume V) as a control parameter of a simulation, however, causes particular problems if the chosen value of V falls in the 'forbidden region' of this jump. It means that in thermal equilibrium the system should separate into two coexisting phases (e.g. if we cool down a box containing water molecules from high temperature to room temperature at any intermediate density N/V between that of water vapor and that of water at room temperature). This separation can be

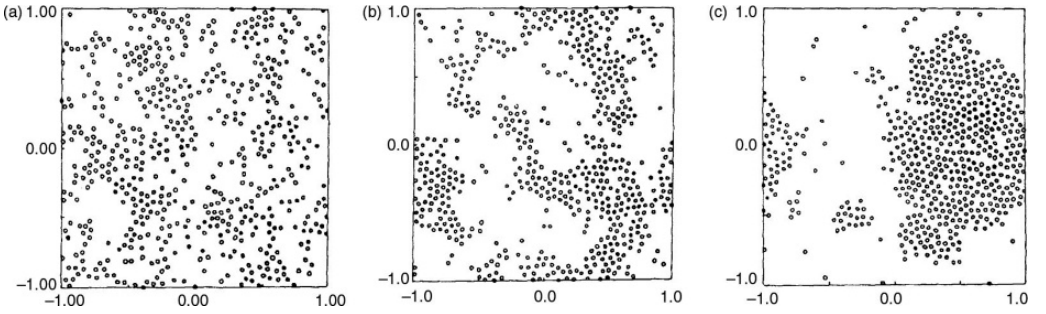

Fig. 6.1 Snapshots of 576 particles at a density $\rho^* = 0.3$ for $T^* =$ (a) 0.7, (b) 0.5, and (c) 0.45. Here ρ^*, T^* are density and temperature in reduced units, i.e. the Lennard–Jones parameters σ and ε/k_B are used as units of length and temperature, respectively. From Rovere *et al.* (1990).

observed in the framework of NVT simulations in simple cases, e.g. for a two-dimensional Lennard–Jones fluid this is seen in the snapshots (Rovere *et al.*, 1990) in Fig. 6.1, but reaching equilibrium in such a computer simulation of phase separation is rather cumbersome. Also, averaging any observables in such a two-phase coexistence regime is a tricky business – obviously in Fig. 6.1 it would be hard to disentangle which features are due to the gas phase, which are due to the liquid phase, and which are attributed to the interface. (By the way, interfaces are slowly fluctuating objects and are hard to characterize quantitatively, see Section 4.2.3.6.) Sometimes phase separation is even missed, either because the system is too small, or because of hysteresis. As a result, for a study of phase transitions in off-lattice systems it is often preferable to use the NpT ensemble (or the grand canonical μVT ensemble where the chemical potential μ rather than the pressure p is used as a second intensive thermodynamic variable to characterize the static system). For systems with continuous potentials the first use of the NpT ensemble dates back to 1972 (McDonald, 1972). We follow Frenkel and Smit (1996) in deriving it from statistical mechanics. To begin with we consider the partition function $Z(N, V, T)$ in the canonical (NVT) ensemble for a box $V = L^3$ in three dimensions,

$$Z(N, V, T) = \frac{1}{\Lambda^{3N} N!} \int_0^L \cdots \int_0^L d\mathbf{r}_1 \ldots d\mathbf{r}_N \exp[-U(\mathbf{r}_1, \ldots, \mathbf{r}_N)/k_B T], \tag{6.18}$$

where the prefactors ensure the proper normalization of entropy via the quasi-classical limit of quantum mechanics (Λ is the thermal de Broglie wavelength of the atoms and the factor $1/N!$ accounts for the indistinguishability of the particles).

In the NpT ensemble the volume V, and hence the linear dimension L, is not fixed but is a fluctuating quantity. It is convenient to define scaled coordinates $\mathbf{s}_i$ by

$$\mathbf{r}_i = L\mathbf{s}_i, \qquad \text{for } i = 1, 2, \ldots, N, \tag{6.19}$$

and treat the $\{\mathbf{s}_i\}$ and the linear dimension L as separate variables $\{\mathbf{s}_i, L\}$. The (Helmholtz) free energy $F(N, V, T)$ thus is written as

$$\begin{aligned} F(N, V, T) &= -k_B T \ln Z(N, V, T) \\ &= -k_B T \ln \left\{ \frac{[V/\Lambda^3]^N}{N!} \right\} \\ &\quad - k_B T \ln \int_0^1 \cdots \int_0^1 d\mathbf{s}_N \exp\left[-\frac{U(\mathbf{s}_1, \ldots, \mathbf{s}_N, L)}{k_B T} \right] \\ &= F_{ig}(N, V, T) + \Delta F(N, V, T), \end{aligned} \tag{6.20}$$

where the first term has been identified as the well-known expression for the free energy of the ideal gas, $F_{ig}(N, V, T)$; and $\Delta F(N, V, T)$ is the non-trivial part involving all the interactions among the particles. Of course, U depends originally on the actual coordinates $\mathbf{r}_1, \ldots, \mathbf{r}_N$, and when we write U in terms of the $\{\mathbf{s}_i\}$ we must allow for L as an additional variable.

Now we consider the situation in which the system under consideration is actually a subsystem of a much larger ideal gas system of volume V_0, with $V_0 \gg V$, which acts as a heat bath (exchange of energy but not of particles is possible), and from which it is separated by a piston which is free to move. Denoting the total number of atoms as M, we find that there are hence $(M - N) \gg N$ atoms in the reservoir. The partition function of the total system is simply the product of the partition functions of these two subsystems,

$$\begin{aligned} &Z(N, M - N, V, V_0 - V, T) \\ &= \frac{V^N (V_0 - V)^{M-N}}{N!\,(M - N)!} \Lambda^{-3M} \int_0^1 \cdots \int_0^1 d\mathbf{s}'_1 \ldots d\mathbf{s}'_{M-N} \int_0^1 \cdots \int_0^1 d\mathbf{s}_1 \ldots d\mathbf{s}_N \\ &\quad \times \exp\left[-\frac{U(\mathbf{s}_1, \ldots, \mathbf{s}_N, L)}{k_B T} \right]. \end{aligned} \tag{6.21}$$

Note that the integral over the $3(M - N)$ scaled coordinates $\mathbf{s}'_1, \ldots, \mathbf{s}'_{M-N}$ of the ideal gas particles simply yields unity. The probability density $P(V)$ that the N-particle subsystem has the volume V then is

$$\begin{aligned} &P(V) \\ &= \frac{V^N (V_0 - V)^{M-N} \int_0^1 \cdots \int_0^1 d\mathbf{s}_1 \cdots d\mathbf{s}_N \exp[-U(\mathbf{s}_1, \ldots, \mathbf{s}_N, L)/k_B T]}{\int_0^{V_0} dV' V'^N (V_0 - V')^{M-N} \int_0^1 \cdots \int_0^1 d\mathbf{s}_1 \cdots d\mathbf{s}_N \exp[-U(\mathbf{s}_1, \ldots, \mathbf{s}_N, L')/k_B T]}. \end{aligned} \tag{6.22}$$

Let us now exploit the fact that we consider the limit $V_0 \to \infty, M \to \infty$ but with $(M - N)/V_0 = \rho$ held fixed. In that limit, a minor volume change of the small system does not alter the pressure p of the large system. In order to introduce

the pressure p in Eqns. (6.21) and (6.22), in the limit $V/V_0 \to 0$ we can write

$$\begin{aligned}(V_0 - V)^{M-N} &= V_0^{M-N}[1 - (V/V_0)]^{M-N} \\ &\approx V_0^{M-N} \exp[-(M-N)\,V/V_0] = V_0^{M-N} \exp[-\rho V]\end{aligned} \tag{6.23}$$

and simply use the ideal gas law $\rho = p/k_B T$ to replace the exponential factor in Eqn. (6.23) by $\exp(-pV/k_B T)$. Integrating the partition function over the volume V and splitting off the partition function of the reservoir, ${V_0}^{M-N}/[(M-N)!\Lambda^3(M-N)]$, we obtain the partition function $Y(N, p, T)$ in the NpT ensemble

$$\begin{aligned}Y(N, p, T) \equiv \frac{p/k_B T}{\Lambda^{3N} N!} \int dV\, V^N \exp(-pV/k_B T) \int_0^1 \cdots \int_0^1 d\mathbf{s}_1 \cdots d\mathbf{s}_N \\ \times \exp[-U(\mathbf{s}_1, \ldots, \mathbf{s}_N, L)/k_B T].\end{aligned} \tag{6.24}$$

The probability density $P(V)$ then becomes

$$\begin{aligned}&P(V) \\ &= \frac{V^N \exp(-pV/k_B T) \int_0^1 \cdots \int_0^1 d\mathbf{s}_1 \cdots d\mathbf{s}_N \exp[-U(\mathbf{s}_1, \ldots, \mathbf{s}_N, L)/k_B T]}{\int_0^{V_0} dV' V'^N \exp(-pV'/k_B T) \int_0^1 \cdots \int_0^1 d\mathbf{s}_1 \cdots d\mathbf{s}_N \exp[-U(\mathbf{s}_1, \ldots, \mathbf{s}_N, L)/k_B T]}.\end{aligned} \tag{6.25}$$

The partition function $Y(N, p, T)$ yields the Gibbs free energy as usual, $G(N, p, T) = -k_B T \ln Y(N, p, T)$. Equation (6.25) is now the starting point for the NpT Monte Carlo method. We note that the probability density of finding the subsystem in a specific configuration of the N atoms (as specified by $\mathbf{s}_1, \ldots, \mathbf{s}_N$) and a volume V is

$$\begin{aligned}P(\mathbf{s}_1, \ldots \mathbf{s}_N, V) &\propto V^N \exp(-pV/k_B T) \exp[-U(\mathbf{s}_1, \ldots \mathbf{s}_N, L)/k_B T] \\ &= \exp\{-[U(\mathbf{s}_1, \ldots \mathbf{s}_N, L) + pV - Nk_B T \ln V]/k_B T\}.\end{aligned} \tag{6.26}$$

Equation (6.26) looks like the Boltzmann factor for traditional Monte Carlo sampling if the square bracket is interpreted as a generalized 'Hamiltonian', involving an extra variable, $V = L^3$. Thus, trial moves which change V have to be carried out, and these must satisfy the same rules as trial moves in the particle positions $\{\mathbf{s}_i\}$. For example, consider attempted changes from V to $V' = V + \Delta V$, where ΔV is a random number uniformly distributed in the interval $[-\Delta V_{\max}, +\Delta V_{\max}]$ so that $V' = L'^3$. In the Metropolis scheme, the

acceptance probability of such a volume changing move is hence

$$W(V \to V') = \min\left\{1, \exp\left(-\frac{1}{k_B T}[U(\mathbf{s}_1, \ldots, \mathbf{s}_N; L') - U(\mathbf{s}_1, \ldots, \mathbf{s}_N; L) + p(V' - V) - k_B T N \ln(V'/V)]\right)\right\}. \quad (6.27)$$

The frequency with which 'volume moves' should be tried in place of the standard particle displacements $\mathbf{r}_i \to \mathbf{r}_i'$ depends on the efficiency with which phase space is then sampled by the algorithm. In general, a volume trial move could mean that all interatomic interactions are recomputed, which would need a CPU time comparable to N trial moves on the atomic positions. Fortunately, for potentials which can be written as a sum over terms U_n that are simple inverse powers of interatomic distances there is a scaling property that makes the volume changing trial move much 'cheaper'. We can see this by writing

$$U_n = \sum_{i<j} \varepsilon(\sigma/|\mathbf{r}_i - \mathbf{r}_j|)^n = L^{-n} \sum_{i<j} \varepsilon(\sigma/|\mathbf{s}_i - \mathbf{s}_j|)^n, \quad (6.28)$$

from which we can infer that $U_n(L') = (L/L')^n U_n(L)$. Note, however, that Eqn. (6.28) is only true for an *untruncated* potential (cf. Section 6.2).

In order to check the equilibration of the system (and the validity of the implementation of the algorithm) it is also advisable to calculate the pressure p from the virial theorem (see Eqns. (6.9) and (6.10)) in such an NpT ensemble, since one can prove that the virial pressure and the externally applied pressure (that appears in the probability, Eqn. (6.27)) must agree. Finally, we mention that in solids (which are intrinsically anisotropic) a generalization of this algorithm applies where one does not consider isotropic volume changes but anisotropic ones. For an orthorhombic crystal it is thus necessary to have a box with three different linear dimensions L_x, L_y, L_z, and in the NpT ensemble these three linear dimensions may change separately. We shall return to an example for this case in Section 6.6.

6.1.3 Grand canonical ensemble

The grand canonical ensemble μVT uses the volume V and the chemical potential μ as independent thermodynamic variables along with the temperature T. While in the NpT ensemble the particle number N was fixed and the volume could fluctuate, here it is exactly the other way around. Of course, in the thermodynamic limit ($N \to \infty$ or $V \to \infty$, respectively) fluctuations are negligible, and the different ensembles of statistical mechanics yield equivalent results. However, in computer simulations one often wishes to choose N and/or V as small as possible, in order to save CPU time. Then the optimal choice of statistical ensembles is a non-trivial question, the answer to which depends both on the type of physical system being studied and the type of properties to be calculated. As an example, consider the study of adsorption of small gas molecules in the pores of a zeolite crystal (see e.g. Catlow, 1992; Smit, 1995). Then the adsorbate in an experiment is in fact in contact with a

gas reservoir with which it can exchange particles, and this is exactly the type of equilibrium described by the μVT ensemble. Choosing this ensemble to simulate an 'adsorption isotherm' (describing the amount of adsorbed gas as a function of the gas pressure in the reservoir) has the advantage that the simulation closely parallels the experiment. It may also be advantageous to choose the μVT ensemble for other cases, e.g. for a study of the liquid/gas transition and critical point of a bulk fluid (Wilding, 1997). Experimental studies of this problem typically are done in the NVT or NpT ensembles, respectively. Simulations of fluid criticality have been attempted as well, both in the NVT ensemble (Rovere *et al.*, 1990) and the NpT ensemble (Wilding and Binder, 1996), but these approaches are clearly less efficient than the simulations in the μVT ensemble (Wilding, 1997).

The grand canonical partition function is written

$$Y(\mu, V, T) = \sum_{N=0}^{\infty} \frac{1}{N!} \left(V/\Lambda^3\right)^N \exp\left(\mu N/k_{\mathrm{B}}T\right) \int d\mathbf{s}_1, \ldots, \int d\mathbf{s}_N \times \exp[-U(\mathbf{s}_1, \ldots, \mathbf{s}_N)/k_{\mathrm{B}}T], \tag{6.29}$$

where the $\mathbf{s}_i$ are the scaled coordinates of the particles, Eqn. (6.19). Note that we again consider only a cubic box in $d = 3$ dimensions here, $V = L^3$. Then the corresponding probability density is

$$\mathcal{N}_{\mu VT}(\mathbf{s}_1, \ldots, \mathbf{s}_N, N) \propto \frac{1}{N!} \left(\frac{V}{\Lambda^3}\right)^N \exp\{-[U(\mathbf{s}_1, \ldots, \mathbf{s}_N) - \mu N]/k_{\mathrm{B}}T\}. \tag{6.30}$$

This probability density can be sampled by a Metropolis Monte Carlo method (see Chapter 4). In addition to trial moves that displace particles (the acceptance probability for such moves is still given by Eqn. (6.8)) trial moves for the insertion or removal of particles from the reservoir are also introduced. The insertion of a particle at a randomly selected position $\mathbf{s}_{N+1}$ is accepted with the probability (Norman and Filinov, 1969)

$$W(N \to N+1) = \min\left\{1, \frac{V}{\Lambda^3(N+1)} \exp\{-[U(\mathbf{s}_1, \ldots, \mathbf{s}_{N+1}) - U(\mathbf{s}_1, \ldots, \mathbf{s}_N) - \mu]/k_{\mathrm{B}}T\}\right\}, \tag{6.31}$$

while the removal of a randomly chosen particle is accepted with the probability

$$W(N \to N-1) = \min\left\{1, \frac{\Lambda^3 N}{V} \exp\{-[U(\mathbf{s}_1, \ldots, \mathbf{s}_N) - U(\mathbf{s}_1, \ldots, \mathbf{s}_{N-1}) + \mu]/k_{\mathrm{B}}T\}\right\}. \tag{6.32}$$

Since the particles are indistinguishable, their labeling is arbitrary, and hence in Eqn. (6.32) we have given the particle that was removed the index N. Obviously, two successive (successful) events in which a particle is removed at a site $\mathbf{s}_N$ and inserted at a site $\mathbf{s}'_N$ have the same effect as a (random) move from $\mathbf{s}_N$ to $\mathbf{s}'_N$ according to Eqn. (6.8). Therefore, these displacement moves are not actually necessary, and one can set up a simulation program that includes random insertions and removals exclusively. For densities which are not too large (but including the critical density of a fluid (Wilding, 1997)), such an algorithm is in effect very efficient, much more so than the simple random displacement algorithm of Eqn. (6.8). This is true because the effective displacements generated are of the order of the linear dimension of the box, while the displacements generated by the algorithm of Eqn. (6.8) are of the order δ, a length typically chosen of the same order as the range σ of the interparticle potential. On the other hand, the efficiency of this straightforward implementation of the grand canonical Monte Carlo algorithm deteriorates very quickly when the density increases – for dense fluids near their fluid–solid transition successful attempts of a particle insertion are extremely rare, and thus the method becomes impractical, at least in this straightforward form.

A particular advantage of grand canonical simulations of gas–fluid criticality is that the analysis in terms of finite size scaling is most natural in this ensemble (Wilding, 1997; see also Section 4.3.5). As has already been discussed in Section 4.3.5, for an accurate analysis of this situation one needs to properly disentangle density fluctuations and energy density fluctuations in terms of the appropriate 'scaling fields'. In this way, critical phenomena in fluids can be studied with an accuracy which is nearly competitive to that in corresponding studies of lattice systems (Chapter 4).

Extensions to binary (A, B) or multicomponent mixtures can also be straightforwardly considered. For the grand canonical simulation of a binary mixture, two chemical potentials μ_A, μ_B are needed, of course, and the term μN in Eqn. (6.30) is generalized to $\mu_A N_A + \mu_B N_B$. Then the moves in Eqns. (6.31) and (6.32) must distinguish between the insertion or removal of an A particle or a B particle. An important extension of the fully grand canonical simulation of mixtures is the so-called *semi-grand canonical simulation* technique, where the total particle number $N_{tot} = N_A + N_B$ is held fixed and only the chemical potential difference $\Delta\mu = \mu_A - \mu_B$ is an independent variable, since then $\mu_A N_A + \mu_B N_B = \Delta\mu N_A + \mu_B N_{tot}$ and the second term $\mu_B N_{tot}$ then cancels out from the transition probability. Thus, the moves consist of the removal of a B particle and insertion of an A particle at the same position, or vice versa. Alternatively, one can consider this move as an 'identity switch': an A particle transforms into B or a B into A. The obvious advantage of this algorithm is that it still can be efficient for very dense systems, where the standard grand canonical algorithm is bound to fail. Thus the semi-grand canonical method can be generalized from simple monatomic mixtures to such complex systems as symmetrical mixtures of flexible polymers (Sariban and Binder, 1987). An entire polymer chain then undergoes such an

'identity switch', keeping its configuration constant. In addition, other moves are needed to sample the possible configurations, and these will be described in Section 6.6 below. However, the extension of the semi-grand canonical ensemble to formulate efficient Monte Carlo algorithms of asymmetric mixtures poses particular challenges. For mixtures of flexible polymers, such an asymmetry is very common due to the differing chain lengths of the constituents, $N_a = N_b$. We shall return to this problem in Section 6.6.2. Another very popular model is a mixture of hard spheres with very different sizes. A variant uses mixtures of hard and soft spheres, e.g. the famous Asakura–Oosawa (AO) model of colloid-polymer mixtures (Asakura and Oosawa, 1954). Here the colloidal particles are represented by impenetrable spheres of radius R_c, and polymers are represented as spheres of radius R_p, such that the potential between a colloidal particle and a polymer is infinite if their distance is less than $R_c + R_p$. Two polymers can overlap with no energy cost, however. (As will be discussed further in Section 6.6, flexible polymers have random walk-like configurations which can easily penetrate each other.) Although this model is only a crude representation of reality, it is nevertheless widely used. Typically the colloids are much larger than the polymers, $R_c \gg R_p$.

Now the general problem in the simulation of asymmetric binary mixtures is that an attempt to insert a large particle inevitably results in an overlap with several small particles, and hence such a trial move will be rejected. Vink and Horbach (2004) solved this problem by inventing a collective move in which a random number n_r of small particles (with $0 \le n_r < m$, where m is an integer that will be specified later) is removed when one tries to insert a large particle (or vice versa). The first step of the move consists of randomly selecting a point in the mixture at which one wants to insert the large particle and drawing a sphere of radius δ around it. (δ must be sufficiently large, e.g. $\delta = R_c + R_p$ is a useful choice). There will be $n_p (= 0, 1, 2, \ldots)$ small particles inside the sphere. If $n_r > n_p$, the move is rejected, but if $n_r \le n_p$, n_r small particles are randomly selected and removed and then the insertion of the large particle is attempted. The new configuration is accepted with probability

$$A_+ = \min\left[1, \frac{z_c V}{N_c + 1} \frac{(n_p)!}{(n_p - n_r)!} \frac{\exp(-\Delta E / k_B T)}{(z_p V_\delta)^{n_r}}\right],$$

where V is the volume of the box and V_δ the volume of the sphere, $V_\delta = 4\pi\delta^3/3$, and $\{z_c, z_p\}$ are the fugacities of all the large and small particles, respectively ($z = \exp(\mu / k_B T)$, where μ is the appropriate chemical potential). Here we have allowed for a potential energy difference ΔE between the initial and the final configuration, since the algorithm is by no means restricted to hard-core systems. Finally, N_c is the number of colloids. The reverse move is constructed such that detailed balance holds. First a large particle is selected at random, and a sphere with radius δ is drawn around the center of this particle. Next, a uniform random integer n_r is chosen from the interval $0 \le n_r < m$, followed by the selection of n_r random sites from inside the sphere. The large

particle then is removed, and n_r small particles are placed on the selected site before the new configuration is accepted with probability

$$A_- = \min\left[1, \frac{N_c}{z_c V}\frac{(n_p)!(Z_p V_\delta)^{n_r}}{(n_p + n_r)!}\exp(-\Delta \mathrm{E}/k_\mathrm{B}T)\right].$$

The algorithm is ergodic and satisfies detailed balance. The integer m must be chosen large enough to allow for the formation of voids, e.g. $m = Z_p V_\delta$ is a reasonable choice if $R_c = 1$ is the unit of length.

When this algorithm is combined with successive umbrella samplings (Virnau and Müller, 2004) and finite size scaling analyses, both the phase diagram and the interfacial tension of this AO model could be accurately estimated (Vink and Horbach, 2004). This work is a good example showing that the great strength of Monte Carlo methods is the possibility of suitably adapting an algorithm to the problem of interest.

Problem 6.4 Demonstrate that the algorithm defined by Eqns. (6.31) and (6.32) satisfies the detailed balance principle with the semi-grand canonical probability distribution, Eqn. (6.30).

Problem 6.5 Write down the transition probabilities and the grand canonical probability distribution for a Monte Carlo algorithm that samples the lattice gas model, Eqn. (2.60), at a given volume of the lattice $V = L^3$, temperature T and chemical potential μ. Discuss the differences between the result and Eqns. (6.30)–(6.32).

6.1.4 Near critical coexistence: a case study

The study of phase transitions in systems without a clear symmetry, which is the situation for many systems in the continuum, is a challenging problem. A good example of such a case is the examination of asymmetric fluid criticality. One particular complication is the possible presence of a Yang–Yang singularity, i.e. the second derivative of the chemical potential $\mu_\sigma(T)$ diverges as the critical point is approached from below. Kim *et al.* (2003) used grand canonical Monte Carlo, together with a finite size analysis to identify and include pressure mixing effects, for the hard-core square-well (HCSW) fluid and for the restricted primitive model (RPM) electrolyte. In Fig. 6.2 we show their results for the density discontinuity as the critical point is approached. This figure demonstrates that very high resolution can now be achieved quite close to the critical point for non-trivial, off-lattice models. The precision of these simulations is, in fact, quite competitive with experimental resolution for real materials. Below T_c the grand canonical description of phase coexistence of the density distribution function is approximated by two Gaussians centered at $\rho^{\pm}(T)$, and the separation of the peaks is a measure of the discontinuity at the transition. As the critical point is approached, however, finite size rounding begins to smear out the discontinuity at the transition and a finite size scaling study of properties such as the fourth order cumulant becomes essential to extracting information about the transition. Kim *et al.* (2003) defined three

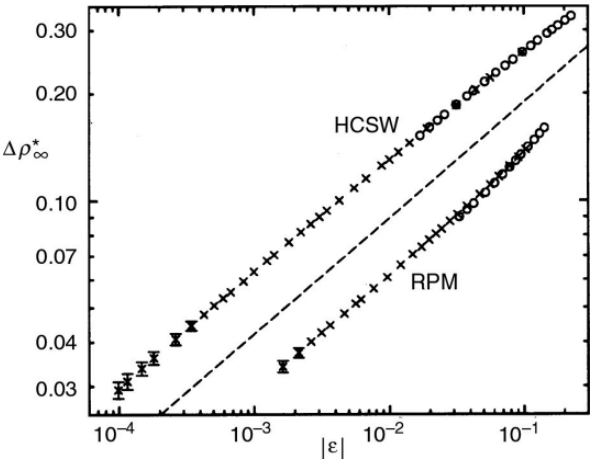

Fig. 6.2 Grand canonical Monte Carlo results for the semi-density jump $\rho^* = (\rho^+ - \rho^-)/2$ vs. $\varepsilon = |T - T_c|/T_c$ for a HCSW fluid with interaction range $1.5a$ (where a is the hard-sphere diameter and $\rho_c^* \sim 0.3067$) and for the RPM with $\rho_c^* \sim 0.079$. The dashed line has the Ising slope $\beta = 0.32$. After Kim *et al.* (2003).

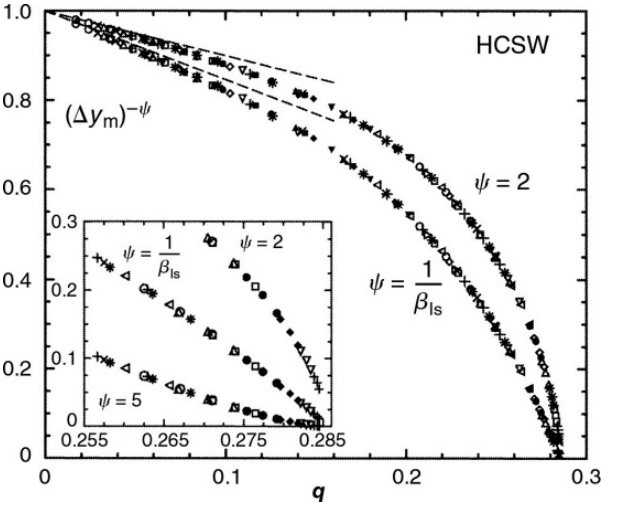

Fig. 6.3 Scaling plots for the HCSW fluid. Note that Δy_m and q are related to the difference in the scaling variable for the mean density and the fourth order cumulant, respectively. After Kim *et al.* (2003).

scaling fields:

$$\begin{aligned} \tilde{p} &= \breve{p} - k_0\varepsilon - l_0\breve{\mu} + \cdots, \\ \tilde{\varepsilon} &= \varepsilon - l_1\breve{\mu} - j_1\breve{p} + \cdots, \\ \tilde{h} &= \mu - k_1\varepsilon - j_2\breve{p}, \end{aligned} \tag{6.33}$$

where $\varepsilon = |1 - T/T_c|$, $\breve{p} = (p - p_c)/p_c k_B T$, and $\breve{\mu} = (\mu - \mu_c)/k_B T$. Finite size scaling then implies that

$$\rho_c \tilde{p} = L^{-d}\, Y(x, z)\,, \tag{6.34}$$

where $x = D\tilde{\varepsilon} L^{1/\nu}$ and $z = U\tilde{h}\,|\tilde{\varepsilon}|^{-\Delta}$ and $Y(x, z)$ is a universal scaling function, D and U are non-universal amplitudes. Looking at the mean value of the minimum of the fourth order cumulant and the difference in the scaling of the mean density, one can make scaling plots (see Fig. 6.3) to determine how the system behaves as the critical point is approached.

The resultant scaling behavior is excellent and allows a quite accurate determination of the location of the critical point and a description of the coexistence curves quite close to this point. It is particularly gratifying that this work is co-authored by one of the pioneers in the development of the theory of phase transitions (MEF) who has been very skeptical about Monte Carlo simulations for many years. Now, however, he helps guide the analysis of these careful simulations with the proper theoretical background – such close interactions between theory and simulation (as shown schematically in Fig. 1.1) provide a good example of how significant progress can be achieved.

6.1.5 Subsystems: a case study

In dense off-lattice systems particle insertions often are very hard to perform, and simulations in the grand canonical ensemble are impractical. Nevertheless, equivalent information often is easily deduced from a study of subsystems of a larger system that is simulated in the standard canonical NVT ensemble (Rovere *et al.*, 1990; Weber *et al.*, 1995). A study of subsystems is attractive because from a single simulation one can obtain information about both finite size behavior and response functions that is not accessible otherwise. In order to explain how this is done, we best proceed by way of an example, and for this purpose we choose the solid–liquid transition of hard disks in $d = 2$ dimensions. Actually this model system has been under study since the very first application of the importance sampling Monte Carlo method (Metropolis *et al.*, 1953), and many classic papers have appeared since then (e.g. Alder and Wainwright, 1962; Zollweg and Chester, 1992).

The total system of size $S \times S$ is divided into $L \times L$ subsystems of linear dimension $L = S/M_b$ with $M_b = 1, 2, 3, 4, \ldots$ up to a value at which the subsystem size becomes too small for a meaningful analysis. The boundaries of these subsystems have no physical effect whatsoever; they only serve to allow a counting of which particle belongs to which subsystems, so information on subsystem properties for all subsystem sizes is deduced simultaneously from the same simulation run. (Actually, one can also choose non-integer M_b to allow a continuous variation of L, choose subsystems of spherical rather than quadratic shape, if desired, etc.) Such subsystem properties are, first of all, the density ρ, and in the present example another quantity of interest is the bond orientational order parameter ψ defined as

$$\psi = \left| \sum_i \sum_j \exp(6i\phi_{ij}) \right| / N_{\text{bond}}, \tag{6.35}$$

where the sum over i runs over all particles in the subsystem and the sum over j runs over all neighbors of i (defined by the criterion that the distance is less than 1.3 times the close packing distance). ϕ_{ij} is the angle between the 'bond' connecting neighbors i and j and an arbitrary but fixed reference axis, and N_{bond} is the number of bonds included in the sums in Eqn. (6.35).

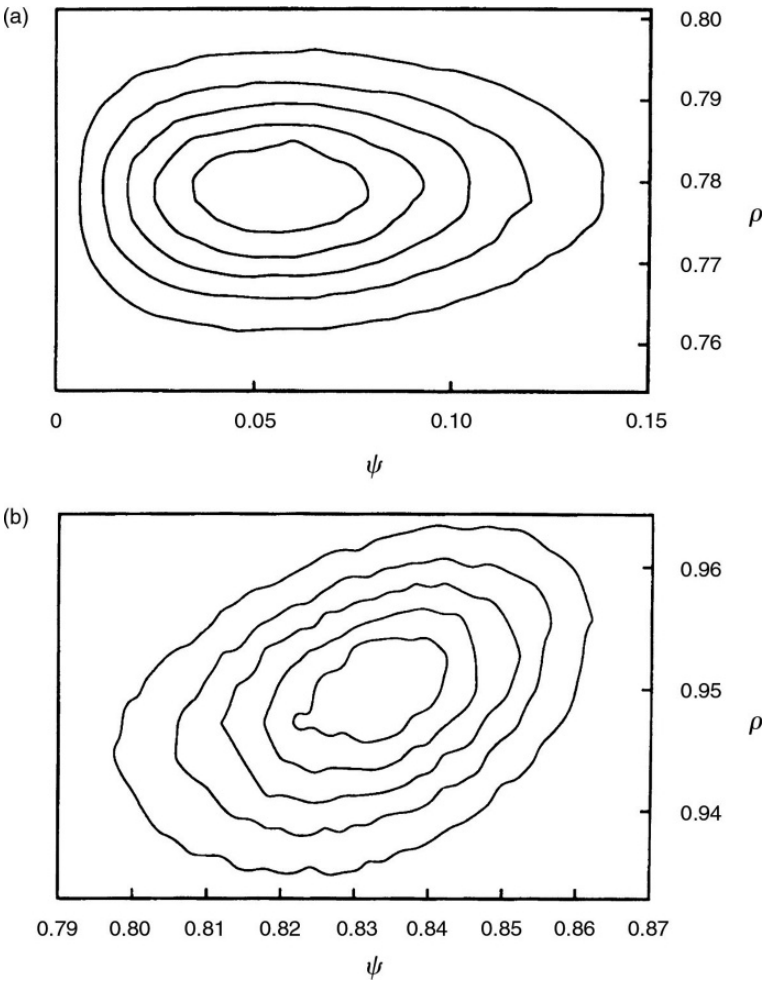

Fig. 6.4 Contour plot of the joint probability distribution $P(\psi, \rho)$ of the bond-orientational order parameter ψ and the subsystem density ρ for subsystems with $M_b = 6$, at a system density (in units of the close packing density) of (a) $\rho = 0.78$ (fluid phase) and (b) $\rho = 0.95$ (solid phase). The total number of particles is $N = 2916$, and averages were taken over 600 000 MCS/particle. From the outermost to the innermost contour the probability increases as $i\Delta p$, $i = 1, 2, 3, 4, 5$, with (a) $\Delta p = 0.000\,965$ and (b) $\Delta p = 0.000\,216$. Note that in the disordered phase the peak of $P(\psi, \rho)$ occurs at a non-zero value of ψ, because ψ is the absolute value of a two-component order parameter. From Weber *et al.* (1995).

A study of the probability distribution $P_L(\phi, \rho)$ is illuminating (see Fig. 6.4) as it allows the estimation of various response functions. While we expect that ρ and ψ fluctuate independently of each other in the disordered phase, this is not so in the ordered phase where an increase of ρ also enhances ψ, and a cross-correlation $\langle \Delta\psi \Delta\rho \rangle$ is thus non-vanishing. For linear dimensions L much larger than the (largest) correlation length ξ we can assume a Gaussian probability distribution (Landau and Lifshitz, 1980; Weber *et al.*, 1995)

$$P_L(\psi, \rho) \propto \exp\left\{ -\frac{L^d}{2} \left[\frac{(\Delta\psi)^2}{\chi_{L,\rho}} - \frac{\Delta\psi\,\Delta\rho}{\gamma_L} + \frac{(\Delta\rho)^2}{\kappa_{L,\psi}} \right] \right\}, \qquad (6.36)$$

with the fluctuations $\Delta\psi \equiv \psi - \langle\psi\rangle_L$ and $\Delta\rho \equiv \rho - \langle\rho\rangle_L$. The bond orientational 'susceptibility' measured in a system of linear dimension L at constant density ρ is denoted by $\chi_{L,\rho}$, and γ_L^{-1} is the coupling parameter measured on the same length scale L, while $\kappa_{L,\psi}$ denotes the compressibility measured on

length scale L at a constant value $\langle\psi\rangle$ of the order parameter. Note that factors $1/k_{\mathrm{B}}T$ have been absorbed in these definitions throughout.

From Eqn. (6.36) we can derive an expression for the differences between the 'susceptibilities' at constant density $\chi_{L,\rho}$ and constant chemical potential $\chi_{L,\mu}$. Note that a subsystem with $L \ll S$ can freely exchange particles with a much larger 'reservoir' (remember that the walls of the subsystems are only virtual boundaries, of course), and hence is at constant chemical potential even if the total system is held at constant density ρ. Thus (for $L \to \infty$ the index L can be omitted)

$$\chi_\mu - \chi_\rho = L^d \langle \Delta\psi \Delta\rho \rangle^2 / \langle (\Delta\rho)^2 \rangle. \tag{6.37}$$

In fact, a distinction between χ_μ and χ_ρ is expected only in the ordered phase, since

$$\langle \Delta\psi \Delta\rho \rangle_L = (\partial \langle\psi\rangle_L / \partial\mu)(L^d / k_{\mathrm{B}}T), \tag{6.38}$$

and $\langle\psi\rangle_{L\to\infty} \equiv 0$ in the disordered phase. As expected, the distribution in Fig. 6.4 has contours with the long axis parallel to the abscissa (no $\psi-\rho$ coupling) in the disordered phase, while in the ordered phase the long axis forms a non-trivial angle with the abscissa, due to the presence of a coupling term in Eqn. (6.36). From Fig. 6.4 both χ_μ, $\langle \Delta\psi \Delta\rho \rangle$, and $\langle (\Delta\rho)^2 \rangle$ can be measured, and one finds susceptibilities χ_μ, χ_ρ in both ensembles (from Eqn. (6.37)) and the isothermal compressibility

$$\kappa = L^d \rho^{-2} \langle (\Delta\rho)^2 \rangle_L \tag{6.39}$$

from a *single* simulation run!

However, it is important to realize that the subsystem fluctuations 'cut off' correlations across the subsystem boundaries, and hence one has to carry out an extrapolation according to (Rovere *et al.*, 1990; Weber *et al.*, 1995)

$$\chi_{L,\mu} = \chi_\mu (1 - \text{ const. } \xi / L), \qquad L \gg \xi, \tag{6.40}$$

where the constant is of order unity. Actually, both the compressibility n (Fig. 6.5) and the susceptibility χ_μ (Fig. 6.6a) have to be found by an extrapolation of the form given by Eqn. (6.40), see Fig. 6.6b, and hence are denoted as κ_∞, χ_∞, in these figures. Figure 6.6b shows that the extrapolation suggested by Eqn. (6.40) does indeed work, but one must discard data for small L^{-1} which bend systematically down to smaller values. This effect is due to crossover from the grand canonical ensemble (small subboxes, $M_b \gg 1$) to the canonical ensemble (realized by $M_b = 1$, of course). Indeed, Eqn. (6.37) shows that $\chi_\mu > \chi_\rho$ in the ordered phase.

The major reason for the great interest in the solid–liquid transition of hard disks is a longstanding controversy about whether the Nelson-Halperin (1979) theory works for this model. According to this theory, melting in two dimensions is not a conventional first order transition (as it is in the three-dimensional case) but rather occurs via a sequence of two continuous

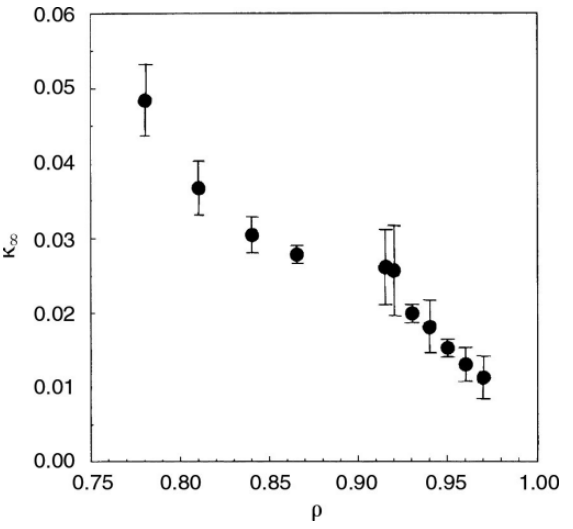

Fig. 6.5 Compressibility κ_∞ of the hard disk model as a function of density ρ, obtained by extrapolation from circular and rectangular subsystems in the solid and fluid phases, respectively. Total number of particles is $N = 576$. From Weber *et al*. (1995).

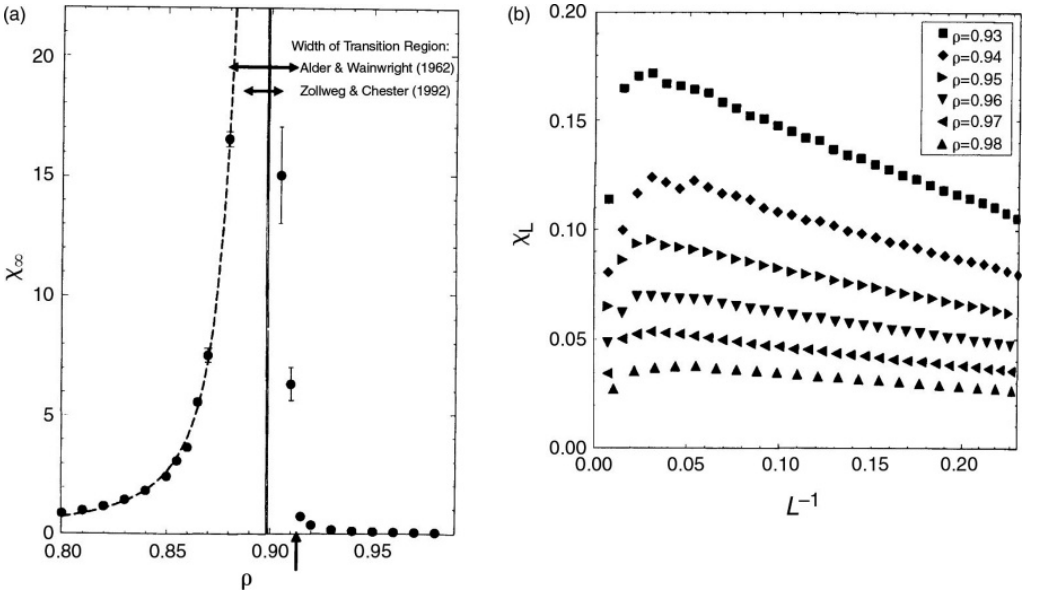

Fig. 6.6(a) Extrapolated 'susceptibility' χ_∞ of the hard disk system vs. density. The data in the fluid are fitted to $\chi_\infty \propto \exp\{b'(\rho_f - \rho)^{-1/2}\}$ where b' is a constant and $\rho_f = 0.913$ is marked with an arrow. The vertical solid line marks the estimated transition density $\rho_{cross} = 0.8985 \pm 0.0005$ obtained from cumulant intersections (Fig. 6.7). Previous estimates for the width of the two-phase region are indicated by horizontal arrows. Error bars are only shown when they exceed the size of the symbols. (b) Susceptibility χ_L as a function of the inverse linear subsystem size L^{-1} in the solid phase away from the transition, for $N = 16\,384$ particles. From Weber *et al*. (1995).

transitions: by increasing the density one leaves the fluid phase through a divergence of the susceptibility χ_∞,

$$\chi_\infty \propto \exp\{b'(\rho_f - \rho)^{-1/2}\}, \tag{6.41}$$

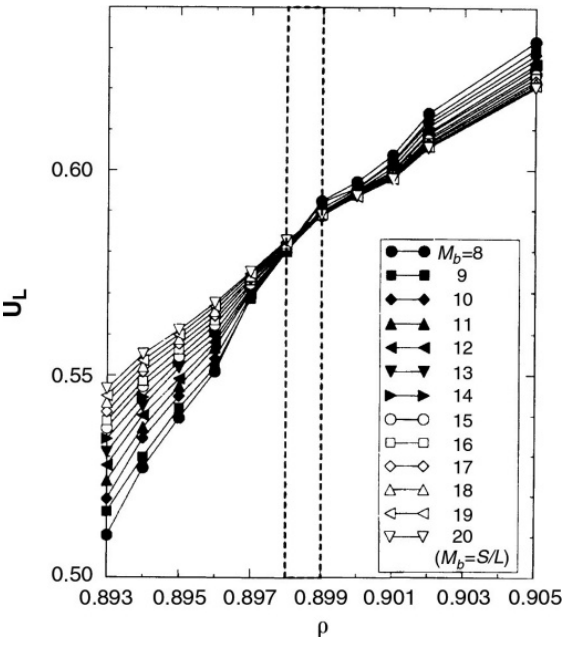

Fig. 6.7 Order parameter cumulants for the bond orientational order parameter, plotted as a function of the total density ρ for various subsystem sizes $L = S/M_b$. The vertical dashed lines mark the range within which the cumulant intersection occurs, i.e. they indicate the error in the estimated transition density of $\rho_{\text{cross}} = 0.8985 \pm 0.0005$. From Weber *et al.* (1995).

where b' is a constant and at ρ_f a transition occurs to a rather unconventional phase, the hexatic phase. In this phase, for $\rho_f < \rho < \rho_f'$, the order parameter $\langle \psi \rangle$ is still zero in the thermodynamic limit $L \to \infty$, but correlation functions of this order parameter decay algebraically, i.e. the correlation length ξ (cf. Eqn. (6.40)) is infinite. Only for $\rho > \rho_f'$ would one have $\langle \psi \rangle > 0$, i.e. a conventional solid.

As Fig. 6.6a shows, Eqn. (6.41) provides a very good fit to the simulation data, but the 'critical' density ρ_f is larger than the density ρ_{cross}, which results from cumulant intersections (Fig. 6.7). As in the case of the Ising model, see Chapter 4, the cumulant of the bond orientational order parameter has been defined as (cf. Eqn. (4.12))

$$U_L = 1 - \langle \psi^4 \rangle_L \big/ \left(3 \langle \psi^2 \rangle_L^2\right). \tag{6.42}$$

Figure 6.7 shows that the intersection occurs in the region $0.898 \leq \rho \leq 0.899$, and this estimate clearly is significantly smaller than $\rho_f \approx 0.913$ extracted from the fit to Eqn. (6.41), cf. Fig. 6.6a. Thus the implication is that at the (first order) transition χ_∞ is still finite, ρ_f only has the meaning of a 'spinodal point' (limit of metastability of the fluid phase). Of course, noting that ρ is the density of an extensive thermodynamic variable, we emphasize that in principle there should be a jump in density from ρ (where one leaves the fluid phase) to ρ_s (where one enters the solid phase). In the 'forbidden' region of densities in between ρ and ρ_s one finds two-phase coexistence (which for large enough L must show up in a double peak distribution for $\rho_L(\psi, \rho)$, rather than the single peaks seen in Fig. 6.4). Unfortunately, even with 16 384 particles no evidence for this ultimate signature of first order melting in two

dimensions is found. The large values found for χ_∞ near the transition at ρ_{cross} in Fig. 6.6a imply that the system is indeed rather close to a continuous melting transition, and previous estimates for the width of the two-phase coexistence region (included in Fig. 6.6a) clearly are too large. This fact that the system is so close to continuous melting also explains why one cannot see a jump singularity of κ_∞ at the transition (Fig. 6.5 rather suggests only a discontinuity of the slope). However, the conclusions are called into question by a finite size scaling analysis for very large systems (Jaster, 1998) which studied χ_∞ much closer to the transition than in the data in Fig. 6.6a and which concluded that there is a continuous transition at $\rho_c \approx 0.900$ compatible with Fig. 6.7.

Originally, the subsystem analysis for off-lattice systems was used to study the gas–liquid transition (Rovere *et al.*, 1990), but it now is evident that for this problem the grand canonical simulation method is more efficient (Wilding, 1997). For very dense systems, however, the subsystem analysis clearly has its merits. Another useful application concerns the analysis of capillary-wave type fluctuations of interfaces between coexisting phases in polymer mixtures (Werner *et al.*, 1997). Thus we suggest that the reader keep this technique in mind as an alternative to the more traditional approaches.

6.1.6 Gibbs ensemble

For a study of many fluids or fluid mixtures one is sometimes not primarily interested in a precise knowledge of critical properties, but rather in an overall description of phase diagrams, involving the description of phase coexistence between liquid and gas, or between an A-rich phase and a B-rich phase in a binary mixture (AB), respectively. The so-called 'Gibbs ensemble' method, pioneered by Panagiotopoulos (1987, 1995), is an efficient (and computationally 'cheap') approach to achieve that goal, and hence is of widespread use for a large variety of systems.

The basic idea of this method is very intuitive. Consider a macroscopic system where gas and fluid phases coexist in thermal equilibrium. The Gibbs ensemble attempts to simulate two microscopic regions within the bulk phase, away from an interface (Fig. 6.8). The thermodynamic requirements for phase coexistence are that each region should be in internal equilibrium and that temperature, pressure, and the chemical potential are the same in both regions. The system temperature in Monte Carlo simulations is specified in advance. The remaining conditions are satisfied by three types of Monte Carlo moves: displacements of particles within each region (to ensure internal equilibrium), exchange of volume between the two regions (to ensure equality of pressures), and particle exchanges (to ensure equality of the chemical potentials).

From this discussion, and from Fig. 6.8, it is evident that the Gibbs ensemble somehow interpolates between the NVT, NpT, and μVT ensembles discussed above; and it is applicable only when grand canonical simulations (or semi-grand canonical ones, for the simulation of phase equilibrium in a mixture) are also feasible, since the transfer of particles from one box to the other one is an indispensable step of the procedure in order to maintain the equality of the

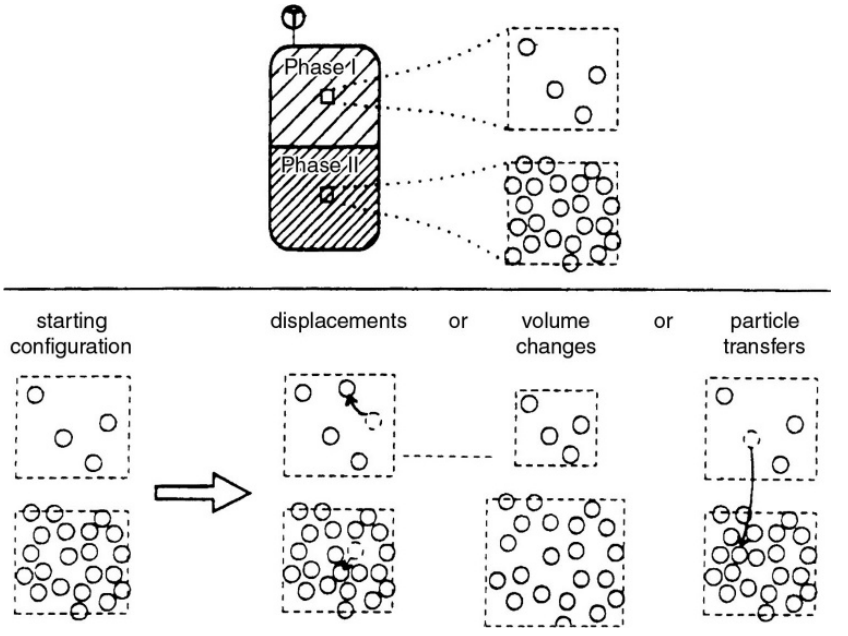

Fig. 6.8 Schematic diagram of the Gibbs ensemble technique. A two-dimensional system is shown for simplicity. Broken lines indicate boundaries where periodic boundary conditions are applied. From Panagiotopoulos (1995).

chemical potentials of the two boxes. Therefore, its application is straightforward for fluid–fluid phase equilibria only and not for phase equilibria involving solid phases (or for complex fluids, such as very asymmetric polymer mixtures).

For a formal derivation of the acceptance rules of the moves shown in Fig. 6.8, one proceeds similarly as in the derivation of rules for the NpT and μVT ensembles. The total particle number $N = N_{\mathrm{I}} + N_{\mathrm{II}}$ and the total volume $V = V_{\mathrm{I}} + V_{\mathrm{II}}$, of the two boxes are kept constant, and hence we apply the canonic partition function, cf. Eqns. (6.18) and (6.21)

$$Z_{NVT} = \frac{1}{\Lambda^{3N} N!} \sum_{N_{\mathrm{I}}=0}^{N} \binom{N}{N_{\mathrm{I}}} \int_0^V d\,V_{\mathrm{I}} V_{\mathrm{I}}^{N_{\mathrm{I}}} (V - V_{\mathrm{I}})^{(N-N_{\mathrm{I}})} \times \int d\mathbf{s}_1 \ldots\, d\mathbf{s}_{N_{\mathrm{I}}} e^{-U_{\mathrm{I}}/k_{\mathrm{B}}T} \int d\mathbf{s}_{N_{\mathrm{I}}+1} \ldots \int d\mathbf{s}_N e^{-U_{\mathrm{II}}/k_{\mathrm{B}}T}. \quad (6.43)$$

U_{I} is the total intermolecular interaction potential of the N_{I} particles in V_{I}, and U_{II} the corresponding quantitiy in V_{II}. The probability density corresponding to Eqn. (6.43) is

$$P(N_{\mathrm{I}}, V_{\mathrm{I}}; N, V, T) \propto \frac{N!}{N_{\mathrm{I}}(N - N_{\mathrm{I}})!} \exp\left\{ N_{\mathrm{I}} \ln V_{\mathrm{I}} + (N - N_{\mathrm{I}}) \ln (V - V_{\mathrm{I}}) - \frac{U_{\mathrm{I}}}{k_{\mathrm{B}}T} - \frac{U_{\mathrm{II}}}{k_{\mathrm{B}}T} \right\}. \quad (6.44)$$

From Eqn. (6.44), one obtains the transition probability for the various types of moves as in Sections 6.1.1–6.1.3. For a displacement step in one of the regions, the situation is exactly the same as in a standard NVT simulation. For

a volume exchange step, we have (cf. Eqn. (6.27))

$$W(V_{\mathrm{I}} \to V_{\mathrm{I}} + \Delta V, V_{\mathrm{II}} \to V_{\mathrm{II}} - \Delta V) = \min\left\{1, \exp\left[-\frac{\Delta U_{\mathrm{I}} + \Delta U_{\mathrm{II}}}{k_{\mathrm{B}}T} + N_{\mathrm{I}} \ln \frac{V_{\mathrm{I}} + \Delta V}{V_{\mathrm{I}}} + (N - N_{\mathrm{I}}) \ln \frac{(V - V_{\mathrm{I}} - \Delta V)}{V - V_{\mathrm{I}}}\right]\right\}. \tag{6.45}$$

The transition probability for particle exchanges (written here for a transfer from region II to region I) is

$$W(N_{\mathrm{I}} \to N_{\mathrm{I}} + 1, N_{\mathrm{II}} \to N_{\mathrm{II}} - 1) = \min\left\{1, \frac{(N - N_{\mathrm{I}})\, V_{\mathrm{I}}}{(N_{\mathrm{I}} + 1)(V - V_{\mathrm{I}})} \exp\left[-\frac{\Delta V_{\mathrm{I}} + \Delta V_{\mathrm{II}}}{k_{\mathrm{B}}T}\right]\right\}. \tag{6.46}$$

Note that beforehand neither the vapor pressure at which phase coexistence occurs nor the associated chemical potential need to be known starting from suitable initial conditions (e.g. one box with density smaller than the gas density at phase coexistence, the other box with a density higher than the corresponding liquid density). The system will automatically develop towards phase coexistence, but of course, the total density N/V must be chosen such that the state point would fall inside the two-phase coexistence region in the thermodynamic limit.

One practical difficulty is that in a long simulation run it can happen (and will inevitably happen close to criticality) that the box labeled by I will sometimes contain the gas phase and sometimes the liquid phase, and so one would not obtain any meaningful results (referring to properties of a pure phase) by simply taking running averages for the two boxes separately. Hence a safer way to analyze the results is to record the density distribution function: as long as it shows two clearly separated peaks, there is no difficulty in ascribing to them the properties of the two coexisting phases. Unlike canonical simulations of phase coexistence (Rovere *et al.*, 1990), equilibrium is established very quickly and the data are not affected so much by interfacial contributions. Near the critical point, however, the accuracy of the method deteriorates, and finite size effects are less straightforward to analyze, since both volumes and particle numbers of the individual boxes fluctuate. Given the current status of our knowledge, the grand canonical method in conjunction with finite size scaling yields clearly superior results (Wilding, 1997). Nevertheless, the Gibbs ensemble method has a suitable place in our 'bag of tricks'; due to its relative simplicity of implementation and modest CPU requirements it has been applied in numerous studies of simple fluids as well as of ionic, associating, and reacting fluids and even for simple models of homopolymers (combining the technique with 'configurational bias' Monte Carlo methods, see e.g. Mooij *et al.* (1992)). We do not give further details here, but draw the reader's attention to the recent extensive reviews presented by Panagiotopoulos (1995) and Frenkel and Smit (1996).

Problem 6.6 Generalize Eqn. (6.46) to a multicomponent system (where at phase coexistence the chemical potentials of all components should be equal).

6.1.7 Widom particle insertion method and variants

The test particle insertion method (Widom, 1963) is a technique which can be used to sample the chemical potential in a fluid. Remember that the chemical potential is defined by

$$\mu = (\partial F/\partial N)_{VT} = (\partial G/\partial N)_{pT}\,. \tag{6.47}$$

Consider first the case of the NVT ensemble where $F = -k_{\mathrm{B}}T \ln Z(N, V, T)$ and the partition function $Z(N, V, T)$ is given by Eqn. (6.18). For $N \gg 1$ we can replace the partial derivative with respect to N by a difference, $\mu = k_{\mathrm{B}}T \ln\{Z(N+1, V, T)/Z(N, V, T)\}$. Again using scaled coordinates $\mathbf{s}_i$ (Eqn. (6.19)) and Eqn. (6.20) to split off the contribution of the ideal gas, $\mu_{\mathrm{id}}(\rho) = -k_{\mathrm{B}}T \ln\{V/[\Lambda^d(N+1)]\}$ with $\rho = N/V$, we find

$$\mu = \mu_{\mathrm{id}}(\rho) + \mu_{\mathrm{ex}}, \tag{6.48}$$

where

$$\mu_{\mathrm{ex}} = -k_{\mathrm{B}}T \left\{ \int_0^1 d\mathbf{s}_1 \cdots \int_0^1 d\mathbf{s}_{N+1} \exp\left[-\frac{U(\mathbf{s}_1, \ldots, \mathbf{s}_{N+1}, L)}{k_{\mathrm{B}}T}\right] \Bigg/ \int_0^1 d\mathbf{s}_1 \cdots \int_0^1 d\mathbf{s}_N \exp\left[-\frac{U(\mathbf{s}_1, \ldots, \mathbf{s}_N, L)}{k_{\mathrm{B}}T}\right] \right\}.$$

We now separate the potential energy U of the $(N+1)$-particle system into the energy of the N-particle system and the interaction energy ΔU of the $(N+1)$th particle with the rest of the system, i.e.

$$U(\mathbf{s}_1, \ldots, \mathbf{s}_{N+1}, L) = U(\mathbf{s}_1, \ldots, \mathbf{s}_N, L) + \Delta U. \tag{6.49}$$

We immediately realize that μ_{ex} then can be rewritten as

$$\mu_{\mathrm{ex}} = -k_{\mathrm{B}}T \ln \int_0^1 d\mathbf{s}_{N+1} \langle \exp(-\Delta U/k_{\mathrm{B}}T) \rangle_N, \tag{6.50}$$

where $\langle \ldots \rangle_N$ is a canonical ensemble average over the configuration space of the N-particle system. This average now can be sampled by the conventional Monte Carlo methods. In practice one proceeds as follows: one carries out a standard NVT Monte Carlo simulation of the system of N particles (as described in Section 6.1.1). Often one randomly generates additional coordinates $\mathbf{s}_{N+1}$ of the test particle, *uniformly distributed* in the d-dimensional unit cube in order to carry out the remaining integral in Eqn. (6.50). With this value of $\mathbf{s}_{N+1}$, one computes ΔU from Eqn. (6.49) and samples then $\exp(-\Delta U/k_{\mathrm{B}}T)$.

Thus one computes the average of the Boltzmann factor associated with the random insertion of an additional particle in an N-particle system, but actually this insertion is never carried out, because then we would have created an $(N+1)$-particle system, but we do need an N-particle system for the averaging in Eqn. (6.50).

Care is necessary when applying this method to other ensembles. One can show that (for details see e.g. Frenkel and Smit, 1996) in the NpT ensemble Eqns. (6.48) and (6.50) are replaced by

$$\begin{aligned} \mu &= \mu_{\mathrm{id}}(p) + \mu_{\mathrm{ex}}(p), \\ \mu_{\mathrm{id}}(p) &= -k_{\mathrm{B}}T \ln(k_{\mathrm{B}}T/p\Lambda^d), \\ \mu_{\mathrm{ex}}(p) &= -k_{\mathrm{B}}T \ln\left\langle \frac{pV}{(N+1)k_{\mathrm{B}}T} \int_0^1 d\mathbf{s}_{N+1} \exp(-\Delta U/k_{\mathrm{B}}T) \right\rangle. \end{aligned} \tag{6.51}$$

Thus one uses the ideal gas reference state at the same pressure (rather than at the same density as in Eqn. (6.48)) as the investigated system, and the quantity that is sampled is $V\exp(-\Delta U/k_{\mathrm{B}}T)$ rather than $\exp(-\Delta U/k_{\mathrm{B}}T)$.

An obvious extension of the particle insertion method is to binary mixtures (A, B) where one often is interested only in chemical potential differences $\mu_{\mathrm{A}} - \mu_{\mathrm{B}}$ rather than in individual chemical potentials μ_{A}, μ_{B}. Then trial moves can be considered in which one attempts to transform a particle of species A into one of species B (without ever accepting such a transformation, of course).

While the Widom test particle method works well for moderately dense fluids (such as near and below the critical density), it breaks down long before the triple point density of a fluid is reached, simply because the probability $\exp(-\Delta U/k_{\mathrm{B}}T)$ that a random insertion is accepted becomes too small. Even for hard spheres, the insertion probability is down to 4×10^{-5} at a packing fraction of 0.4, long before the freezing transition is reached. Therefore, substantial effort has been devoted to devising schemes for biasing the insertions (rather inserting them 'blindly') as well as implementing 'gradual insertions'. While the basic idea of a gradual insertion, where the interaction of the test particle with the other particle is turned on in many small steps and the resulting free energy change is computed by thermodynamic integration, is rather straightforward (Mon and Griffiths, 1985), the implementation of such methods needs particular care in order to control the errors (Allen, 1996; Kofke and Cummings, 1997; Fasnacht *et al.*, 2004). Related techniques can also be used to calculate, e.g., the excess free energy of nanoparticles inserted into soft matter systems such as polymer brushes (Milchev *et al.*, 2008).

We conclude this section with a caveat: often the chemical potential is computed in a desire to establish phase diagrams (remember that chemical potentials of coexisting phases are equal). Then very good accuracy is needed, and one must carefully pay attention to systematic errors both due to finite size effects and due to the potential cutoff (if the potential is truncated, see

Section 6.2.1, one may approximately correct for this truncation by applying so-called 'tail corrections', see Frenkel and Smit (1996)).

6.1.8 Monte Carlo phase switch

Another difficult problem of considerable interest is the freezing of a simple fluid. The particular difficulties presented by the freezing transition stem from the distinctive symmetries of the coexisting fluid (F) and crystalline solid (CS) phases that give rise to kinetic problems because the crystal that forms from the fluid is often replete with defects. These defects do not normally anneal out on accessible simulation time scales so the system may become trapped in states from which it cannot escape. Thus, computational studies of freezing have generally relied on indirect approaches, e.g. thermodynamic integration. An innovative technique, known as Phase Switch Monte Carlo (PSMC), which was originally developed for computing free energy differences between distinct crystalline structures where interfacial states are computationally problematic has been extended to permit the study of freezing. The method (Wilding, 2001, 2006; Errington, 2004) samples the disjoint configuration spaces of two coexisting phases within a single simulation using a global coordinate transformation or 'phase switch' which directly maps one pure phase onto the other. Biased sampling methods are employed to enhance the probability of certain 'gateway' states in each phase from which the switch can be successfully launched. The method permits direct determination of equilibrium coexistence-point parameters and prescribes statistical uncertainties transparently.

To illustrate the method we consider N hard spheres simulated within an NpT ensemble with periodic boundary conditions. The configurational weight of a phase may be written as

$$Z_\gamma(N, p) = \int_0^\infty dV e^{-pV} Z_\gamma(N, V) \tag{6.52}$$

with (units are chosen such that $k_B T = 1$ throughout)

$$Z_\gamma(N, V) = \frac{1}{N!} \prod_{i=1}^{N} \int_{V,\gamma} d\{\vec{r}_i\} e^{-E\{\vec{r}\}}, \tag{6.53}$$

where V is the system volume, p the reduced pressure and γ (CS-crystalline solid or F-fluid) labels the phase. The hard sphere configurational energy is E, and the factor of $(N!)^{-1}$ corrects for indistinguishability. The γ-label denotes some constraint that picks out configurations $\{\vec{r}\}$ that 'belong' to phase γ. In a Monte Carlo simulation, this constraint is formulated as follows. Denote some *representative* configuration $\vec{R}_1^\gamma \ldots \vec{R}_N^\gamma = \{\vec{R}\}^\gamma$ as the reference state of phase γ. The constraint picks out those configurations which can be reached from $\{\vec{R}\}^\gamma$ on a simulational time scale which is presumed to be sufficiently long to allow exploration of one phase, but still short compared to spontaneous inter-phase traverses. Such a situation is realized if the freezing transition is

sufficiently strongly first order. The reference sites $\{\vec{R}\}^\gamma$ are the origins of the particle coordinates defined via some arbitrary association between the N particles and the N reference sites. The particle positions can then be written as

$$\vec{u}_i = \vec{r}_i - \vec{R}_i, \tag{6.54}$$

which serves to define the set of displacement vectors $\vec{u}_i$ (independent of the phase label γ) linking each particle i to its associated reference site $\vec{R}_i$. The configurational energy is then

$$E^\gamma(\{\vec{u}\}) \equiv E(\{\vec{R}^\gamma + \vec{u}\}). \tag{6.55}$$

In the case of the F-phase all contributing configurations are reachable from any one and so

$$Z_F(N, V) = \frac{1}{N!}\prod_{i=1}^{N}\int_{V,\{\vec{R}\}^F} d\{\vec{u}_i\} e^{-E^F\{\vec{u}\}}, \tag{6.56}$$

where $\{\vec{R}\}^F$ is an arbitrary fluid configuration which can be selected at random in the course of Monte Carlo exploration of the fluid phase.

For the CS phase, $\{\vec{R}\}^{CS}$ can be chosen to be the sites of a FCC lattice. In contrast to the F-phase, the Monte Carlo simulation does not sample the complete CS configuration space, which is composed of several mutually inaccessible fragments corresponding essentially to the different permutations of particles between lattice sites. In the absence of self-diffusion, Monte Carlo sampling will visit only the states within the fragment in which it is initiated. By symmetry each fragment should contribute equally to the configurational weight, so the total weight of the CS phase is the product of the contribution of one fragment times the number of fragments, i.e. the number of distinct permutations of N distinguishable particles amongst N fixed lattice sites in a periodic system. This number is not $N!$ but $(N-1)!$ since certain permutations are reachable from others via a global translation (permitted via the boundary conditions) (Wilding, 2001). Thus,

$$Z_{CS}(N, V) = \frac{1}{N}\prod_{i=1}^{N}\int_{V,\{R\}^{CS}} d\{\vec{u}_i\} e^{-E^{CS}\{\vec{u}\}} \tag{6.57}$$

and the Gibbs free energy difference is

$$\Delta g = g_{CS}(N, P) - g_F(N, P) = \frac{1}{N}\ln(Z_F/Z_{CS}). \tag{6.58}$$

The key to a Monte Carlo algorithm that visits both phases is the observation that the system may be transformed between the CS and F reference states simply by switching the representative vectors $\vec{R}_i^F \leftrightarrow \vec{R}_i^{CS}$ for all i. Hence, any $CS(F)$ configuration that is close enough to the reference may be transformed, and the phase switch can itself be implemented as a Monte Carlo step, so that the phase label γ becomes a stochastic variable. However, the set of configurations

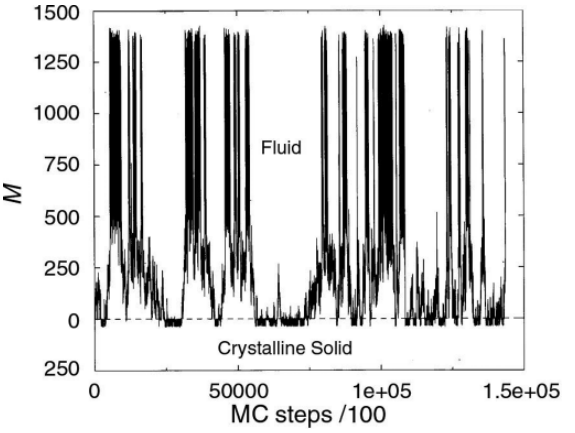

Fig. 6.9 The MC time evolution of the order parameter M for the $N = 256$ system. Phase switches occur between $M = 0$ states. After Wilding and Landau (2003). (For further details, see text.)

for which the Monte Carlo switch will be accepted will generally constitute only a small fraction of the respective configuration spaces and multicanonically biased sampling (see Chapter 7) is needed to enhance the probabilities with which these 'gateway' regions are visited. To that end an order parameter M can be defined that measures the overlap (between particle i and its neighbors) which would be created by a phase switch. The equilibrium states of both phases are characterized by large M values. The 'overlap' term contributes in both phases: swapping the $\{\vec{R}\}$ vectors will, in general, produce a configuration of the 'other' phase in which spheres overlap. A 'tether' term contributes only in the F-phase where particles may drift arbitrarily far from the sites with which they are nominally associated; the tethers provide the means to 'pull' the fluid towards the reference sites. The gateway states are those for which $M = 0$, i.e. for which a phase switch can be implemented without incurring hard sphere overlaps.

Simulations in the resultant ensemble measure the joint probability distribution $p(M, V, \gamma | N, p, \{\eta\})$ and thus permit the unfolding of the bias due to the weights to infer the true equilibrium distribution $p(M, V, \gamma | N, p)$. The desired free energy difference between the two phases follows by integrating over the contributions associated with each γ to give the a priori probabilities of the respective phases. (Of course, histogram reweighting techniques described in Chapter 7 can be employed to determine the value at neighboring pressures, thereby permitting a very precise determination of the coexistence pressure.)

Before the simulation is performed, values must be assigned to the parameters appearing in the definition of the order parameter, and there is some license in making this choice. Simulations were performed using systems of $N = 256$ particles using suitable weights obtained by iterative means. In Fig. 6.9 we show a typical portion of the evolution of the preweighted order parameter M as a function of Monte Carlo time. For clarity of presentation, states in the F-phase are denoted by positive values of M, while negative values correspond to CS phase states. Note that the range of M values sampled in the CS phase is quite small because particles are localized near their reference sites by the

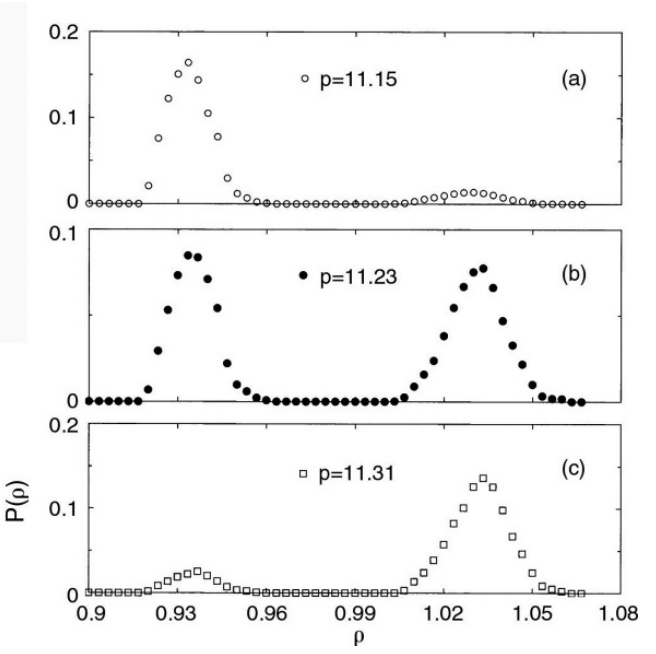

Fig. 6.10 The distribution of the density of the system of $N = 256$ particles at pressures: (a) just below; (b) at; (c) just above coexistence for this N. The mean single phase density averages are $\rho_F = 0.934(3)$ and $\rho_{CS} = 1.031(4)$. From Wilding and Bruce (2000).

suppression of the global translation mode. By contrast, much larger values of M are explored in the F-phase because the particles can drift far from the reference site to which they are associated. Nevertheless the whole range can be spanned relatively quickly by virtue of the highly efficient associations updates which permit large-scale changes in tether lengths.

The density distribution $P(\rho)$ was obtained from the measured distribution $p(M, V, \gamma | N, p, \{\eta\})$ by marginalizing with respect to the volume V and unfolding the effect of the weights. The results for the $N = 256$ system in the vicinity of the coexistence pressure are shown in Fig. 6.10. The distributions are derived from histogram reweighting of simulation data obtained at $p = 11.1$. Coexistence, identified by the equality of the area under each peak, occurs for $p = 11.23(3)$. With the use of this method, it is possible to locate the solid–liquid transition in a system of hard spheres with impressive accuracy. (Note: the finding that this transition actually occurs was made in the 1950s and represented one of the first major new discoveries made via computer simulations.) Current resolution is competitive to the most extensive alternative approaches, e.g. thermodynamic integration. Applications of Phase Switch Monte Carlo to transitions between different crystalline phases also exist (Bruce *et al.*, 1997; Jackson *et al.*, 2002).

6.1.9 Cluster algorithm for fluids

How to devise a general cluster flipping method for off-lattice systems, e.g. fluids, was not immediately obvious. The first step was taken by Dress and Krauth (1995) who used geometric operations to design a cluster algorithm for

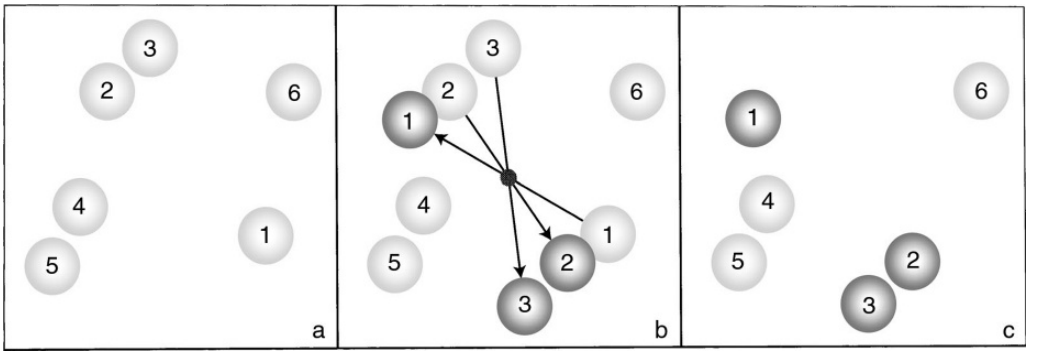

Fig. 6.11 Two-dimensional illustration of the continuous space cluster algorithm. Light and dark objects represent the particle before and after movement, respectively. The pivot is marked by the small dot at the center of the figure. Configurations are: (a) the initial particle state; (b) state resulting from point reflection of particles 1–3; (c) final state. From Liu and Luijten (2004).

hard spheres. They would take a configuration, choose a pivot point randomly, rotate the entire system about that pivot, and superimpose the rotated configuration with the original one to produce a joint system. Overlapping clusters in the *joint* system are identified. Then, either the clusters with even numbers of particles or pairs of clusters with an odd number of particles are flipped, i.e. those in the rotated configuration replace those in the original configuration. (This choice is made so that the total number of particles is conserved and the simulation is in the canonical ensemble.) The resultant configuration will then, in general, differ significantly from the original one because non-local moves have been made.

Later, Liu and Luijten (2004) generalized this method in the following way. They considered particles with 'soft' interactions that extend out to some cutoff distance r_c. A random pivot is chosen, and one randomly chosen particle, at position $\vec{r}_i$, is moved via a point reflection with respect to the pivot to position $\vec{r}_i'$. Two classes of particles are then identified: those that interact with particle i in its original position; and those that interact with it in its new position. Particle i is always moved, and subsequent particles j are added to the cluster with probability

$$p_{ij} = \max[1 - e^{-\Delta_{ij}/k_B T}, 0], \tag{6.59}$$

where $\Delta_{ij} = V(|\vec{r}_i' - \vec{r}_j|) - V(|\vec{r}_i - \vec{r}_j|)$. This means that the probability of adding particle j to the cluster depends only on the energy difference that would result from a change in the relative position of particles i and j. If particle j is added to the cluster, all of its interacting neighbors are considered in an iterative fashion, just as in the original Wolff algorithm, until the cluster stops growing. The positions of the particles in the cluster are accepted and a new, random pivot is chosen to continue the process. The procedure is shown, schematically, in Fig. 6.11. This method offers the potential for the acceleration of simulations for models representing many different physical systems and we expect it to be of great importance.

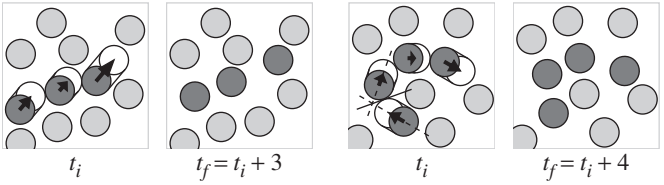

Fig. 6.12 Move of an event chain algorithm. The individual displacements, in this example of three disks, add up to a distance of l. From Bernard *et al*. (2009).

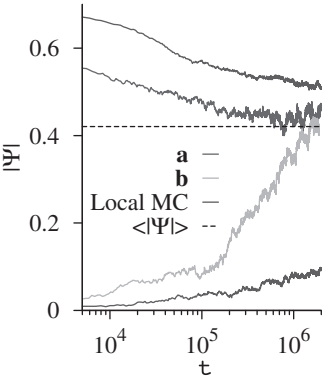

Fig. 6.13 Absolute value of the orientational order parameter showing the approach to thermal equilibrium for a 1024^2 hard disk system at density $\rho = 0.708$. Data are shown post-quenching for: (a) a high-density crystal; and (b) a low-density liquid. Results from both the event-driven algorithm and the usual local move algorithm are shown. From Bernard and Krauth (2011).

6.1.10 Event chain algorithms

An interesting rejection free algorithm has been proposed for treating hard disk/sphere systems (Bernard *et al*., 2009, 2011) and then extended to generalized potentials (Bernard and Krauth, 2012). This event-driven algorithm starts with a randomly chosen disk that moves in a random direction until it encounters another disk. It then stops but the second disk begins moving in the same direction until it hits another disk and the process repeats until the total distance traveled by all of the disks equals some pre-determined, fixed length l. The algorithm is shown schematically in Fig. 6.12. The usual 'local move' algorithms that have been applied attempt to move each hard disk in turn, but at high densities the rejection rate becomes very great.

This new method was applied in rather spectacular fashion to the long-standing problem of melting of hard disks in two dimensions (Bernard and Krauth, 2011). Simulating systems as large as 1024^2, they were able to show that the melting occurs neither via a single first order transition nor the two-step, continuous KTHNY scenario (Kosterlitz and Thouless, 1973; Halperin and Nelson, 1978; Young, 1979). Instead, a continuous hexatic–liquid transition is followed by a first order hexatic–solid transition as the density is decreased from its close-packing value. As can be seen in Fig. 6.13, the convergence of the orientational order parameter at a density of $\rho = 0.708$ starting from two

very different initial states can be achieved with the event-driven algorithm. In contrast, the usual 'local move' algorithm is still very far from convergence, even after more than 10^6 MCS have elapsed.

6.2 'SHORT RANGE' INTERACTIONS

6.2.1 Cutoffs

One significant advantage of a potential like Lennard–Jones is that it falls off quite fast, and only those particles within a nearby environment have much effect. As a consequence it is possible to limit, or 'cut off', the maximum range of the interaction at a distance r_c. This effectively introduces a step function into the distance dependence, but the hope is that if the potential has already decayed substantially, this effect will be small. (The situation is perhaps less complex than for molecular dynamics for which this cutoff can introduce a singularity in the force; there the potential is then often 'shifted' so that the force is quite small at r_c.) The choice of cutoff radius is somewhat arbitrary and depends upon the potential used. For Lennard–Jones a convenient choice is often $r_c = 2.5\sigma$. The use of a cutoff dramatically reduces the number of near neighbors which must be included in the calculation of energy of the new trial state, but in order to take advantage of this fact one must use an intelligent data structure. One simple, but very good choice, is discussed in the next subsection. In general one must balance the desire to speed up the program by using a small cutoff with the concern that the cutoff may change the physics.

6.2.2 Verlet tables and cell structure

A very simple method to reduce the amount of work needed to calculate energy changes is to construct a table of neighbors for each particle which contains only those neighbors which are closer than r_c. This can be further improved by making the following observation: as particles move due to the acceptance of Monte Carlo moves they may leave the 'interaction volume' or new particles may enter this region. The recalculation of the table following each successful move may be avoided by keeping track of all particles within some distance $r_{max} > r_c$ where $(r_{max} - r_c) = n\delta_{max}$ is large enough that no particle can enter the 'interaction volume' in n Monte Carlo steps of maximum size δ; the table is then only recalculated after every n steps. For very large systems even this occasional recalculation can become very time consuming, so an additional step can be introduced to further limit the growth in time requirement as the system size increases. The system can be divided into a set of cells of size l which are small compared to the size of the simulation box L but larger than the cutoff radius r_c. The only interacting neighbors must then be found within the same cell or the neighboring cells, so the remainder of the simulation volume need not be searched.

6.2.3 Minimum image convention

Periodic boundary conditions may be easily implemented by simply attaching copies of the system to each 'wall' of the simulation volume. An 'image' of each particle is then replicated in each of the fictitious volumes; only the distance between the nearest neighbor, including one of the 'images' is used in computing the interaction.

6.2.4 Mixed degrees of freedom reconsidered

Often one of the degrees of freedom in the semi-canonical ensemble is continuous. An example that we considered earlier was Si/Ge mixtures for which the choice of atom was determined by a discrete (Ising) variable and a continuous variable was used to determine the movement of the particles. In this case a three-body interaction was included so that the table structure became more complicated. Since the interactions of a 'trimer' needed to be calculated, it was sometimes necessary to calculate the position of the neighbor of a neighbor, i.e. both the nearest neighbor distance as well as the bond angle. This effectively extends the range of the interaction potential substantially. An instructive example of the combination of the positional and magnetic degrees of freedom is the study of the phase transition in a ferromagnetic fluid. Nijmeijer and Weis (1995) studied a Heisenberg fluid with magnetic interactions that decayed with distance out to 2.5σ beyond which a cutoff was imposed. Their Monte Carlo simulations used Metropolis sampling for the positional degrees of freedom and the Wolff cluster flipping/embedding trick for the magnetic degrees of freedom. A finite size scaling analysis for systems as large as 2916 particles was employed and critical behavior that was different from that of a lattice system was observed.

6.3 TREATMENT OF LONG RANGE FORCES

Long range interactions represent a special challenge for simulation because they cannot be truncated without producing drastic effects. In the following we shall briefly describe several different methods which have been used to study systems with long range interactions (Pollock and Glosli, 1996).

6.3.1 Reaction field method

This approach is taken from the continuum theory of dielectrics and is effective for the study of dipolar systems. We consider a system of N particles each of which has a dipolar moment of magnitude μ. The dipole–dipole interaction between two dipoles i and j is given by

$$v_{\mathrm{dd}} = \frac{\boldsymbol{\mu}_i \cdot \boldsymbol{\mu}_j}{r_{ij}^3} - \frac{3(\boldsymbol{\mu}_i \cdot \mathbf{r}_{ij})(\boldsymbol{\mu}_j \cdot \mathbf{r}_{ij})}{r_{ij}^5}, \tag{6.60}$$

and the total energy of a given dipole is determined by summing over all other dipoles. An approximation to the sum may be made by carving out a spherical cavity about the dipole, calculating the sum exactly within that cavity, and treating the remaining volume as a continuum dielectric. In the spirit of dielectric theory, we can describe the volume within the cavity of radius r_c by a homogeneous polarization, which in turn induces a 'reaction field' $\mathbf{E}_R$,

$$\mathbf{E}_R(i) = \frac{2(\varepsilon - 1)}{r_c^3(2\varepsilon + 1)} \sum_j^N \boldsymbol{\mu}_j, \tag{6.61}$$

which acts on each dipole. The correct choice of the dielectric constant ε is still a matter of some debate. The total dipolar energy of a particle is thus given by the sum of the 'local' part within the cavity and the 'global' part which comes from the reaction field.

6.3.2 Ewald method

The Ewald method is not new; in fact it has long been used to sum the Coulomb energy in ionic crystals in order to calculate the Madelung constant. The implementation to the simulation of a finite system is straightforward with the single modification that one must first periodically replicate the simulation volume to produce an 'infinite' array of image charges. Each cell is identified by the integer n and the vector $\mathbf{r}_n$ is the replication vector. The electrostatic energy is calculated, however, only for those charges in the original cell. The potential at charge q_i is

$$v_i(r) = \sum_j^N \sum_{n=n_i}^{\infty} \frac{q_j}{|\mathbf{r} - \mathbf{r}_j + \mathbf{r}_n|} \qquad \begin{cases} n_i = 0, & j \neq i \\ n_i = 1, & j = i \end{cases} \tag{6.62}$$

which excludes self-interaction. The trick is to add and subtract a Gaussian charge distribution centered at each site $\mathbf{r}_j$ and separate the potential into two sums, one in real space and one in reciprocal space. The Coulomb potential then becomes

$$v_i(\mathbf{r}) = v_i^r(\mathbf{r}) + v_i^k(\mathbf{r}), \tag{6.63}$$

with

$$v_i^k(\mathbf{r}) = \sum_{m \neq 0} W(k_m) S(k_m) e^{2\pi \mathbf{k}_m \cdot \mathbf{r}} - 2\sqrt{\frac{2}{\pi}} \frac{q_i}{\alpha} \tag{6.64}$$

where the second term corrects for the self-energy, and

$$W(k_m) = \frac{1}{\pi L^3 k_m^2} e^{-2\pi^2 k_m^2 \alpha^2}, \tag{6.65a}$$

$$S(k_m) = \sum_j^N q_j e^{-2\pi i \mathbf{k}_m \cdot \mathbf{r}_j}. \tag{6.65b}$$

The width of the Gaussian distribution is α. By proper choice of α the sums in both real space and reciprocal space in Eqn. (6.63) can be truncated.

Instead of replicating the simulation cell for computing the Ewald sum, Caillot (1992) showed that it was possible to map the system onto the three-dimensional surface of a four-dimensional hypersphere. Although the use of non-Euclidean geometry would seem to complicate the problem, program coding is simple, and for system size of about 10^3 particles the increase in performance is about a factor of 3.

6.3.3 Fast multipole method

The fast multipole method (Greengard and Rokhlin, 1987) plays a particularly important role in calculating Coulomb interactions in large systems because it exhibits $O(N)$ scaling, where N is the number of particles. The method relies on two expansions which converge for large distances and short distances, respectively. The multipole expansion is

$$V(r) = 4\pi \sum_{l,m}^{l_{\max}} \frac{M_{lm}}{(2l+1)} \frac{Y_{lm}(\Omega)}{r^{l+1}} + \cdots, \tag{6.66}$$

where $Y_{lm}(\Omega)$ is a spherical harmonic, the multipole moment is

$$M_{lm} = \sum_{i}^{N} q_i r_i^l Y_{lm}^*(\Omega_i), \tag{6.67}$$

and the 'local' expansion is

$$V(r) = 4\pi \sum_{l,m}^{l_{\max}} L_{lm} r^l Y_{lm}(\Omega) + \cdots, \tag{6.68}$$

where the 'local' moment is

$$L_{lm} = \sum_{l} \frac{q_i}{(2l+1)} \frac{Y_{lm}^*(\Omega_i)}{r_i^{l+1}} + \cdots. \tag{6.69}$$

The algorithm is implemented in the following way:

Fast multipole method

(1) Divide the system into sets of successively smaller subcells.
(2) Shift the origin of the multipole expansion and calculate the multipole moments at all subcell levels starting from the lowest level.
(3) Shift the origin of the local expansion and calculate the local expansion coefficients starting from the highest level.
(4) Evaluate the potential and fields for each particle using local expansion coefficients for the smallest subcell containing the particle.

This procedure becomes increasingly efficient as the number of particles is made larger.

6.4 ADSORBED MONOLAYERS

6.4.1 Smooth substrates

The study of two-dimensional systems of adsorbed atoms has attracted great attention because of the entire question of the nature of two-dimensional melting. In the absence of a periodic substrate potential, the system is free to form an ordered structure determined solely by the inter-particle interactions. As the temperature is raised this planar 'solid' is expected to melt, but the nature of the transition is a matter of debate.

6.4.2 Periodic substrate potentials

Extensive experimental data now exist for adsorbed monolayers on various crystalline substrates and there have been a number of different attempts made to carry out simulations which would describe the experimental observations. These fall into two general categories: lattice gas models, and off-lattice models with continuous, position dependent potentials. For certain general features of the phase diagrams lattice gas models offer a simple and exceedingly efficient simulations capability. This approach can describe the general features of order–disorder transitions involving commensurate phases. (For early reviews of such work see Binder and Landau (1989) and Landau (1991). An extension of the lattice gas description for the ordering of hydrogen on palladium (100) in the c(2×2) structure has been proposed by giving the adatoms translational degrees of freedom within a lattice cell (Presber *et al.*, 1998).

The situation is complicated if one wishes to consider orientational transitions involving adsorbed molecules since continuous degrees of freedom must be used to describe the angular variables. Both quadrupolar and octupolar systems have been simulated. For a more complete description of the properties of adsorbed monolayers it is necessary to allow continuous movement of particles in a periodic potential produced by the underlying substrate. One simplification which is often used is to constrain the system to lie in a two-dimensional plane so that the height of the adatoms above the substrate is fixed. The problem is still difficult computationally since there may be strong competition between ordering due to the adatom–adatom interaction and the substrate potential and incommensurate phases may result. Molecular dynamics has been used extensively for this class of problems but there have been Monte Carlo studies as well. One of the 'classic' adsorbed monolayer systems is Kr on graphite. The substrate has hexagonal symmetry with a lattice constant of 2.46 Å whereas the lattice constant of a compressed two-dimensional krypton solid is 1.9 Å. The 1×1 structure is thus highly unfavorable and instead we find occupation of next-nearest neighbor graphite hexagons leading to a

($\sqrt{3} \times \sqrt{3}$) commensurate structure with lattice constant 4.26 Å. This means, however, that the krypton structure must expand relative to an isolated two-dimensional solid. Thus, there is competition between the length scales set by the Kr–Kr and Kr–graphite interactions. An important question was thus whether or not this competition could lead to an incommensurate phase at low temperatures. This is a situation in which boundary conditions again become an important consideration. If periodic boundary conditions are imposed, they will naturally tend to produce a structure which is periodic with respect to the size of the simulation cell. In this case a more profitable strategy is to use free edges to provide the system with more freedom. The negative aspect of this choice is that finite size effects become even more pronounced. This question has been studied using a Hamiltonian

$$\mathcal{H} = \sum_i V(\mathbf{r}_i) + \frac{1}{2} \sum_{i \neq j} \upsilon_{\mathrm{LJ}}(\mathbf{r}_{ij}), \tag{6.70}$$

where the substrate potential is given by

$$V(\mathbf{r}_i) = V_0(z_{\mathrm{eq}}) + 2V_1(z_{\mathrm{eq}})\{\cos(\mathbf{b}_1 \cdot \mathbf{r}_i) + \cos(\mathbf{b}_2 \cdot \mathbf{r}_i) + \cos[(\mathbf{b}_1 + \mathbf{b}_2) \cdot \mathbf{r}_i]\}, \tag{6.71}$$

where $\mathbf{b}_1$ and $\mathbf{b}_2$ are the reciprocal lattice vectors for the graphite basal plane, and υ_{LJ} is the Lennard–Jones potential of Eqn. (6.4). The strength of the corrugation potential is given by V_1. The order parameter for the ($\sqrt{3} \times \sqrt{3}$) registered phase is

$$\Phi = \frac{1}{3N} \sum_i \{\cos(\mathbf{b}_1 \cdot \mathbf{r}_i) + \cos(\mathbf{b}_2 \cdot \mathbf{r}_i) + \cos[(\mathbf{b}_1 + \mathbf{b}_2) \cdot \mathbf{r}_i]\}. \tag{6.72}$$

A local order parameter can also be defined using the reciprocal lattice vectors appropriate to each of the three possible sublattices. A canonical Monte Carlo study (Houlrik *et al.*, 1994) showed that there was a first order transition between a low temperature incommensurate phase and a high temperature commensurate ($\sqrt{3} \times \sqrt{3}$) structure. Both the smearing of the transition and the shift in the transition temperature decrease rapidly as the system size increases. At higher temperature still the ($\sqrt{3} \times \sqrt{3}$) ordered structure melts.

Similar potentials as that given in Eqn. (6.70) can also be used when the substrate surface has square or rectangular symmetry, as would be appropriate for (100) and (110) faces of cubic crystals (Patrykiejew *et al.*, 1995, 1998). Interesting effects due to competition occur since the adsorbed layer prefers a triangular structure for weak corrugation.

6.5 COMPLEX FLUIDS

By the term 'complex fluids' as opposed to 'simple fluids' one means systems such as colloidal dispersions, surfactant solutions (microemulsions) and their

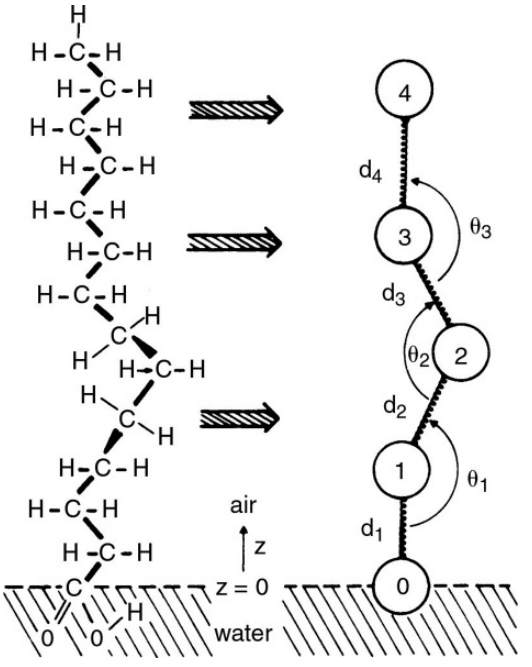

Fig. 6.14 Schematic picture of a fatty acid molecule at the air–water interface and a possible coarse-grained model, where a few successive CH_2 groups are combined into one effective monomer. The effective bonds between these effective monomers are represented by springs, and the stiffness of the chain is controlled by a potential depending on the angle θ_i between the effective bonds. From Haas *et al.* (1996).

various microphase-separated structures (sponge phases, phases with lamellar superstructure, solutions containing micelles or vesicles, etc.), polymer solutions and melts, liquid crystalline systems with various types of order (nematic, smectic, cholesteric, etc.). Unlike simple atomic fluids (whose basic constituents, the atoms, e.g. fluid Ar, have nothing but their positional degree of freedom) and unlike diatomic molecules (such as N_2, O_2, etc.), whose basic constituents have just positional and orientational degrees of freedom (neglecting the high frequency small amplitude molecular vibrations, these molecules are just treated as two point particles kept at a rigidly fixed distance), these complex fluids typically have a large number of atomic constituents. Typically they contain several species of atoms and involve different types of interactions, and sometimes they have a large number of internal degrees of freedom. Typical examples are surfactant molecules such as fatty acids that form monomolecular layers (so-called 'Langmuir monolayers', e.g. Gaines (1996)) at the air–water interface (a related system known to the reader from daily life is a thin soap film). Typically, these surfactant molecules exhibit self-assembly at an interface because of their structure, comprising a hydrophilic head group and a hydrophobic tail (e.g. a short alkane chain, cf. Fig. 6.14). Similar surfactant molecules have important practical applications as detergents, for oil recovery (when small oil droplets are dispersed in water, surfactants that gather at the oil–water interfaces are useful), and also the biological membranes that are the basis of all biological functions in the living cell are formed from similar amphiphilic phospholipid molecules.

Simulation of such systems in full atomistic detail is a very difficult task, since the single molecule is already a rather large object, with complicated interactions which are often only rather incompletely known, and since a common feature of these systems is a tendency to organize themselves in supramolecular structures on mesoscopic length scales, thermal equilibrium is rather hard to obtain. Figure 6.14 indicates one possibility to simplify the model by a kind of coarse-graining procedure: first of all, the water molecules are not considered explicitly (simulation of water and water surfaces is a difficult task itself, see Alejandre *et al.* (1995); note that there is not even a consensus on a good effective potential for water that is 'good' under all physical conditions, because of the tendency of water molecules to form bridging hydrogen bonds). Thus, the air–water interface here is simply idealized as a flat plane at $z = 0$, and it is assumed that the interaction between the hydrophilic head groups and the water substrate is so strong that the head groups are also fixed at $z = 0$, they are simply described as point-like particles which interact with a Lennard–Jones-type potential. Similar Lennard–Jones-type potentials are also assumed to act between the effective monomers. In addition, a bond angle potential $V(\theta) \propto (1 - \cos\theta)$ is used. Sometimes one even ignores the internal flexibility of these alkane chains (at low temperatures $V(\theta) \gg T$ apart from the case $\theta = 0$), and treats them as rigid rods with a single orientational degree of freedom (or, more precisely, two polar angles ϑ, φ specifying the orientation of the rod with respect to the z-axis, see Scheringer *et al.* (1992)). While this rigid-rod model clearly is too crude to exhibit much similarity with actual Langmuir monolayers, the model shown in Fig. 6.14 can describe at least qualitatively some of the experimentally observed phases of dense monolayers, such as the untilted structure and phases where the head groups form a regular triangular lattice, while the tails are uniformly tilted towards nearest or next-nearest neighbors, respectively (Schmid *et al.*, 1998). However, at present there exists no model yet that could describe all the experimentally observed phases, that include solid structures with herringbone-type ordering of the CH_2-groups in the xy-plane parallel to the water surface, for instance. However, only for these simplified models has it been possible to study phase changes (applying techniques such as finite size scaling, constant pressure simulations with variable shape of the simulation box, etc.), see Haas *et al.* (1996) and Schmid *et al.* (1998).

While these techniques are straightforwardly generalized from simple to complex fluids, other techniques (such as grand canonical ensemble, Gibbs ensemble, etc.) require special methods, because the particle insertion step for a large surfactant molecule will be rejected in the overwhelming majority of cases. Such special methods (like the 'configurational bias' method) will be discussed later in this chapter.

The situation is similar, as far as the phase behavior of surfactants in bulk solution (rather than at the air–water interface) is concerned. The classic problem is micelle formation in dilute solution (Degiorgio and Corti, 1985). Suppose molecules as shown in Fig. 6.14 are dissolved in a good solvent for

alkanes (e.g. benzene or toluol, etc.) while the solvent is a bad solvent for the head group. Then the solution behaves as ideal (i.e. a random, geometrically uncorrelated arrangement of the solute molecules) only at extreme dilution, while for larger concentrations the surfactants cluster together into aggregates, such that the hydrophilic heads form the core of the aggregate, while the tails form the 'corona' of this (star polymer-like) 'micelle'. The transition from the ideal 'gas' of individual surfactant molecules in solution to a 'gas' of micelles occurs relatively sharply at the 'cmc' (critical micelle concentration), although this is not a thermodynamic phase transition. Questions that one likes to answer by simulations concern the precise molecular structure of such micelles, the distribution of their sizes near the cmc, possible transitions between different shapes (spherical vs. cylindrical), etc. Again, there is a wide variety of different models that are used in corresponding simulations: fully atomistic models (Karaborni and O'Connell, 1990) are valuable for a description of the detailed structure of a given isolated micelle of a priori chosen size, but cannot be used to study the micellar size distribution – there one needs a very large simulation box containing many micelles (to avoid finite size effects) and a very fast simulation algorithm, because in equilibrium many exchanges of surfactant molecules between the different micelles must have occurred. Many different types of coarse-grained models have been used; often it is more realistic to have the hydrophobic and hydrophilic parts comparable in size (unlike the molecule shown in Fig. 6.14), and then one may use symmetric or asymmetric dumbbells (two point-like particles with different Lennard–Jones potential are connected by a spring of finite extensibility (see Rector *et al.*, 1994)) or short flexible chains of type A-A-B-B, where A stands for hydrophilic and B for hydrophobic (von Gottberg *et al.*, 1997; Viduna *et al.*, 1998), etc. In addition, a model where the hydrophilic part is a branched object has also been studied (Smit *et al.*, 1993). Here we cannot review this rapidly developing field, but we only try to convey to the reader the flavor of the questions that one asks and the spirit of the model-building that is both possible and necessary. Due to structure formation on mesoscopic scales, and the large number of mesophases that are possible both at interfaces and in the bulk, this field of 'soft condensed matter' is rapidly growing and still incompletely explored. Since entropy is a dominating factor regarding structure on mesoscopic scales, it is very difficult to develop analytical theories, and hence simulation studies are expected to play a very important rôle. We elaborate on this fact only for one particular example of 'complex fluids', namely polymer solutions and melts, to be described in the next section.

6.5.1 Application of the Liu–Luijten algorithm to a binary fluid mixture

A simple fluid model that nonetheless shows slow relaxation is a binary fluid mixture where the two kinds of particles are two different-sized spherical particles. Liu and Luijten (2004) simulated a system with 150 large particles and between 1200 and 506 250 small particles with size ratio varying from

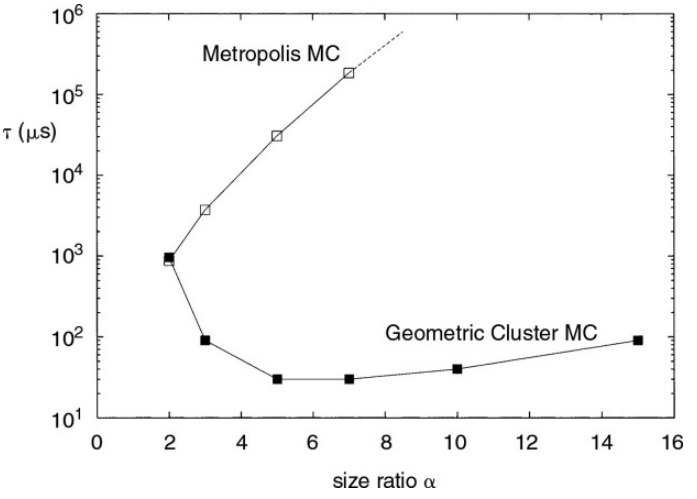

Fig. 6.15 Energy autocorrelation time for a Metropolis algorithm (open symbols) and the continuous space cluster algorithm (filled symbols) for a size asymmetric system of Yukawa particles as a function of the size asymmetry. From Liu and Luijten (2004).

2 to 15. All interactions involving small particles are hard core, but the large particles interact amongst themselves with a Yukawa repulsion

$$U_{22}(r) = \begin{cases} +\infty & r \leq \sigma_{22}, \\ \mathcal{J} \exp[-\kappa\,(r - \sigma_{22})]/\,(r/\sigma_{22}) & r > \sigma_{22}, \end{cases} \tag{6.73}$$

where $\beta\mathcal{J} = 3.0$ and the screening length $\kappa^{-1} = \sigma_{11}$. The relative efficiency as compared with Metropolis sampling is shown in Fig. 6.15. Beyond a size ratio asymmetry $\alpha = 7$ it was not possible to equilibrate the system with the Metropolis algorithm so no data can be shown for larger ratios; we can, however, anticipate that the characteristic time needed will continue to increase rapidly. For the Liu–Luijten algorithm, however, the autocorrelation time is continuing to increase relatively slowly with increasing ratios.

6.6 POLYMERS: AN INTRODUCTION

6.6.1 Length scales and models

Polymers represent an area where computer simulations are providing an ever increasing amount of information about a complex and very important class of physical systems. Before beginning a discussion of the simulation of polymer models, we want to provide a brief background on the special characteristics which are unique to polymers. For systems of small molecules, such as simple fluids containing rare gas atoms, diatomic molecules, or water etc., it is possible to treat a small region of matter in full atomistic detail. Since away from the critical point the pair correlation function often exhibits no significant structure on a length scale of 10 Å, such systems may be simulated using a box of linear dimensions 20 Å or thereabouts which contains a few thousand atoms.

For macromolecules the situation is quite different, of course (Binder, 1995). Even a single, flexible, neutral polymer in dilute solution exhibits structure

on multiple length scales ranging from that of a single chemical bond (1 Å) to the 'persistence length' (≈10 Å) to the coil radius (100 Å). Note that the persistence length (l_p) describes the length scale over which correlations between the angles formed by subsequent chemical bonds along the 'backbone' of the chain molecule have decayed. Assuming a random walk-like structure is formed by N uncorrelated subunits of length l_p, one concludes that the end-to-end distance R of this 'polymer' should scale like $R \approx l_p\sqrt{N}$ (see Section 3.8). In fact, such a random walk-like structure occurs only in rather special polymer solutions, namely at the so-called 'theta temperature', Θ, where the excluded volume repulsive interaction between the segments of the chains is effectively canceled by an attractive interaction mediated by the solvent (De Gennes, 1979). In 'good solvents', where the excluded volume interactions dominate, the coils are 'swollen' and rather non-trivial correlations in their structure develop. The radius then scales with N according to a non-trivial exponent ν, i.e. $R \propto l_p N^{\nu}$ with $\nu \approx 0.588$ in $d = 3$ dimensions while $\nu = 3/4$ in $d = 2$ dimensions (De Gennes, 1979). We have already discussed these relations in the context of self-avoiding walks on lattices in Chapter 3.

The above description applies to simple synthetic polymers such as polyethylene $(CH_2)_N$ or polystyrene $(CH_2CH(C_6H_5))_N$. Additional length scales arise for liquid-crystalline polymers, for polymers carrying electrical charges (polyelectrolytes carry charges of one sign only; polyampholytes carry charges of both sign), branched polymers, etc. Such macromolecules are not at all unimportant; a biopolymer such as DNA is an example of a rather stiff poly-electrolyte, and for some biopolymers the understanding of structure formation ('protein folding') is one of the 'grand challenge problems' of modern science.

Nevertheless we shall consider neither polyelectrolytes nor branched polymers further, since they pose special problems for simulations, and thus computer simulation of these systems is much less well developed. For polyelectrolytes the explicit treatment of the long range Coulomb interactions among the charges is a problem for the large length scales that need to be considered (Dünweg *et al.*, 1995). For polymer networks (like rubbery materials) or other branched polymers (randomly branched chains near the gel point, etc.) equilibration is a problem, and one may need special algorithms to move the crosslink points of the network. Since the chemical structure of a network is fixed one also needs to average over many equivalent configurations (Kremer and Grest, 1995). We thus restrict ourselves to flexible neutral polymers. Even then the treatment of full chemical detail is rather difficult, and simplified, coarse-grained models are often the only acceptable choice. We have already encountered the extreme case of coarse-grained models for polymers in Chapter 3 of this book where we dealt with random walks and self-avoiding walks on lattices. Of course, the precise choice of model in a simulation dealing with polymers depends very much on the type of problem that one wishes to clarify. Thus, if one wants to estimate precisely the exponent ν mentioned above or associated 'correction to scaling' exponents, the self-avoiding walk on the lattice is indeed the most appropriate model (Sokal, 1995), since these

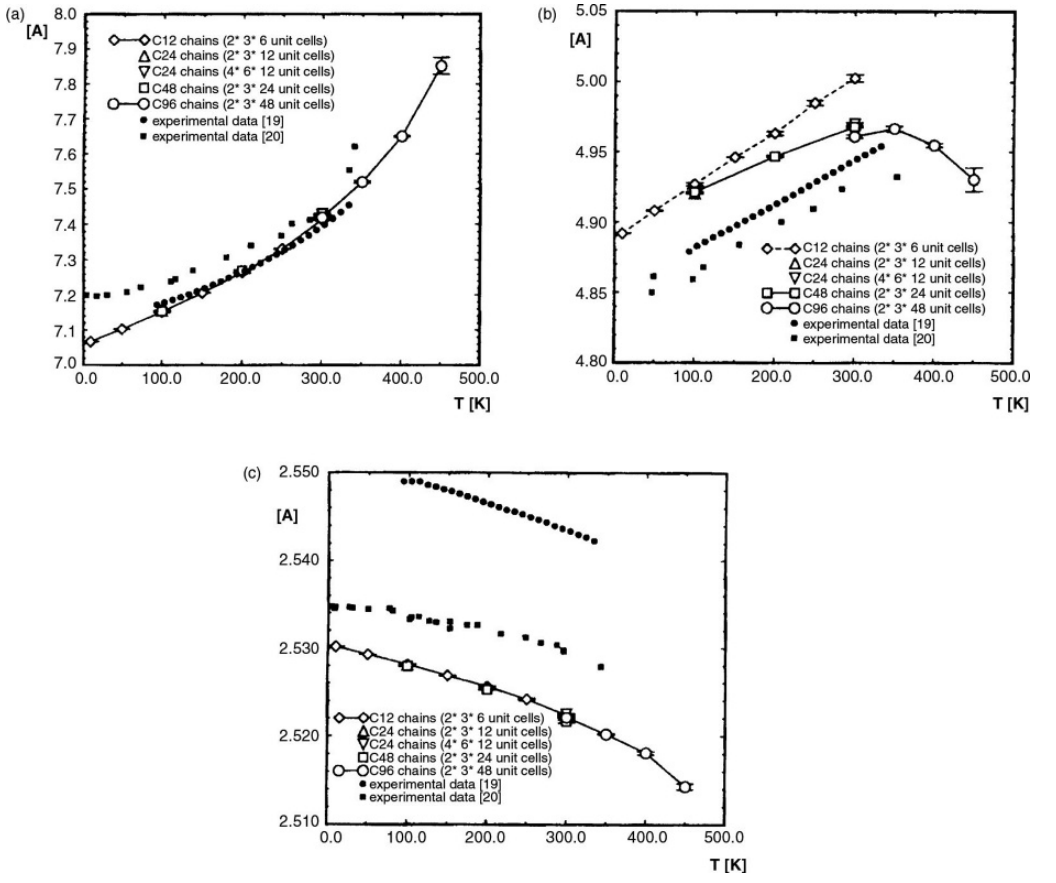

Fig. 6.16 Monte Carlo data for the temperature dependence of the lattice parameters for crystalline polyethylene together with the experimental data of Davies *et al*. (1970) (labeled as [19]) and Dadobaev and Slutsker (1981) (labeled as [20]). Lines are only guides to the eye. From Martonak *et al*. (1997).

exponents are 'universal'. On the other hand, if one wants to elucidate where the anomalous anisotropic thermal expansion of crystalline polyethylene comes from, full chemical detail must be kept in the model. In the orthorhombic phase of solid polyethylene there is a contraction of the lattice parameter c in the z-direction (Fig. 6.16c) while the lattice parameters a, b in the x, y directions expand (Fig. 6.16a, b). These experimental trends are qualitatively reproduced by the simulation but there is no quantitative agreement. (i) The simulation is classical Monte Carlo sampling in the NpT ensemble, and hence the temperature derivatives of lattice parameters $da(T)/dT$ etc. remain non-zero as $T \to 0$, while quantum mechanics requires that $da(T)/dT \to 0$ as $T \to 0$, as is also borne out by the data $T < 100$ K. (ii) There are uncertainties about the accurate choice of the non-bonded interactions, which typically are chosen of the Lennard–Jones form (suitably truncated and shifted). Even for the chemically simplest polymer, polyethylene, potentials for use in classical Monte Carlo or molecular dynamics work are not perfectly known. As one can see from the

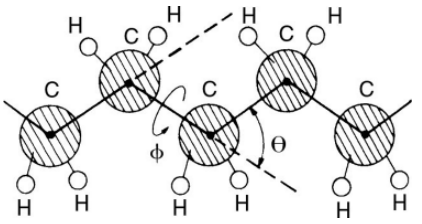

Fig. 6.17 Schematic model for polyethylene: Hydrogen atoms (H) are shown by small white circles, the carbon atoms (C) by larger shaded circles which are connected by harmonic bonds (thick straight lines) of lengths l_i. Segments are labeled consecutively by an index i ($i = 0$ to $N_p - 1$ where N_p is the degree of polymerization). Three successive segments define a bond angle Θ_i, and four successive segments define a torsional angle Φ_i. All the angles $\Phi_i = 0$ in the 'all-trans' configuration.

simulation data in Fig. 6.16, even in the case of polymer crystals there is a need to watch out carefully for finite size effects.

While in a polymer crystal the chain structure is essentially linear, in melts and solutions the chains are coils of random walk or self-avoiding walk type, and their structure needs to be characterized. There are several important quantities which can be used to characterize the behavior of polymer chains. In addition to the mean-square end-to-end distance $\langle R^2 \rangle$, the relative fluctuation of $\langle R^2 \rangle$,

$$\chi(R) = (\langle R^4 \rangle - \langle R^2 \rangle^2)/\langle R^2 \rangle^2, \tag{6.74}$$

and the mean-square gyration radius

$$\left\langle R_g^2 \right\rangle = \frac{1}{N} \sum \langle (\mathbf{r}_i - \mathbf{r}_j)^2 \rangle, \tag{6.75}$$

where $\mathbf{r}_i$ is the position of the ith monomer, are all important quantities to measure. Similarly the mean-square displacement of the center of mass of the chain,

$$g(t) \equiv \langle (\mathbf{r}_{cm}(t) - \mathbf{r}_{cm}(0))^2 \rangle \tag{6.76}$$

leads to an estimate of the self-diffusion constant of the chain from the Einstein relation,

$$D_N = \lim_{t \to \infty} \frac{g(t)}{6t}. \tag{6.77}$$

In the simulation of crystalline polyethylene, in principle the problem of large length scales is extremely severe, since the polymer is stretched out in an 'all-trans' zig-zag type linear configuration (Fig. 6.17), i.e. $R \propto N$ rather than $R \propto N^{\nu}$. This problem is overcome by neglecting the CH_3-groups at the chain ends completely and simply applying a periodic boundary condition in the z-direction. As Fig. 6.16 shows, there are non-trivial finite size effects in one of the other directions if the size of the simulation box is not large enough. In addition, this artificial periodicity prevents a physically reasonable description of the melting transition at high temperature. Significant discrepancies

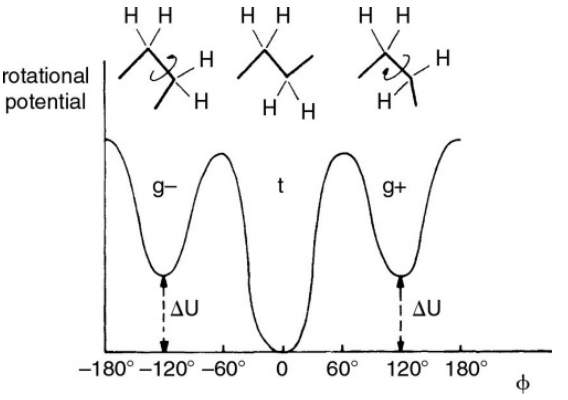

Fig. 6.18 Qualitative sketch of the torsional potential for alkane chains, indicating the three energetically preferred states gauche minus (g−), trans (t), and gauche plus (g+). The minimum of the trans configuration is deeper by an amount ΔU. From Kremer and Binder (1988).

are seen between the sets of experimental data included in Fig. 6.15; however, since polyethylene single crystals do not occur in nature, and lamellar arrangements separated by amorphous regions may occur in the laboratory, measurements may suffer from unknown systematic errors. The aim of the simulation is to realize an ideal sample of a material that cannot yet be prepared in the laboratory. Technically, a simulation of crystalline polyethylene is rather demanding (Martonak *et al.*, 1996), since the potentials for the lengths l_i of the covalent bonds and the angles θ_i between them are rather stiff, and the scale for the barriers of the torsional potential (Fig. 6.18) is an order of magnitude larger than temperatures of interest ($\sim 10^3$ K). Hence the trial displacements (Δx, Δy, Δz) of carbon atoms in the local Monte Carlo moves have to be chosen extremely small, in order to ensure that the acceptance rate of these trial moves is not too low. The relaxation of the (much weaker and slowly varying) non-bonded energy is then very slow. To overcome such problems where the Hamiltonian contains terms with very different energy scales, it is advisable to randomly mix different types of Monte Carlo moves. In the present example, global displacements of chains by amounts Δx_c, Δy_c, Δz_c were chosen, as well as rigid rotations around the c-axis, in addition to the standard local moves. In this way a reasonable convergence was achieved. If one is interested in the properties of molten polyethylene at high temperatures (i.e. $T \geq 450$ K), a study of models that include hydrogen atoms explicitly is only possible for rather small N_p (Yoon *et al.*, 1993). An approach which allows the study of larger chains is to model the system using the 'united atom' model where an entire CH_2-monomer is treated as an effective spherical entity. With such models it is still possible to equilibrate polyethylene melts at $T = 500$ K and $N_p = 100$ (Paul *et al.*, 1995). Actually these studies of melts are carried out mostly using molecular dynamics techniques rather than by Monte Carlo, simply because of the lack of efficient Monte Carlo moves for these locally stiff chains. For the study of isolated chains with realistic interactions, however, Monte Carlo techniques are very efficient, and chains as long as $N_p = 4096$ can be simulated (Ryckaert, 1996). However, it is difficult to relate a simulation of such an isolated chain in vacuum to a physically meaningful situation

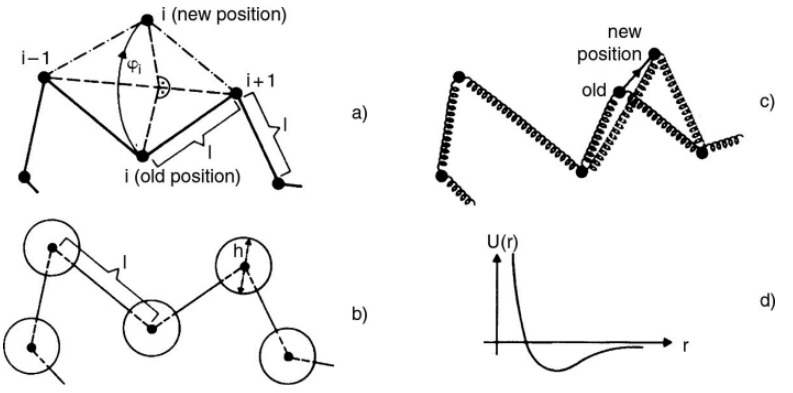

Fig. 6.19 (a–c) Several off-lattice models for polymer chains; (d) Lennard–Jones potential. For further explanations see text.

(Baschnagel *et al.*, 1992). We shall therefore not discuss such single chain simulations further, although many sophisticated Monte Carlo techniques which have already proven useful for lattice models (Sokal, 1995) are applicable to the off-lattice case as well.

In polymer science, in addition to the explanation of material properties of specific macromolecular substances by simulations, an important goal is the clarification of qualitative questions such as whether polymer chains in a melt 'reptate' (Lodge *et al.*, 1990). By 'reptation' (De Gennes, 1979) one means a snake-like motion of polymer chains along their own contour, since the 'entanglements' with other chains create an effective 'tube' along the contour that constrains the motions. Since this type of motion is a universal phenomenon, it can be studied by coarse-grained models of polymers (Fig. 6.19) where one dispenses with much of the chemical detail such as the torsional potential (Fig. 6.18). Rather one considers models where effective bonds are formed by treating $n \approx 3$–5 successive covalent bonds along the backbone of the chain in one effective subunit. While the chains are generally treated as being completely flexible, i.e. the only potentials considered are bond length potentials and non-bonded forces, a treatment of stiff chains by bond angle potentials is straightforward (Haas *et al.*, 1996). Such models are useful for describing the alkane tails in monolayers of amphiphilic fatty acids at the air–water interface (Haas *et al.*, 1996). In the freely jointed chain (a) rigid links of length l are jointed at beads (shown by dots) and may make arbitrary angles with each other. The stochastic chain conformational changes, which on a microscopic level come about by jumps between the minima of the torsional potential (Fig. 6.18), are modeled by random rotations about the axis connecting the nearest neighbor beads along the chain, as indicated. A new bead position i may be chosen by assigning an angle φ_i, drawn randomly from the interval $[-\Delta\varphi, +\Delta\varphi]$ with $\Delta\varphi \leq \pi$. For the simulation of melts, freely joined chains are often supplemented by a Lennard–Jones-type potential (Fig. 6.19) between any pairs of beads (Baumgärtner and Binder, 1981). An alternative model is the pearl-necklace model (b), where the beads are at the center of hard spheres of diameter h, which must not intersect each other. By varying the ratio h/l

one can to some extent control the persistence length of the polymer chains. With this model studies of rather long chains have been possible (Baumgärtner, 1984). The most popular model, however, is the bead-spring model (c), which is used both for Monte Carlo simulations as indicated (Milchev *et al.*, 1993) and for molecular dynamics simulations (Kremer and Grest, 1995). In both cases the non-bonded interactions are modeled by Lennard–Jones potentials among the beads or by Morse potentials, respectively. These coarse-grained off-lattice models exist in several variants, and defining a model that is optimally suited for the desired application is the first step of a successful Monte Carlo simulation in polymer science.

Problem 6.7 Write a Monte Carlo algorithm that generates recursively freely jointed chains containing N rigid links of length ℓ, i.e. start from the origin and build up a random walk step-by-step. For $N = 10$, 20, 30, 40, and 50 generate a sample of $n = 10\,000$ configurations. Use these configurations to calculate the mean-square end-to-end distance $\langle R^2 \rangle$ and the mean-square gyration radius. Analyze the ratio $\langle R^2 \rangle / \langle R_g^2 \rangle$ as a function of N.

Problem 6.8 Using the algorithm of Problem 6.7 calculate the relative fluctuation of $\langle R^2 \rangle$, i.e. $\chi(R)$, see Eqn. (6.74), as a function of N. How can you interpret the result?

Problem 6.9 Use a configuration generated in Problem 6.7 as the initial state for the algorithm shown in Fig. 6.19a, with $\Delta\phi = \pi/4$. (End bonds may rotate freely by arbitrary angles to a new point on the surface of a sphere of radius ℓ and center at the monomer adjacent to the end.) Calculate the mean-square displacement of the center of mass of the chain. Obtain the self-diffusion constant D_N of the chain from the Einstein relation (Eqn. (6.77)). Choose the time unit such that each bead on average is chosen randomly for a move once. Analyze the behavior D_N vs. N on a log–log plot.

Problem 6.10 Use a configuration of Problem 6.7 as a starting configuration for the algorithm in Fig. 6.19a, but with a Lennard–Jones interaction between the beads with $\sigma = 1/2$, $\varepsilon = 3$. Study the relaxation of the end-to-end distance. Analyze $\langle R^2 \rangle$ vs. N on a log–log plot and compare the result to the self-avoiding walk problem.

6.2.2 Asymmetric polymer mixtures: a case study

Many aspects of Monte Carlo simulations of polymeric systems are in fact rather similar to those of simulations of systems composed of atoms or small molecules. This fact will become apparent from the case study treated in this subsection, where we consider a mixture of two polymers (A, B) with different chain lengths, $N_A < N_B$. In other physical properties (shape and size of monomeric units, chain stiffness, etc.) the two types of chains are assumed to be identical, but a choice of pair–wise interaction parameters is made which

leads to unmixing:

$$\varepsilon_{AB}(\mathbf{r}) = \varepsilon_{AA}(\mathbf{r}) = \varepsilon_{BB}(\mathbf{r}) = \infty, \qquad r < r_{min}, \tag{6.78}$$

$$\varepsilon_{AB}(\mathbf{r}) = -\varepsilon_{AA}(\mathbf{r}) = -\varepsilon_{BB}(\mathbf{r}) = T\varepsilon, \qquad r_{min} \le r \le r_{max}, \tag{6.79}$$

$$\varepsilon_{AB}(\mathbf{r}) = \varepsilon_{AA}(\mathbf{r}) = \varepsilon_{BB}(\mathbf{r}) = 0, \qquad r > r_{max}. \tag{6.80}$$

If, in addition, $N_A = N_B$, there would be a symmetry in the problem with respect to the interchange of A and B, and due to that symmetry phase coexistence between unmixed A-rich and B-rich phases could only occur at a chemical potential difference $\Delta\mu = \mu_A - \mu_B = 0$ between the two species. The critical value ρ_c of the concentration ρ of species A, defined in terms of the densities of monomers ρ_A, ρ_B as $\rho = \rho_A/(\rho_A + \rho_B)$, would thus be simply $\rho_c = 1/2$ due to this symmetry between A, B. In the case of chain length asymmetry, however, this symmetry is destroyed, and then phase coexistence between the A-rich and the B-rich phase occurs along a non-trivial curve $\Delta\mu = \Delta\mu_{coex}(T)$ in the plane of variables (temperature T, chemical potential difference $\Delta\mu$). Also ρ_c now has a non-trivial value. Problems of this sort are of interest in materials science, since polymer blends have many practical applications. As a consequence we would very much like to understand to what extent simple mean-field theories of this problem, such as the Flory–Huggins theory (Binder, 1994), are reliable. These predict the critical point to be at

$$\rho_c = \left(\sqrt{N_A/N_B} + 1\right)^{-1}, \qquad (2z\varepsilon_c)^{-1} = 2\left(1/\sqrt{N_A} + 1/\sqrt{N_B}\right)^{-2}, \tag{6.81}$$

where z is the effective number of monomers within the interaction range specified in Eqn. (6.79) and ε_c is the effective value of ε (see Eqn. (6.79)) at the critical point.

An actual study of this problem has been carried out by Müller and Binder (1995) in the framework of the bond fluctuation lattice model of polymers (see Section 4.7). We nevertheless describe this case study here, because the problem of asymmetric mixtures is rather typical for the off-lattice simulations of binary mixtures in general. For the bond fluctuation model, $r_{min} = 2a$, where a is the lattice spacing, and $r_{max} = \sqrt{6}a$.

We now describe how such a simulation is carried out. The first step consists of choosing an initial, well-equilibrated configuration of an athermal ($T \to \infty$) polymer melt, consisting purely of B-chains, at the chosen total monomer density $\rho_m = \rho_A + \rho_B$. This part of the simulation is a standard problem for all kinds of polymer simulations of dense polymeric systems, because if we fill the available volume of the simulation box by putting in simple random walk type configurations of polymers, the excluded volume interaction, Eqn. (6.78), would not be obeyed. If we put in the chains consecutively, growing them step by step as growing self-avoiding walk type configurations, we would create a bias with subtle correlations in their structure rather than creating the configurations typical for chains in dense melts which do respect excluded volume interactions locally but behave like simple random walks on large length

scales, since then the excluded volume interactions are effectively screened out. Thus, whatever procedure one chooses to define the initial configuration, it needs to be carefully relaxed (e.g. by applying the 'slithering snake' algorithm or the 'random hopping' algorithm, cf. Section 4.7 for lattice models of polymers and the previous subsection for off-lattice models). In the case where large boxes containing many short polymers are simulated, one may simply put them into the box until the memory of this ordered initial configuration is completely lost. Of course, this particular choice requires that the linear dimension L of the box exceeds the length of the fully stretched polymer chain.

When dealing with problems of phase coexistence and unmixing criticality of mixtures, it is advisable to work in the semi-grand canonical ensemble, with temperature T and chemical potential difference $\Delta\mu$ being the independent thermodynamic variables. This is exactly analogous to the problem of phase coexistence and criticality in simple fluids, see Section 6.1 of the present chapter, where we have also seen that the grand canonical ensemble is preferable. However, while there it is straightforward to use Monte Carlo moves where particles are inserted or deleted, the analogous move for a mixture (an A-particle transforms into a B-particle, or vice versa) is straightforward to use only for the case of symmetric polymer mixtures (we can take out an A-chain and replace it by a B-chain in the identical conformation: essentially this identity switch is just a relabeling of the chain). Of course, there is no problem in taking out a long B-chain and using part of the emptied volume to insert a shorter A-chain, but the inverse move will hardly ever be successful for a dense polymeric system, because of the excluded volume interaction the acceptance probability for such chain insertions in practice always is zero.

But this problem can be overcome in the special situation $N_B = kN_A$, when k is an integer ($k = 2, 3, 4, \ldots$), by considering the generalized semi-grand canonical moves where a single B-chain is replaced by k A-chains, or vice versa. In the net effect, one has to cut (or insert, respectively) $k - 1$ covalent bonds together with the relabeling step. While the cutting of bonds of a B-chain is unique, the reverse step of bond insertion is non-unique, and hence one must use carefully constructed weighting factors in the acceptance probability of such moves to ensure that the detailed balance principle holds.

We shall not dwell on these weighting factors here further but rather discuss how one can find the chemical potential difference $\Delta\mu_{\mathrm{coex}}(T)$ where phase coexistence occurs, applying such an algorithm. This is done exactly with the same 'equal weight rule' that we have discussed in Section 4.2 in the context of finite size effects at first order transitions: the distribution function $P_L(\rho)$ in the $L \times L \times L$ box (with periodic boundary conditions as usual) will exhibit a double-peak structure for $\Delta\mu$ near $\Delta\mu_{\mathrm{coex}}(T)$, and at $\Delta\mu_{\mathrm{coex}}\,(T)$ the weights of the two peaks have to be equal. In practice, histogram reweighting techniques are needed (and for T far below T_c, even the application of the 'multicanonical' method is advisable, see Chapter 7) in order to sample $P_L(\rho)$ efficiently. Furthermore, several choices of L need to be studied, in order to check for finite size effects. The analysis of finite size effects is subtle particularly near the critical point, because there the 'field mixing' problem (order

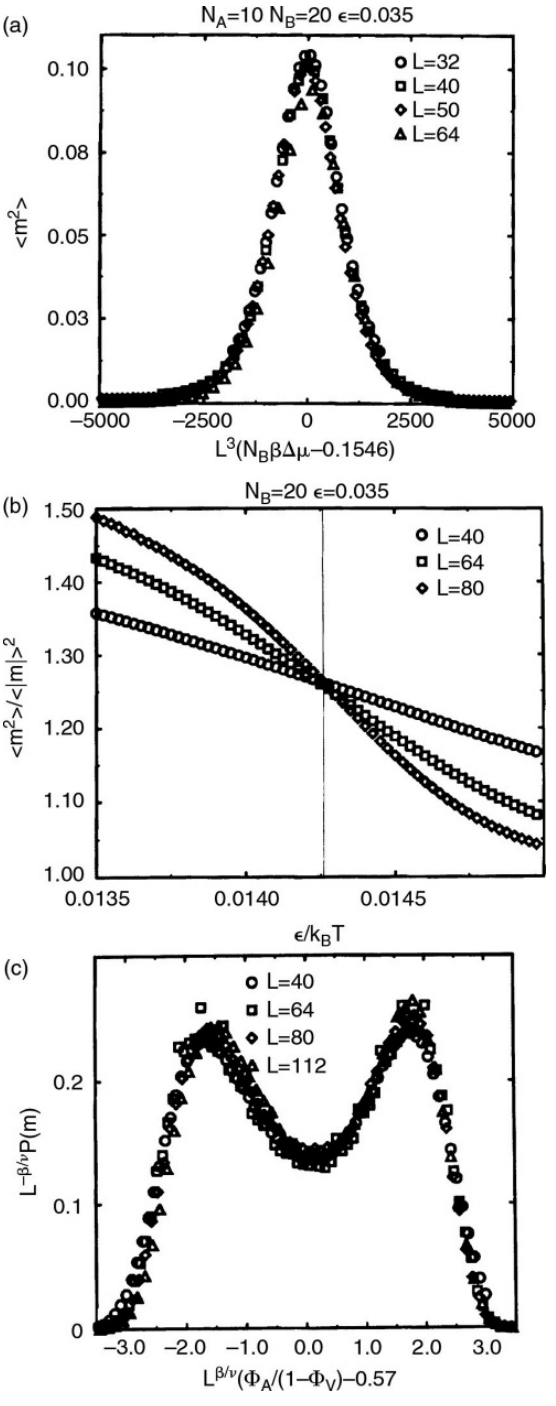

Fig. 6.20 Data for asymmetric polymer mixtures. Scaling of the second moment of the order parameter at $\varepsilon/k_B\,T = 0.035$ (a); locating the critical temperature from the intersection of moment ratios (b); scaled order parameter distribution at criticality (c). In all cases the different symbols indicate different linear dimensions L.

parameter density and energy density are coupled for asymmetric systems, see Section 4.2.3) comes into play, too.

Figure 6.20 shows typical results from the finite size scaling analysis applied to this problem. For a given choice of N_A, N_B and the normalized energy ε/k_BT, we have to find $\Delta\mu_{coex}(T)$ such that the second moment $\langle m^2\rangle$ of the order parameter $m \equiv (\rho_A - \rho_A^{crit})/(\rho_A + \rho_B)$ satisfies the finite size scaling characteristic of first order transitions as long as $T < T_c$, namely $\langle m^2\rangle$ is a universal function of $L^3(\Delta\mu - \Delta\mu_{coex}(T))$, in $d = 3$ dimensions (Fig. 6.20a). Along the line $\Delta\mu = \Delta\mu_{coex}(T)$ one can then apply the moment analysis as usual, recording ratios such as $\langle m^2\rangle/\langle|m|\rangle^2$ and $1 - \langle m^4\rangle/3\langle m^2\rangle^2$ for different choices of L, in order to locate the critical temperature T_c from the common size-independent intersection point (Fig. 6.20b). The consistency of this Ising-model type finite size scaling description can be checked for $T = T_c$ by analyzing the full order parameter distribution (Fig. 6.20c). We see that the same type of finite size scaling at T_c as discussed in Chapter 4 is again encountered, the order parameter distribution $P(m)$ scales as $P(m) = L^{\beta/\nu}\tilde{P}(mL^{\beta/\nu})$, where $\beta = 0.325$, $\nu = 0.63$ are the Ising model critical exponents of order parameter and correlation length, respectively, and the scaling function $\tilde{P}(\zeta)$ is defined numerically from the 'data collapse' of $P(m)$ as obtained for the different linear dimensions L in the figure. Of course, this data collapse is not perfect – there are various sources of error for a complicated model like the present asymmetric polymer mixture. Neither $\Delta\mu_{coex}(T)$, nor T_c and ρ_A^{crit} (= 0.57 here, see Fig. 6.20c) are known without error, there are statistical errors in the simulation data for $P(m)$ and systematic errors due to finite size scaling, etc., but the quality of this data collapse is good enough to make this analysis credible and useful. For the example chosen ($N_A = 40$, $N_B = 80$) one expects from Eqn. (6.81) that $\rho_c \approx 0.586$ and hence the finding $\rho_c = \rho_A^{crit}/(\rho_A + \rho_B) \approx 0.57$ (Fig. 6.20c) deviates from the prediction only slightly.

6.6.3 Applications: dynamics of polymer melts; thin adsorbed polymeric films

The reptation concept alluded to above is only effective if the chain length N far exceeds the chain length N_e between 'entanglements'. For short chains, with $N \approx N_e$ or less, entanglements are believed to be ineffective, and neighboring chains only hinder the motion of a chain by providing 'friction' and random forces acting on the bonds of the chain. In more mathematical terms, this is the content of the 'Rouse model' (Rouse, 1953) of polymer dynamics, where one considers the Langevin equation for a harmonic bead-spring chain exposed to a heat bath. Now it is clear that random motions of beads as considered in Fig. 6.19c can be considered as discretized realizations of such a stochastic dynamical process described by a Langevin equation. Monte Carlo moves are thus suitable for the modeling of the slow Brownian motion of polymer chains in melts, and since the non-bonded potentials can be chosen such that they have the side effect that no chain intersections can occur in the course of the

random motions of the beads, all essential ingredients of the reptation mechanism are included in the Monte Carlo algorithm. As a consequence, various Monte Carlo studies of models shown in Fig. 6.19 have been made to attempt to clarify questions about reptation theory (Bäumgartner, 1984). These simulations supplement molecular dynamics studies (Kremer and Grest, 1990) and Monte Carlo work on lattice models, e.g. Paul *et al.* (1991). One typical example is the crossover behavior in the self-diffusion of chains. From Fig. 6.19c it is clear that random displacements $\Delta\mathbf{r}$ will lead to a mean-square displacement of the center of mass of a chain of the order $(\Delta\mathbf{r}/N)^2 N \propto l^2/N$ after N moves (the natural unit of time is such that every monomer experiences an attempted displacement on average once, and the mean-square distances between the old and new positions are of the same order as the bond length square, l^2). This shows that the self-diffusion constant of the Rouse model, D_{Rouse}, should scale with chain length like $D_{\text{Rouse}} \propto 1/N$. The characteristic relaxation time, τ_{Rouse}, can be found as the time needed for a chain to diffuse its own sizes $l\sqrt{N}$. Putting $D_{\text{Rouse}}\tau_{\text{Rouse}} \propto (l\sqrt{N})^2$ and using $D_{\text{Rouse}} \propto l^2/N$ yields $\tau_{\text{Rouse}} \propto N^2$. This behavior is indeed observed both in single chain simulations at the θ-temperature (Milchev *et al.*, 1993) and for melts of very short chains (Baumgärtner and Binder, 1981).

If we consider instead the motion of very long chains, we can argue that this can be again described by a Rouse-like diffusion but constrained to take place in a tube. During the Rouse time the chain has traveled a distance proportional to $l\sqrt{N}$ along the axis of the tube. However, the axis of the tube follows the random-walk-like contour of the chain, which hence has a length proportional to lN rather than $l\sqrt{N}$. A mean-square distance of order l^2N^2, i.e. the full length of the contour, hence is only traveled in a time of order $\tau_{\text{Rouse}}N \propto N^3$. Hence the characteristic time τ_{Rep} for a chain to 'creep out' of its tube scales like N^3. On the other hand, the distance traveled in the coordinate system of laboratory space (not along the tube contour) is no more than the chain radius, $R \approx l\sqrt{N}$. Putting again a scaling relation between diffusion constant D_N and relaxation time, $D_N\tau_{\text{Rep}} \propto (l\sqrt{N})^2$ we conclude $D_N \propto N^{-2}$. In general, then, one expects that $D_N \propto N^{-1}$ for $N \ll N_e$ and $D_N \propto N^{-2}$ for $N \gg N_e$, with a smooth crossover for $N \approx N_e$.

Figure 6.21 shows that these expectations indeed are borne out by the simulations. Rescaling D by D_{Rouse} and N by N_{e} (which can be estimated independently by other means, such as an analysis of the mean-square displacement of inner monomers) one finds that Monte Carlo data for the bond fluctuation model (Paul *et al.*, 1991) and molecular dynamics data for the bead-spring model with purely repulsive Lennard–Jones interaction (Kremer and Grest, 1990) fall on a common curve. The bond fluctuation model is actually a lattice model, but unlike the self-avoiding walk model of Chapter 3 where a bead is a lattice site and a bond connects two nearest neighbor sites of the lattice, the discretization is rather fine: a bead takes all eight sites of the elementary cube of the lattice, an effective bond has a length of $\sim$3 lattice spacings, and rather than six bond vectors connecting nearest neighbor sites on the simple cubic lattice one has 108 bond vectors. The result is a rather close approximation to the

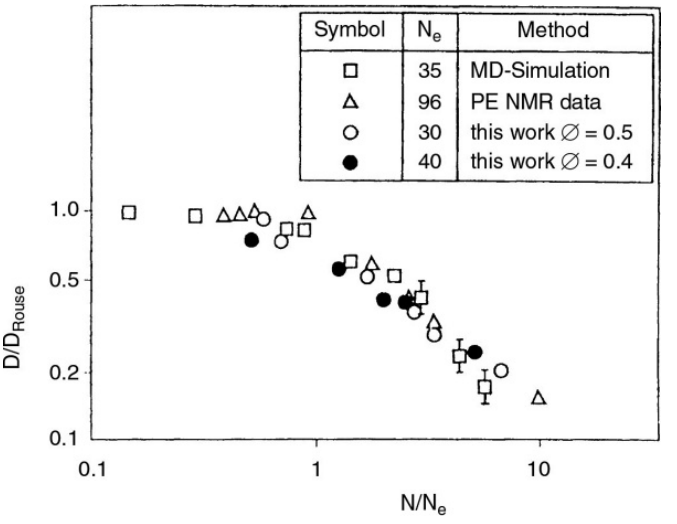

Fig. 6.21 The self-diffusion constant D of polymer melts vs. chain length N, normalized by the diffusion constant in the short chain Rouse limit, D_{Rouse}. The entanglement chain length is N_e. Circles are Monte Carlo results for the bond fluctuation model at two volume fractions Φ of occupied sites, squares are molecular dynamics results of Kremer and Grest (1990), and triangles are experimental data for polyethylene (Pearson *et al.*, 1987). From Paul *et al.* (1991).

properties of continuum models. Although Monte Carlo methods certainly omit many aspects of the dynamics of polymer melts – from bond length vibrations to hydrodynamic flows – they can model the slow Brownian diffusive motion of polymer chains rather well. This is indicated by the agreement with the experimental data on polyethylene (Pearson *et al.*, 1987). Note that there is no inconsistency in the observation that the experimental value of N_e is about three times as large as in the simulation: here the count is simply the degree of polymerization, i.e. number of C-C bonds along the backbone of the chain, while in the simulations each effective bond corresponds to $n \approx 3$–5 such C–C bonds.

As a final example, we briefly mention thin polymeric films adsorbed on walls. While the adsorption of single chains at walls from dilute solution has been studied for a long time, both in the framework of lattice (Eisenriegler *et al.*, 1982) and continuum models (Milchev and Binder, 1996), the study of many-chain systems at surfaces in equilibrium with surrounding solution has just begun. A particular advantage of the off-lattice models is that, from the virial theorem, it is straightforward to obtain the components $p_{\alpha\beta}(z)$ of the local pressure tensor as a function of the distance z from the attractive wall (Rao and Berne, 1979)

$$p_{\alpha\beta}(z) = \rho(z) k_B T \delta_{\alpha\beta} - \frac{1}{2A} \sum_{i \neq j} (\mathbf{r}_{ij})_\alpha \frac{\partial U(\mathbf{r}_{ij})}{\partial (\mathbf{r}_{ij})_\beta} \theta[(z - z_i)/z_{ij}] \theta[(z_j - z)/z_{ij}]/|z_{ij}| \quad (6.82)$$

where $p(z)$ is the local density, A is the surface area of the wall in the simulated system, θ is the step function, and U is the total potential. This pressure tensor, which generalizes the expression for the average pressure given in Eqn. (6.9), provides a good criterion for judging whether the simulation box is large enough that bulk behavior in the solution coexisting with the adsorbed layer is actually reached, since in the bulk solution the pressure tensor must be isotropic,

$$p_{xx}(z) = p_{yy}(z) = p_{zz}(z), \tag{6.83}$$

and independent of z. On the other hand, the anisotropy of the pressure tensor near the wall can be used to obtain interfacial free energies (e.g. Smit, 1988). For a geometry where the wall at $z = 0$ is attractive while the wall at the opposite surface, $z = D$, is purely repulsive, even two different interfacial free energies can be estimated (Pandey *et al.*, 1997; Nijmeijer *et al.*, 1990)

$$\gamma_{\mathrm{I}}^{\mathrm{att}} = \int_0^{D/2} dz \left[p_{zz}(z) - (p_{xx}(z) + p_{yy}(z))/2 - \rho(z) z \frac{d}{dz} \phi^{\mathrm{att}}(z) \right], \tag{6.84}$$

$$\gamma_{\mathrm{I}}^{\mathrm{rep}} = \int_{D/2}^{D} dz \left[p_{zz}(z) - (p_{xx}(z) + p_{yy}(z))/2 - \rho(z) z \frac{d}{dz} \phi^{\mathrm{rep}}(z) \right], \tag{6.85}$$

if the thickness of the system is large enough such that in the center (near $z = D/2$) the pressure tensor is isotropic. Here $\phi^{\mathrm{att}}(z)$, $\phi^{\mathrm{rep}}(z)$ denote the attractive and repulsive wall potentials.

Of course, understanding the dynamics of chains in these adsorbed layers is a particular challenge (Milchev and Binder, 1996, 1997; Pandey *et al.*, 1997). Also, non-equilibrium phenomena such as 'dewetting' can be observed (Milchev and Binder, 1997): if at time $t = 0$ the strength of the adsorption potential is strongly reduced, a densely adsorbed, very thin polymer film becomes thermodynamically unstable, and it breaks up into small droplets which slowly coarsen as time passes, similar to the coarsening observed in intermediate and late stages of spinodal decomposition of mixtures (Fig. 6.22). While some features of such simulations are qualitatively similar to those found in some experiments, one must consider the possibility that effects due to hydrodynamic flow, which are not included in the Monte Carlo 'dynamics', could be important.

Thus, for simulation of polymers it is particularly important for the reader to consider quite carefully the question of which models and simulation technique are most suitable for the investigation of a particular problem. We have not attempted to give an exhaustive survey but hope that our treatment provides a feeling for the considerations that need to be made.

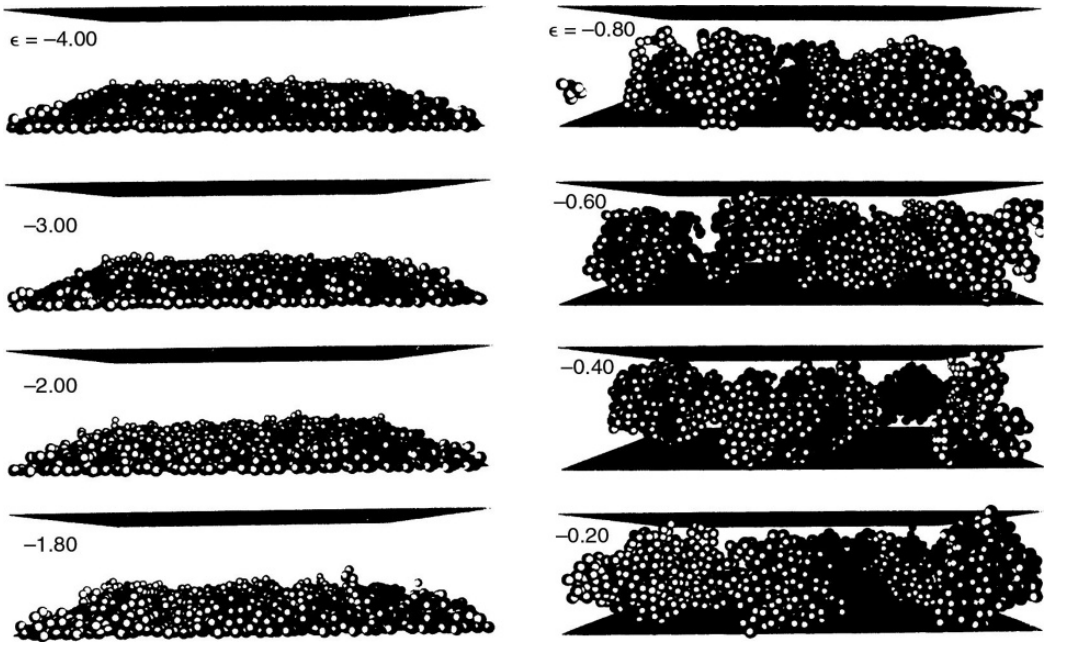

Fig. 6.22 Snapshots of a system with 64 chains, each containing $N = 32$ beads, in an $L \times L \times D$ box with $L = 32$, $D = 8$. There are periodic boundary conditions in x- and y-directions, while at $z = 0$ and $z = D$ there are impenetrable hard walls; at the bottom wall there is also an attractive square-well potential of strength ε and range $\delta = 1/8$. The chains are described by a bead-spring model with a preferred bond length of 0.7. Note that the springs between the beads are not shown. From Milchev and Binder (1997).

6.6.4 Polymer melts: speeding up bond fluctuation model simulations

In studies of melts of long polymer chains with a dynamic Monte Carlo method involving local moves (such as those in Fig. 6.19 for off-lattice models, or the random hopping algorithm for the bond fluctuation lattice model in Section 4.7.3), equilibration becomes very difficult. This should be obvious from the preceding sections, where such effects were discussed in the Rouse model (Rouse, 1953). The relaxation time τ_N increases with chain length N as $\tau_N \propto N^2$, whereas when the inability of chains to cross during their motions is taken into account in the reptation model (De Gennes, 1979), $\tau_N \propto N^3$. This dramatic slowing down in the motion of polymers is reminiscent of the problem of 'critical slowing down' (Section 4.2.5) in Ising models when the temperature approaches the critical point. In the latter case, substantial progress in improving the efficiency of the simulation algorithms was possible by using suitably constructed large-scale moves ('cluster flipping', see Section 5.1) instead of local, single spin-flip Monte Carlo moves. As shown in Fig. 5.19, algorithmic improvements were more important to speeding up the simulations than was hardware development.

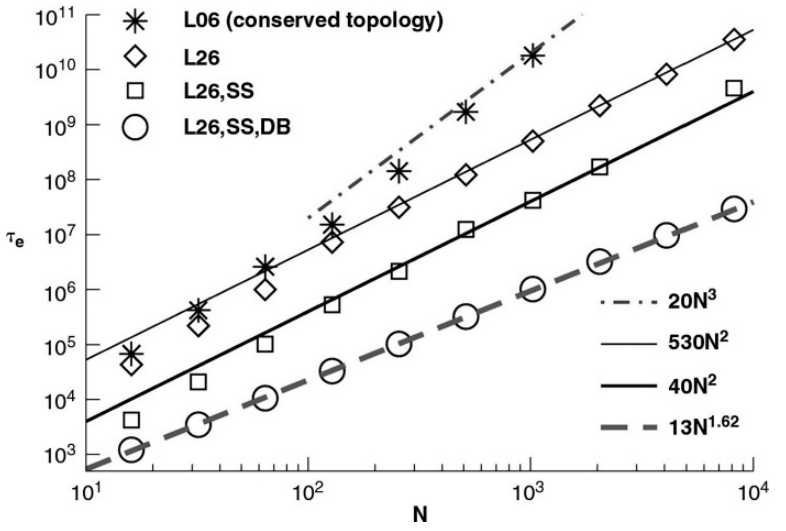

Fig. 6.23 Log–log plot of relaxation time τ_e (defined from the time needed for a chain to diffuse over its end-to-end distance) vs. chain length N for different algorithms for the bond fluctuation model at a volume fraction of the importance sampling $\phi = 0.5$. Asterisks denote the L06 algorithm, diamonds the L26 algorithm, squares the algorithm (where L26 and SS moves are randomly mixed), and circles show the algorithm where DB moves are also included (see the text). Straight lines show fits to power laws $\tau_e \propto N^3$ (dash–dotted), $\tau_e \propto N^2$ (full lines), and $\tau_e \propto N^{1.62}$ (broken line). From Wittmer *et al.* (2007).

Thus, an obvious matter of concern is whether the problem of slowing down for long polymers in dense melts (where large-scale moves like the pivot algorithm, see Fig. 4.26, are impractical since their acceptance rate would be essentially zero) can be remedied by a more clever choice of moves. This problem was recently tackled by Wittmer *et al.* (2007) who succeeded in equilibrating dense melts of polymer chains described by the bond fluctuation model, using chain lengths up to $N = 8192$ for a large system. (For a cubic simulation box of linear dimension $L = 256$ with a fraction $\phi = 0.5$ of occupied sites, which corresponds to a melt density, their system then contained $2^{20} \approx 10^6$ effective monomers.) This progress was due to the implementation of two ideas: first, rather than choosing a trial, new monomer position from only one of the six positions one lattice spacing away (the 'L06 move'), they allowed for somewhat larger local moves by picking one of 26 positions of the cube surrounding the current monomer site (the 'L26' move). The latter move allows the chains to cross each other, while the former does not; however, excluded volume constraints (each lattice site must belong to at most a single monomer) are strictly respected by both moves. Thus, with respect to the static configurations of the melt that can be sampled, there is no difference. Moreover, for the L26 move entanglement constraints are no longer effective, so one no longer expects crossover towards reptation to take place. Instead, simple Rouse-like behavior, $\tau \propto N^2$, should occur even for $N \to \infty$. Figure 6.23 shows that, for $N \leq 100$, the chains, indeed, satisfy this expectation nicely, and for $N = 1000$ already two orders of magnitude in efficiency are gained. Actually, for

$N = 8192$, simulations with the standard L06 algorithm were not possible, due to excessive demands in computer resources: we estimate that there the gain is a factor of 10^3. However, one can do even better. By combining the L26 algorithm with 'slithering snake' moves (denoted 'SS' in Fig. 6.23) we can reduce the relaxation time by a factor of 10 for all chain lengths. However, it would not be appropriate to use only slithering snake moves (Fig. 4.26) in melts, because strong back-jump correlations would render the algorithm very inefficient for large N.

An additional, remarkable improvement can be made by including 'double bridging' (DB) moves, where chain segments are switched between two different chains. Only chain segments of equal subchain lengths are swapped, so the monodisperse character of the melt (all chains have the same chain length N) is strictly conserved. All 108 bond vectors that are possible in the bond fluctuation model are tried in attempting such moves. Since it is crucial that detailed balance be satisfied, this is ensured by refusing all moves which would be possible with more than one swap partner. (This needs to be checked both for the move and the reverse move.) As one can see from Fig. 6.23, for $N = 1024$ the relaxation time is smaller than that of the standard L06 algorithm by more than four orders of magnitude (and for the largest chain length studied, $N = 8192$, the gain would be about a factor of 10^6!). With this algorithmic improvement, Wittmer *et al*. (2007) could demonstrate the (unexpected!) presence of intramolecular, long range correlations in dense polymer melts. For example, the structure factor $S(q)$ of the chains is not the structure factor $S_0(q)$ of Gaussian chains since a correction $S(q)/S_0(q) - 1 \propto q$ must be included. The DB moves can also be implemented for off-lattice models and are very useful for investigating such systems (Theodorou, 2002; Mavrantzas, 2005).

6.7 CONFIGURATIONAL BIAS AND 'SMART MONTE CARLO'

If the trial states generated in attempted Monte Carlo moves are chosen completely 'blindly', without paying particular attention to the state the system is in when the move is attempted, sometimes the acceptance rate of such a move is very small. An example is the insertion of a rod-like molecule in a nematic liquid crystal, where the molecules have some preferred orientation characterized by the nematic order parameter: if the molecule to be inserted is randomly oriented, it is very likely that the repulsive interaction with the other molecules would be too strong, and hence the trial move would be rejected. Under these circumstances it is an obvious idea to choose an 'orientational bias'. Of course, one has to be very careful that the algorithm that is devised still satisfies detailed balance and provides a distribution with Boltzmann weights in the sampling. In practice, this can be done by a suitable modification of the transition probability $W(\mathrm{o} \to \mathrm{n})$ by which the move from the old (o) to the new (n) configuration is accepted (see Frenkel and Smit (1996) for an extensive discussion). Suppose now the a priori transition probability (i.e. without

consideration of the Boltzmann factor) depends on the potential energy $U(\mathrm{n})$ of the new configuration through a biasing function $f[U(\mathrm{n})]$, $W_{\text{a priori}}(\mathrm{n} \to \mathrm{o}) = f[U(n)]$. For the reverse move we would have $W_{\text{a priori}}(\mathrm{n} \to \mathrm{o}) = f[U(\mathrm{o})]$. Then the proper choice of transition probability is a modified Metropolis criterion

$$W(\mathrm{o} \to \mathrm{n}) = \min\left\{1, \frac{f[U(\mathrm{n})]}{f[U(\mathrm{o})]} \exp\{-[U(\mathrm{n}) - U(\mathrm{o})]/k_{\mathrm{B}}T\}\right\}. \qquad (6.86)$$

This prescription is not only appropriate for the case of rigid molecules where we choose a bias for the trial orientation of a molecule that is inserted, but also holds for other cases too. For example, for flexible chain molecules the insertion of a chain molecule in a multichain system, if it is done blindly, very likely creates a configuration that is 'forbidden' because of the excluded volume interaction. Thus one biases the configuration of the chain that is inserted such that these unfavorable interactions are avoided. We emphasize that the configurational bias Monte Carlo method is not only useful in the off-lattice case, but similarly on lattices as well. In fact, for the lattice case these methods were developed first (Siepmann and Frenkel, 1992). Here the biased configuration of the chain that is inserted is stepwise grown by the Rosenbluth scheme (Rosenbluth and Rosenbluth, 1955). There one 'looks ahead' before a new bond is attached to the existing part of the chain, to see for which directions of the new bond the excluded volume constraint would be satisfied. Only from the subset of these 'allowed' bond directions is the new bond direction then randomly chosen. As has been discussed in the literature elsewhere (Kremer and Binder, 1988), we note that such biased sampling methods have serious problems for very long chains, but for chains of medium length (e.g. less than 100 steps on a lattice) the problem of estimating the statistical errors resulting from such techniques is typically under control. In this step-wise insertion of the polymer chain, one constructs the Rosenbluth weight $W(\mathrm{n})$ of this chain – which is the analog of the biasing function f mentioned above – according to the usual Rosenbluth scheme. In order to be able to introduce the appropriate correction factor $W(\mathrm{n})/W(\mathrm{o})$ in the modified Metropolis criterion, one has to select one of the chains, that are already in the system at random, and retrace it step by step from one end to calculate its Rosenbluth weight. Of course, this type of algorithm can also be extended to the off-lattice case. The configurational bias algorithm works very well for polymer solutions but becomes less efficient as the monomer density increases. For relatively dense polymer systems, an extension of the configurational bias method termed 'recoil growth' (Consta *et al.*, 1999) seems rather promising. Alternative methods for dense polymer systems were already treated in Section 4.7.

Still another type of biased sampling, that sometimes is useful, and can even be applied to simple fluids, is force bias sampling (Ceperley *et al.*, 1977; Pangali *et al.*, 1978): one does not choose the trial move of a chosen particle completely blindly at random, but biases the trial move along the forces and torques acting on the particles. One wishes to choose the transition probability W_{ij} to move

from state i to state j proportional to the Boltzmann factor $\exp(U_j/k_BT)$: then detailed balance will be automatically satisfied. Assuming that states i and j are close by in phase space, differing only by center of mass displacements $\mathbf{R}_m(j) - \mathbf{R}_m(i)$ of molecule m and by an angular displacement $\boldsymbol{\Omega}_m(j) - \boldsymbol{\Omega}_m(i)$ (in a formulation suitable for rigid molecules, such as water, for instance). Then one can expand the energy of state j around the energy of state i to first order, which yields

$$W_{ij} = \frac{W_{ij}^{\mathrm{M}}}{Z(i)} \exp\left\{\frac{\lambda}{k_BT}(\mathbf{F}_m(i)\cdot[\mathbf{R}_m(j)-\mathbf{R}_m(i)] + \mathbf{N}_m(i)\cdot[\boldsymbol{\Omega}_m(j)-\boldsymbol{\Omega}_m(i)])\right\}, \tag{6.87}$$

where W_{ij}^{M} is the usual Metropolis acceptance factor $\min\{1, \exp[-(U_j - U_i)/k_BT]\}$, and $\mathbf{F}_m(i)$ is the total force acting on molecule m in state, and $\mathbf{N}_m(i)$ is the corresponding torque. Here $Z(i)$ is a normalization factor and λ is a parameter in the range $0 \le \lambda \le 1$: $\lambda = 0$ would be the unbiased Metropolis algorithm, of course. Note that the displacements have to be limited to fixed (small) domains around the initial values $\mathbf{R}_m(i)$ and $\boldsymbol{\Omega}_m(i)$.

An alternative force bias scheme proposed by Rossky *et al.* (1978) was inspired by the 'Brownian dynamics' algorithm (Ermak, 1975), where one simulates a Langevin equation. For a point particle of mass m this Langevin equation describes the balance of friction forces, deterministic, and random forces:

$$\ddot{\mathbf{r}} = -\dot{\mathbf{r}}\zeta + (\mathbf{F} + \boldsymbol{\eta}(t))\,m,$$

where ζ is the friction coefficient, $\mathbf{F} = -\nabla U$ is the force due to the potential, and $\boldsymbol{\eta}(t)$ is a random force, which is linked to ζ in thermal equilibrium by a fluctuation–dissipation relation. A simulation of this Langevin equation could be done by discretizing the time derivatives $\dot{\mathbf{r}} = d\mathbf{r}/dt$ as $\Delta\mathbf{r}/\Delta t$ to find

$$\Delta\mathbf{r} = (D/k_BT)\mathbf{F}\Delta t + \Delta\boldsymbol{\rho}, \tag{6.88}$$

where $\Delta\mathbf{r}$ is the change of $\mathbf{r}$ in a time step Δt, $\mathbf{F}$ is the force on the particle at the beginning of the step, D is the diffusion constant of the particle in the absence of interparticle interactions, and $\Delta\boldsymbol{\rho}$ is the random displacement corresponding to the random force. For a faithful description of the dynamics that would follow from the Langevin equation, Δt and $\Delta\boldsymbol{\rho}$ would have to be very small. However, if we are interested in static equilibrium properties only, we can allow much larger Δt, $\Delta\rho$ and use the corresponding new state obtained from $\mathbf{r}' = \mathbf{r} + \Delta\mathbf{r}$ as a trial move in a Metropolis Monte Carlo sampling. This is the basic idea behind the algorithm proposed by Rossky *et al.* (1978) and called 'smart Monte Carlo'.

A very straightforward type of biased sampling is useful for dilute solutions (Owicki and Scheraga, 1977): one does a preferential sampling of molecules close to a solute molecule. In fact, this idea is similar to the preferential

selection of sites near external surfaces or internal interfaces which has already been discussed for lattice models, e.g. in Section 5.9.1.

There are many conditions where such biased Monte Carlo methods produce equilibrium faster than do the standard Monte Carlo methods; but often molecular dynamics (Chapter 12) is then even more efficient. Thus the choice of 'which algorithm and when' remains a subtle problem.

6.8 ESTIMATION OF EXCESS FREE ENERGIES DUE TO WALLS FOR FLUIDS AND SOLIDS

For a fluid (or solid) confined by two planar walls at $z = 0$ and $z = D$, assuming N particles in a volume $V = L^2 D$ with periodic boundary conditions in x and y directions, the free energy F of the system for large enough D can be written as the sum of a bulk and surface terms,

$$F = L^2 D f_{\mathrm{b}}(T, \rho) + 2L^2 \gamma_{\mathrm{I}}(T, \rho), \qquad \rho = N/V, \tag{6.89}$$

where $f_{\mathrm{b}}(T, \rho)$ is the bulk free energy density, and $\gamma_{\mathrm{I}}(T, \rho)$ is the excess free energy per unit area due to the fluid–wall interface. We have already mentioned the estimation of this interfacial free energy via the method based on the anisotropy of the stress tensor (Sections 6.1 and 6.6); however, this method is plagued by low accuracy because of the difficulty in determining a small excess by subtracting two large numbers from each other. The same problem occurs when estimating the absolute free energy of the fluid (e.g. with a version of thermodynamic integration devised by Schilling and Schmid, 2009) for different film thickness D (Deb *et al.*, 2012), using Eqn. (6.89) directly. While the feasibility of this brute-force approach has been demonstrated for a fluid of hard spheres (Deb *et al.*, 2012), alternative routes for the computation of γ_{I} that avoid the computationally costly computation of F are desirable.

At this point we mention that the estimation of γ_{I} is of particular interest for fluids under conditions where they can exist in two phases: a simple fluid can exist as vapor (v) or liquid (ℓ) near the condensation transition, or as liquid or crystal near solidification. For a binary (A, B) mixture, phase separation into A-rich and B-rich phases may occur. In all such cases, estimating γ_{I} is valuable within the context of wetting phenomena. For example, for a fluid at vapor–liquid coexistence one may distinguish the state of the wall as 'wet' or 'partially wet' when the wall is in contact with the vapor.

For the case of partial wetting, a liquid droplet attached to the wall will have a contact angle θ described by Young's equation,

$$\gamma_{wv}(T) - \gamma_{w\ell}(T) = \gamma(T) \cos\theta, \qquad 0 < \theta < \pi, \tag{6.90}$$

where $\gamma_{wv}(T)$, $\gamma_{w\ell}(T)$ are the wall–vapor and wall–liquid interfacial tensions, while $\gamma(T)$ is the interfacial tension between coexisting vapor and liquid phases. When $\gamma_{wv}(T) - \gamma_{w\ell}(T) \geq \gamma(T)$, (complete) wetting occurs, while the opposite case ($\gamma_{wv}(T) - \gamma_{w\ell}(T) \leq -\gamma(T)$) corresponds to 'drying'. Note that

unlike Eqn. (6.89), which does not refer to phase coexistence, the temperature T has been written as a single argument in all interfacial tensions. This is because the condition of vapor–liquid phase coexistence implies equality of the chemical potentials and pressures of both coexisting phases. Due to these equations, the densities ρ_v, ρ_ℓ at phase coexistence are already fixed.

For many physical phenomena knowledge of contact angles of droplets (and related quantities like the 'line tension', the excess free energy due to the three-phase contact line vapor–liquid–wall) is of interest. However, estimating them from direct observation of sessile droplets attached to walls is cumbersome since these droplets undergo strong, long-lived fluctuations (Milchev and Binder, 2001), and hence indirect methods were developed (for a review see Binder *et al.*, 2011).

For systems that exhibit symmetry between the two coexisting phases, a thermodynamic integration approach is convenient for obtaining the necessary difference in wall free energies that is needed for Young's equation. As an example, a case study of a binary Lennard–Jones mixture will be presented in Section 6.9.

In the general case, for phase coexistence of fluids or fluid mixtures there is no symmetry between the coexisting phases and no reference state for which the contact angle is known from symmetry. In this case, however, the reference state that can be used for a thermodynamic integration approach is a system with fully periodic boundary conditions, i.e. without walls. Then, $\gamma_{\mathrm{I}}(T, \rho)$ in Eqn. (6.89) is simply zero, and the goal is to construct a path in phase space that connects this system with a system confined by walls so that Eqn. (6.89) applies. This can be done by defining an intermediate Hamiltonian $\mathcal{H}(\vec{X})$ that interpolates between a system of N particles in a volume V without ($\mathcal{H}_1(\vec{X})$) and an equivalent system with walls ($\mathcal{H}_2(\vec{X})$),

$$\mathcal{H}(\vec{X}) = (1-\kappa)\mathcal{H}_1(\vec{X}) + \kappa\mathcal{H}_2(\vec{X}), \tag{6.91}$$

where $\vec{X}$ again describes a point in configuration space (or 'microstate'), and the parameter $\kappa \in [0, 1]$ needs to be varied to compute the free energy difference between systems 1 and 2, which is exactly the second term on the right-hand side of Eqn. (6.89).

The system described by the Hamiltonian in Eqn. (6.91) can never be realized in a laboratory experiment but is readily implemented in a computer simulation. This again nicely illustrates how simulation can go beyond experiment. In practice, computing the free energy difference between systems 1 and 2 still is a challenge, since when $f_{\mathrm{I}}\sigma^2/k_{\mathrm{B}}T$ is of order unity, the free energy difference that needs to be computed is larger by a factor $2(L/\sigma)^2$, σ being the molecular length of interest (Lennard–Jones diameter, or hard sphere diameter, etc.). Since $L/\sigma \gg 1$ is necessary, the task of using Eqn. (6.91) to calculate the free energy difference resulting from the introduction of walls is rather demanding. In practice, this is solved by discretizing the interval for κ into a large number (e.g. 100) discrete states $\{\kappa_i\}$ and considering Monte Carlo moves from a system with $\kappa = \kappa_i$ to a neighboring system κ_{i+1} or κ_{i-1}, respectively. The relative probability $P(i)$ of residing in state i can be

estimated by Wang–Landau sampling (see Section 7.8) or successive umbrella sampling (see Section 7.1.2). The free energy difference between the two states i and $i+1$ is given by $k_B T[\ln P(i) - \ln P(i+1)]$. In this way, it is possible to compute the free energy difference $\Delta F(D)$ for a chosen cross-sectional area L^2 and perform the extrapolation

$$\gamma_I = \lim_{D\to\infty} \Delta F(D)/(2L^2). \tag{6.92}$$

The extrapolation written in Eqn. (6.92) is necessary, since a system with walls generally has an interfacial excess density, $\rho(T, D, \mu) = \rho_b(T, \mu) + (2/d)\rho_I(T, \mu)$. In the canonical ensemble at temperature T, we fix $\rho_b = N/V$; but if we eliminate μ in favor of ρ_b it is clear that the density of a system with walls differs by a $1/D$-correction from ρ_b, and this leads to a $1/D$-correction in γ_I as well. Since the number of discrete values $\{\kappa_i\}$ needs to be of the order of $(L/\sigma)^2$, this method requires a significant sampling effort. But, unlike the method based on the anisotropy of the pressure tensor, Eqns. (6.91) and (6.92) also yield useful results for crystals (remember that in a crystal the pressure tensor reflects the crystal anisotropy in the bulk). Deb *et al.* (2012) have demonstrated the usefulness of this approach for both the simple hard-sphere model of the fluids and the Asakura–Oosawa model of colloid–polymer mixtures.

When we wish to vary the wall potential, e.g. the parameter ε_a in Eqns. (6.93) and (6.94), see Section 6.9, it should be possible to use the method based on Eqns. (6.91) and (6.92) only for the construction of a reference system for which γ_I is known. Data may then be obtained for other values of ε_a by a thermodynamic integration as we shall show in the case study in the next section.

6.9 A SYMMETRIC, LENNARD–JONES MIXTURE: A CASE STUDY

We consider an (A, B) Lennard–Jones mixture, with Lennard–Jones potential parameters (see Eqn. (6.4)) $\sigma_{AA} = \sigma_{AB} = \sigma_{BB} = \sigma$ and $\varepsilon_{AA} = \varepsilon_{BB} = 2\varepsilon_{AB} = \varepsilon$. For a thin film with 'antisymmetric' wall potentials, e.g. the potential acting on A-particles is

$$u_A(z) = \frac{2\pi\rho}{3}\left\{\varepsilon_r\left[\left(\frac{\sigma}{z+\delta}\right)^9 + \left(\frac{\sigma}{D+\delta-z}\right)^9\right] - \varepsilon_a\left(\frac{\sigma}{z+\delta}\right)^3\right\}, \tag{6.93}$$

and similarly for B-particles

$$u_B(z) = \frac{2\pi\rho}{3}\left\{\varepsilon_r\left[\left(\frac{\sigma}{z+\delta}\right)^9 + \left(\frac{\sigma}{D+\delta-z}\right)^9\right] - \varepsilon_a\left(\frac{\sigma}{D+\delta-z}\right)^3\right\} \tag{6.94}$$

Here the parameter $\delta = \sigma/2$ is used to avoid singularities at the walls, and the repulsive parts of the wall potentials (proportional to ε_r) ensure the confinement of the particles in the film. We see that A-particles are attracted to the wall at $z = 0$ with the same strength (ε_a) as B-particles are attracted to the wall at $z = D$. For $\varepsilon_a = 0$ an interchange of A and B leaves the model invariant, and we conclude that $\gamma_{w,\text{A-rich}}(T) = \gamma_{w,\text{B-rich}}(T)$ and $\theta = \pi/2$, i.e. interfaces between the A-rich and B-rich phases are oriented perpendicularly to the walls. Thus, we have a reference state that can conveniently be used for thermodynamic integration.

In order to derive a relation that can be used for thermodynamic integration, we take a derivative of the free energy with respect to ε_a,

$$F = -k_\text{B}T \ln Z = -k_\text{B}T \ln \int d\vec{X} \times \exp\left\{ -\beta\mathcal{H}_b(\vec{X}) - \beta\mathcal{H}_w^r(\vec{X}) + \beta\varepsilon_a L^2(2\pi\rho/3) \times \left[\int_0^D \rho_\text{A}(z)\left(\frac{\sigma}{z+\delta}\right)^3 dz + \int_0^D \rho_\text{B}(z)\left(\frac{\sigma}{D+\delta-z}\right)^3 dz \right] \right\}, \quad (6.95)$$

where $\vec{X}$ denotes the microstate of the system, $\mathcal{H}_b(\vec{X})$ describes the bulk part of the potential energy, and $\mathcal{H}_w^r(\vec{X})$ the energy due to the repulsive part of the wall potential. This yields derivatives of the interfacial free energies with respect to ε_a expressed in terms of convolutions of the average density profiles $\langle\rho_\text{A}(z)\rangle$, $\langle\rho_\text{B}(z)\rangle$ of the particles with the attractive part of the wall potential (Das and Binder, 2011),

$$\left(\frac{\partial\gamma^{(z=0)}}{\partial\varepsilon_a}\right)_T = \frac{2\pi\rho}{3}\int_0^D dz\left(\frac{\sigma}{z+\delta}\right)^3\langle\rho_\text{A}(z)\rangle, \quad (6.96)$$

$$\left(\frac{\partial\gamma^{(z=D)}}{\partial\varepsilon_a}\right)_T = \frac{2\pi\rho}{3}\int_0^D dz\left(\frac{\sigma}{D+\delta-z}\right)^3\langle\rho_\text{B}(z)\rangle. \quad (6.97)$$

These equations are readily integrated to yield an expression for the contact angle, using Young's equation for the binary mixture

$$\gamma_\text{AB}(T)\cos\theta = (2\pi\rho/3)\int_0^{\varepsilon_a} d\varepsilon_a' \int_0^D dz \left[\langle\rho_\text{A}(z)\rangle_\text{A-rich}\left(\frac{\sigma}{z+\delta}\right)^3 - \langle\rho_\text{B}(z)\rangle_\text{A-rich}\left(\frac{\sigma}{D+\delta-z}\right)^3 \right]. \quad (6.98)$$

Note that $\gamma_\text{AB}(T)$ is conveniently estimated from sampling the height of the peak of the negative logarithm of the order parameter distribution, as will be

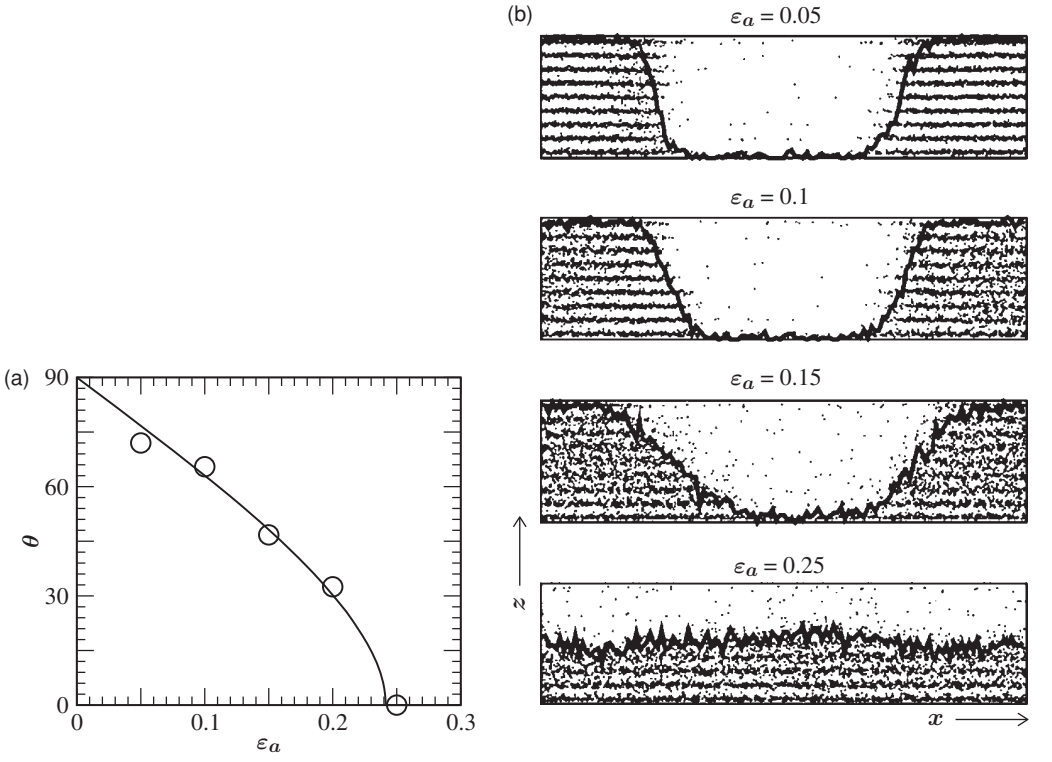

Fig. 6.24 (a) Contact angle θ as a function of the attractive surface potential ε_a for a symmetric, binary Lennard–Jones mixture at $T/T_c = 0.703$. Open circles show estimates from direct observation of inclined interfaces for films in the canonical ensemble for a 50–50% AB system; the full curve is from Eqn. (6.98). (b) Snapshots of an $L \times L \times D$ system with $L = 32$, $D = 8$, displaying only the A-particles as black dots projected into the xz-plane. Thick curves show instantaneous interface positions (averaged over the y-coordinate). The contact angle is estimated from the maximum slope of these profiles. Note that in this dense system ($\rho\sigma^3 = 0.80$) the total density $\rho(z)$ exhibits strong layering throughout the film. From Das and Binder (2011).

discussed in Section 7.6.4. For the binary mixture the order parameter is the relative concentration of species A.

Figure 6.24 shows an example, recorded for $T/T_c = 0.703$, plotting the contact angle θ versus ε_a for this binary Lennard–Jones model. For comparison snapshots of systems at 50% relative concentration are included, where the interfaces can be directly observed. For $\varepsilon_a = 0.25$, complete wetting has occurred, and it is then favorable for the system to form a single A–B interface parallel to the wall. Note that the snapshots are from a simulation carried out in a canonical ensemble where both particle numbers N_A, N_B are separately conserved ($N_A = N_B = N/2$). The application of Eqn. (6.98), however, uses a semi-grand-canonical ensemble with vanishing chemical potential difference between the particles, so the density profiles $\langle \rho_A(z) \rangle_{A\text{-rich}}$, $\langle \rho_B(z) \rangle_{A\text{-rich}}$ are computed from configurations that contain no A–B interfaces (see Das and Binder (2011) for more details).

6.10 FINITE SIZE EFFECTS ON INTERFACIAL PROPERTIES: A CASE STUDY

When studying properties relating to interfaces between coexisting phases by Monte Carlo simulation, one inevitably deals with a situation of phase coexistence between distinct phases inside the simulation box. In such a situation, typically finite size effects are more pronounced than in the study of properties of a single homogeneous system for which there is only a single bulk phase contained in the simulation box.

Grzelak and Errington (2010) demonstrated by a model calculation that a particularly convincing control of finite size effects on interfacial properties is possible when one combines information obtained from systems simulated in different statistical mechanical ensembles, e.g. (for a monatomic system) the canonical (cn) and grand canonical (gc) ensemble. Of course, in the thermodynamic limit the results from the different ensembles (which then are related via Legendre transformations, see Section 2.1) are strictly equivalent, but the finite size corrections generally differ. A study of the size dependence of properties of the same system in different ensembles is then a viable strategy to enable a reliable extrapolation to the thermodynamic limit.

The model of Grzelak and Errington (2010) was a simple Lennard–Jones (LJ) fluid (truncated at a cutoff distance $r_c = 2.5\sigma$, σ being the range parameter of the LJ potential), while the system contained adsorbing walls (a distance $H = 40\sigma$ apart) at which a (9, 3) potential acts

$$u_w(z) = \frac{2\pi}{3}\rho_w\sigma_{w\ell}^3\varepsilon_{w\ell}\left[\frac{2}{15}\left(\frac{\sigma_{w\ell}}{z}\right)^9 - \left(\frac{\sigma_{w\ell}}{z}\right)^3\right], \tag{6.99}$$

where the parameters were chosen as $\rho_w\sigma_{w\ell}^3 = 0.988$, $\sigma_{w\ell}/\sigma = 1.0962$, $\varepsilon_{w\ell}/\varepsilon = 1.1494$, and we focus here on a choice of temperature $k_BT/\varepsilon = 0.8$, ε being the energy parameter of the LJ potential. Thus, the simulation is done far below the vapor–liquid critical point of the fluid in the bulk, any finite size effects associated with criticality hence are not our concern here.

This system undergoes a so-called 'prewetting' phase transition during which the surface excess density of the vapor (which is at the pressure where it is still under-saturated in the bulk) exhibits (in the thermodynamic limit) a jump from a very small value to a somewhat larger value. Analyzing the particle number distribution functions for finite cross-sectional area $A = L^2$ (with periodic boundary conditions in the directions parallel to the walls, as usual) one finds that the chemical potential at the prewetting transitions μ^{pre} varies as

$$\mu^{\text{pre}}(L) = \mu^{\text{pre}}(\infty) + c\,L^{-2}, \tag{6.100}$$

where c is a constant whose value depends on the statistical ensemble that is used (Fig. 6.25). Note that a prewetting transition is a first order transition in a two-dimensional volume (since it can be considered as a singularity of a surface excess free energy of the system), so the power (–2) of the finite size

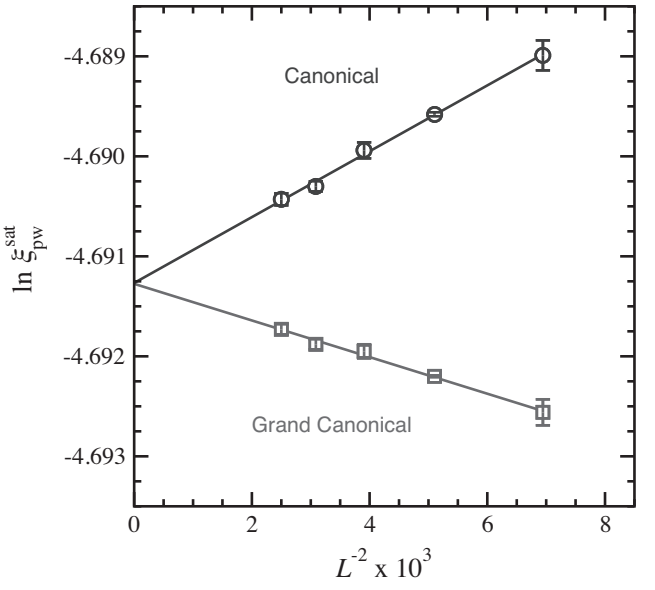

Fig. 6.25 System size dependence of the normalized chemical potential $\mu^{pre}(L)/k_B T$ (which is written here as logarithm of the activity coefficient $\ln \zeta_{pre}^{sat}$) at $k_B T/\varepsilon = 0.8$ for a truncated LJ fluid exposed to a wall where the potential Eqn. (6.99) acts. Circles and squares represent canonical and grand canonical based estimates, for linear dimensions $L/\sigma = 12$, 14, 16, 18, and 20. From Grzelak and Errington (2010).

correction in the above equation is nothing but a 1/(volume) correction, as expected. Figure 6.25 demonstrates that $\mu^{pre}(\infty)$ estimated in this way agrees nicely for both ensembles, and this agreement is evidence that the accuracy of the estimates for finite L used in this extrapolation is well under control. However, using only a single value of L (in one of the ensembles) the presence of the cL^{-2} correction would provide a significant systematic error. In many studies of bulk phase behavior of various systems, such size effects are ignored completely, and hence we emphasize the caveat that (1/volume)-corrections due to the finite size are very often present, although rarely documented.

Of course, obtaining the precise locations of $\mu^{pre}(L)$ is already a demanding task, making a very precise estimation of the variation of the particle number distribution $P_L(N)$ with the chemical potential μ necessary. There are various methods to do this, as discussed in various instances in this book, e.g. successive umbrella sampling or Wang–Landau sampling. Grzelak and Errington (2010) used transition matrix Monte Carlo (Errington, 2003) for this purpose.

Within the context of the study of wetting phenomena of fluids, it is also of interest to study the interfacial tension $\gamma_{\ell v}$ between coexisting bulk liquid (ℓ) and vapor (v) phases, as well as the corresponding wall tensions γ_{sv}, $\gamma_{s\ell}$ between the surface (s) of the confining container and the vapor or liquid, respectively. As was discussed in Section 6.8, under conditions of incomplete wetting, these interfacial tensions control the contact angle. A related quantity of interest is the 'spreading coefficient' $s = \gamma_{s\ell} - (\gamma_{sv} + \gamma_{\ell s})$: it changes sign at the wetting transition.

Also these quantities can be extracted from sampling the particle number distributions, but under conditions corresponding to liquid-vapor phase coexistence in the bulk. Figure 6.26 presents an analogous finite size extrapolation of βs ($\beta = 1/k_B T$) vs. $\ln(L)/L^2$. The presence of a $\ln(L)/L^2$ correction can

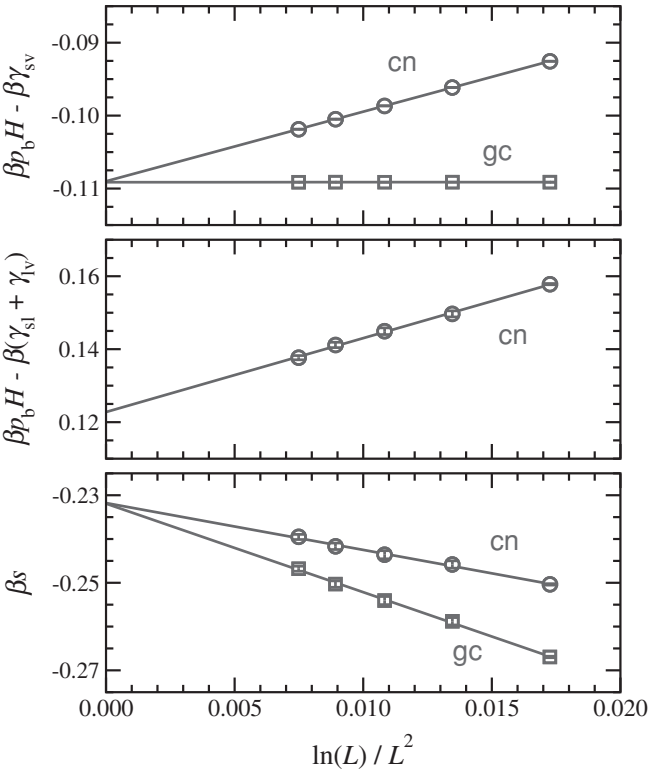

Fig. 6.26 Spreading coefficient βs plotted vs $\ln(L)/L^2$, for the same system as in Fig. 6.25, but for conditions of phase coexistence in the bulk, at a temperature $k_B T/\varepsilon = 0.65$. From Grzelak and Errington (2010).

presumably be attributed to the translational entropy of the slab configuration used to estimate $\gamma_{\ell v}$ from the particle number distribution using a simulation of a system with periodic boundary conditions also in the direction perpendicular to the slab (Binder, 1982; Errington, 2003). Note that in two-dimensional systems (with a one-dimensional interface) a stronger $\ln(L)/L$ correction can be proven to occur in the Ising model (Privman, 1988) due to capillary waves. Again the good agreement between the extrapolation carried out in the *gc* and *cn* ensembles lends additional credibility to the chosen approach. Thus, the present case study shows that the examination of wetting phenomena for simple off-lattice models of fluids by Monte Carlo simulations has reached a state of maturity, where quantitatively reliable results can be extracted. We emphasize again the statement, however, that the claim often made in the literature 'finite size effects far away from critical points are negligible' is not valid in general.

6.11 OUTLOOK

For off-lattice systems the determination of the free energy may be particularly important for the identification of 'ordered states' in systems with complex free energy landscapes as well as for the location of phase transitions. This is not

an altogether trivial task, and a good overview of the current status of ways in which the free energy can be calculated can be found in Müller and de Pablo (2006). At this juncture we also wish to mention to the reader that the modifications to the Wang–Landau sampling method for use in continuous systems, to be described in Section 7.8.2, provide a means by which the free energy in such systems may be readily determined.

REFERENCES

Alder, B. J. and Wainwright, T. E. (1962), *Phys. Rev.* **127**, 359.

Alejandre, J., Tildesley, D. J., and Chapela, G. A. (1995), *J. Chem. Phys.* **102**, 4574.

Allen, M. P. (1996), in *Monte Carlo and Molecular Dynamics of Condensed Matter Systems*, eds. K. Binder and G. Ciccotti (Società Italiana di Fisica, Bologna), p. 255.

Asakura, S. and Oosawa, F. (1954), *J. Chem. Phys.* **12**, 1255.

Baschnagel, J., Qin, K., Paul, W., and Binder, K. (1992), *Macromolecules* **25**, 3117.

Baumgärtner, A. (1984), *Ann. Rev. Phys. Chem.* **35**, 419.

Baumgärtner, A. and Binder, K. (1981), *J. Chem. Phys.* **75**, 2994.

Bernard, E. P. and Krauth, W. (2011), *Phys. Rev. Lett.* **107**, 155704.

Bernard, E. P. and Krauth, W. (2012), *Phys. Rev. E* **86**, 017701.

Bernard, E. P., Krauth, W., and Wilson, D. B. (2009), *Phys. Rev. E* **80**, 056704.

Binder, K. (1982), *Phys. Rev. A* **25**, 1699.

Binder, K. (1994), *Adv. Polymer Sci.* **112**, 181.

Binder, K. (ed.) (1995), *Monte Carlo and Molecular Dynamics Simulations in Polymer Science* (Oxford University Press, New York and Oxford).

Binder, K. and Landau, D. P. (1989), in *Advances in Chemical Physics: Molecule-Surface Interaction*, ed. K. P. Lawley (Wiley, New York), p. 91.

Binder, K., Block, B., Das, S. K., Virnau, P., and Winter, D. (2011), *J. Stat. Phys.* **144**, 690.

Bruce, A. D., Jackson, A. N., Ackland, G. J., and Wilding, N. B. (2000), *Phys. Rev. E* **61**, 906.

Bruce, A. D., Wilding, N. B., and Ackland, G. J. (1997), *Phys. Rev. Lett.* **79**, 3002.

Caillot, J. M. (1992), *J. Chem. Phys.* **96**, 1455.

Catlow, C. R. A. (ed.) (1992), *Modelling of Structure and Reactivity in Zeolites* (Academic Press, London).

Ceperley, D., Chester, C. V., and Kalos, M. H. (1977), *Phys. Rev. B* **16**, 3081.

Consta, S., Wilding, N. B., Frenkel, D., and Alexandrowicz, Z. (1999), *J. Chem. Phys.* **110**, 3220.

Dadobaev, G. and Slutsker, A. I. (1981), *Sov. Phys. Solid State* **23**, 1131.

Das, S. K. and Binder, K. (2011), *Molec. Phys.* **109**, 1043.

Davies, G. T., Eby, K., and Colson, J. P. (1970), *J. Appl. Phys.* **41**, 4316.

De Gennes, P. G. (1979), *Scaling Concepts in Polymer Physics* (Cornell University Press, Ithaca).

De Miguel, E. and Jackson, G. (2006), *Molec. Phys.* **104**, 3717.

Deb, D., Wilms, D., Winkler, A., Virnau, P., and Binder, K. (2012), *Int. J. Mod. Phys. C* **23**, 1240011.

Degiorgio, V. and Corti, M. (eds.) (1985), *Physics of Amphiphiles: Micelles, Vesicles and Microemulsions* (North-Holland, Amsterdam).

Dress, C. and Krauth, W. (1995), *J. Phys. A* **28**, L597.

Dünweg, B., Stevens, M., and Kremer, K. (1995), in *Monte Carlo and Molecular Dynamics Simulations in*

Polymer Science, ed. K. Binder (Oxford University Press, New York and Oxford), p. 125.
Eisenriegler, E., Kremer, K., and Binder, K. (1982), *J. Chem. Phys.* **77**, 6296.
Ermak, D. L. (1975), *J. Chem. Phys.* **62**, 4189.
Errington, J. R. (2003), *Phys. Rev. E* **67**, 012102.
Errington, J. R. (2004), *J. Chem. Phys.* **120**, 3130.
Fasnacht, M., Swendsen, R. H., and Rosenberg, J. M. (2004), *Phys. Rev.* **E69**, 056704.
Frenkel, D. and Smit, B. (1996), *Understanding Molecular Simulation: From Algorithms to Applications* (Academic Press, New York).
Gaines, G. L. Jr. (1996), *Insoluble Monolayers at Liquid-Gas Interfaces* (Intersciences, New York).
Greengard, L. and Rokhlin, V. (1987), *J. Comp. Phys.* **73**, 325.
Grzelak, E. M. and Errington, J. R. (2010), *J. Chem. Phys.* **132**, 224702.
Haas, F. M., Hilfer, R., and Binder, K. (1996), *J. Phys. Chem.* **100**, 15290.
Halperin, B. I. and Nelson, D. R. (1978), *Phys. Rev. Lett.* **41**, 121.
Houlrik, J., Landau, D. P., and Knak Jensen, S. (1994), *Phys. Rev. E* **50**, 2007.
Jackson, A. N., Bruce, A. D., and G. J. Ackland (2002), *Phys. Rev. E* **65**, 036710.
Jaster, A. (1998), *Europhys. Lett.* **42**, 277.
Karaborni, S. and O'Connell, J. P. (1990), *J. Phys. Chem.* **94**, 2624.
Kim, Y. C, Fisher, M. E., and Luijten, E. (2003), *Phys. Rev. Lett.* **91**, 065701.
Kofke, D. A. and Cummings, P. T. (1997), *Molecular Phys.* **92**, 973.
Kosterlitz, J. M. and Thouless, D. J. (1973), *J. Phys. C* **6**, 1181.
Kremer, K. and Binder, K. (1988), *Computer Phys. Rep.* **7**, 259.
Kremer, K. and Grest, G. S. (1990), *J. Chem. Phys.* **92**, 5057.
Kremer, K. and Grest, G. S. (1995), in Binder, K. (1995), p. 194.
Landau, D. P. (1991), in *Phase Transitions and Surface Films* 2, eds. H. Taub, G. Torzo, H. J. Lauter, and S. C. Fain, Jr., p. 11.
Landau, L. D. and Lifshitz, E. M. (1980), *Statistical Physics,* 3rd edn, Part 1 (Pergamon Press, Oxford).
Liu, J. and Luijten, E. (2004), *Phys. Rev. Lett.* **92**, 035504.
Lodge, T. P., Rotstein, N. A., and Prager, S. (1990), in *Advances in Chemical Physics*, Vol. **79**, eds. I. Prigogine and S. A. Rice (Wiley, New York), p. 1.
Martonak, R., Paul, W., and Binder, K. (1996), *Computer Phys. Commun.* **99**, 2.
Martonak, R., Paul, W., and Binder, K. (1997), *J. Chem. Phys.* **106**, 8918.
Mavrantzas, V. G. (2005), in *Handbook of Materials Modelling, Vol. I: Methods and Models*, ed. S. Yip (Springer, Berlin).
McDonald, I. R. (1972), *Mol. Phys.* **23**, 41.
Metropolis, N. *et al.* (1953), *J. Chem. Phys.* **21**, 1087.
Milchev, A. and Binder, K. (1996), *Macromolecules* **29**, 343.
Milchev, A. and Binder, K. (1997), *J. Chem. Phys.* **106**, 1978.
Milchev, A. and Binder, K. (2001), *J. Chem. Phys.* **115**, 983.
Milchev, A., Dimitrov, D. I., and Binder, K. (2008), *Polymer* **49**, 3611.
Milchev, A., Paul, W., and Binder, K. (1993), *J. Chem. Phys.* **99**, 4786.
Mon, K. K. and Griffiths, R. B. (1985), *Phys. Rev.* **A31**, 956.
Mooij, G. C. A. M., Frenkel, D., and Smit, B. (1992), *J. Phys. Condens. Matter* **4**, L255.
Müller, M. and Binder, K. (1995), *Macromolecules* **28**, 1825.
Müller, M. and de Pablo, J. J. (2006), in *Computer Simulations in Condensed Matter: From Materials to Chemical Biology*, eds. M. Ferrario, G. Ciccotti, and K. Binder (Springer, Heidelberg), vol. 1, p. 67.

Nelson, D. R. and Halperin, B. I. (1979), *Phys. Rev. B* **19**, 2457.
Nijmeijer, M. J. P. and Weis, J. J. (1995), *Phys. Rev. Lett*. **75**, 2887.
Nijmeijer, M. J. P., Bruin, C., Bakker, A. F., and van Leeuwen, M. J. M. (1990), *Phys. Rev. A* **42**, 6052.
Norman, G. E. and Filinov, V. S. (1969), *High Temp. (USSR)* **7**, 216.
Owicki, J. C. and Scheraga, H. A. (1977), *Chem. Phys. Lett*. **47**, 600.
Panagiotopoulos, A. Z. (1987), *Molecular Physics* **61**, 813.
Panagiotopoulos, A. Z. (1995), in *Observation Prediction and Simulation of Phase Transitions in Complex Fluids*, eds. M. Baus, L. F. Rull and J. P. Ryckaert (Kluwer Academic Publ., Dordrecht), p. 463.
Pandey, R. B., Milchev, A., and Binder, K. (1997), *Macromolecules* **30**, 1194.
Pangali, C., Rao, M., and Berne, B. J. (1978), *Chem. Phys. Lett*. **55**, 413.
Patrykiejew, A., Sokolowski, S., Zientarski, T., and Binder, K. (1995), *J. Chem. Phys*. **102**, 8221.
Patrykiejew, A., Sokolowski, S., Zientarski, T., and Binder, K. (1998), *J. Chem. Phys*. **108**, 5068.
Paul, W., Binder, K., Heermann, D. W., and Kremer, K. (1991), *J. Phys. II (France)* **1**, 37.
Paul, W., Yoon, D. Y., and Smith, G. D. (1995), *J. Chem. Phys*. **103**, 1702.
Pearson, D. S., Verstrate, G., von Meerwall, E., and Schilling, F. C. (1987), *Macromolecules* **20**, 1133.
Pollock, E. L. and Glosli, J. (1996), *Comput. Phys. Commun*. **95**, 93.
Presber, M., Dünweg, B., and Landau, D. P. (1998), *Phys. Rev. E* **58**, 2616.
Privman, V. (1988), *Phys. Rev. Lett*. **61**, 183.
Rao, M. and Berne, B. J. (1979), *Mol. Phys*. **37**, 455.
Rector, D. R., van Swol, F., and Henderson, J. R. (1994), *Molecular Physics* **82**, 1009.
Rosenbluth, M. N. and Rosenbluth, A. W. (1955), *J. Chem. Phys*. **23**, 356.
Rossky, P. J., Doll, J. D., and Friedman, H. L. (1978), *J. Chem. Phys*. **69**, 4628.
Rouse, P. E. (1953), *J. Chem. Phys*. **21**, 127.
Rovere, M., Heermann, D. W., and Binder, K. (1990), *J. Phys. Cond. Matter* **2**, 7009.
Ryckaert, J. P. (1996), in *Monte Carlo and Molecular Dynamics of Condensed Matter Systems*, eds. K. Binder and G. Ciccotti (Società Italiana di Fisica, Bologna), p. 725.
Sariban, A. and Binder, K. (1987), *J. Chem. Phys*. **86**, 5859.
Scheringer, M., Hilfer, R., and Binder, K. (1992), *J. Chem. Phys*. **96**, 2296.
Schilling, T. and Schmid, F. (2009), *J. Chem. Phys.* **131**, 231102.
Schmid, F., Stadler, C., and Lange, H. (1998), in *Computer Simulation Studies in Condensed-Matter Physics X*, eds. D. P. Landau, K. K. Mon, and H.-B. Schüttler (Springer, Berlin), p. 37.
Siepmann, J. I. and Frenkel, D. (1992), *Mol. Phys*. **75**, 90.
Smit, B. (1988), *Phys. Rev. A* **37**, 3481.
Smit, B. (1995), *J. Phys. Chem*. **99**, 5597.
Smit, B., Esselink, K., Hilbers, P. A. J., van Os, N. M., Rupert, L. A. M., and Szleifer, I. (1993), *Langmuir* **9**, 9.
Sokal, A. D. (1995), in *Monte Carlo and Molecular Dynamics Simulations in Polymer Science*, ed. K. Binder (Oxford University Press, New York and Oxford), p. 47.
Theodorou, D. N. (2002), in *Bridging Time Scales: Molecular Simulations for the Next Decade*, eds. P. Nielaba, M. Mareschal, and G. Ciccotti (Springer, Berlin).
Viduna, D., Milchev, A., and Binder, K. (1998), *Macromol. Theory and Simul*. **7**, 649.
Vink, R. L. C. and Horbach, J. (2004), *J. Chem. Phys*. **121**, 3253.
Virnau, P. and Müller, M. (2004), *J. Chem. Phys*. **120**, 10925.

Von Gottberg, F. K., Smith, K. A., and Hatton, T. A. (1997), *J. Chem. Phys.* **106**, 9850.
Weber, H., Marx, D., and Binder, K. (1995), *Phys. Rev.* B **15**, 14636.
Werner, A., Schmid, F., Müller, M., and Binder, K. (1997), *J. Chem. Phys.* **107**, 8175.
Widom, B. (1963), *J. Chem. Phys.* **39**, 2808.
Wilding, N. (2006), in *Computer Simulations in Condensed Matter: From Materials to Chemical Biology*, eds. M. Ferrario, G. Ciccotti, and K. Binder (Springer, Heidelberg), vol. 1, p. 39.
Wilding, N. B. (1997), *J. Phys. Condensed Matter* **9**, 585.
Wilding, N. B. (2001), *Am. J. Phys.* **69**, 1147.
Wilding, N. B. and Binder, K. (1996), *Physica A* **231**, 439.
Wilding, N. B. and Bruce, A. D. (2000), *Phys. Rev. Lett.* **85**, 5138.
Wilding, N. B. and Landau, D. P. (2003), in *Bridging Time Scales: Molecular Simulations for the Next Decade*, eds. P. Nielaba, M. Marechal, and G. Ciccotti (Springer, Heidelberg).
Wittmer, J. P., Beckrich, P., Meyer, H., Cavallo, A., Johner, A., and Baschnagel, J. (2007), *Phys. Rev. E* **76**, 011803.
Yoon, D. Y., Smith, G. D., and Matsuda, T. (1993), *J. Chem. Phys.* **98**, 10037.
Young, A. P. (1979), *Phys. Rev. B* **19**, 1855.
Zollweg, J. A. and Chester, G. V. (1992), *Phys. Rev. B* **46**, 11187.